UCRL-13964

CENTER FOR ELECTROMECHANICS

THE UNIVERSITY OF TEXAS
COLLEGE OF ENGINEERING
TAYLOR HALL 167
AUSTIN, TEXAS, 78712
512/471-4496

PULSED POWER SUPPLIES FOR LASER FLASHLAMPS

LAWRENCE LIVERMORE LABORATORY

Subcontract No. 1823209

Final Report

October, 1978

Prepared by

Center for Electromechanics
The University of Texas at Austin

William F. Weldon, Technical Director and Co-Principal Investigator
H. G. Rylander, Director and Co-Principal Investigator
Herbert H. Woodson, Associate Director and Co-Principal Investigator

This report written and compiled by

William L. Bird, Jr., Project Engineer
Mircea D. Driga, Faculty Associate
David J. T. Mayhall, Research Engineer
Michael Brennan, Research Engineer

NOTICE

This report was prepared by the Center for Electromechanics at The University of Texas at Austin as an account of work sponsored by the Lawrence Livermore Laboratory (LLL) under subcontract No. 1823209. Neither LLL, members of LLL, The University of Texas, nor any persons acting on behalf of either: (a) makes any warranty or representation, express or implied, with respect to the accuracy, completeness, or usefulness of the information contained in this report, or that the use of any information, apparatus, method or process disclosed in this report may not infringe privately owned rights; or (b) assumes any liabilities with respect to the use of, or for damages resulting from the use of, any information, apparatus, method, or process disclosed in this report.

ABSTRACT

A preliminary engineering design of a compensated pulsed alternator for driving laser flashlamps is presented. The work performed by the Center for Electromechanics at The University of Texas at Austin also includes the optimization and revision of the prototype design for a compensated pulsed alternator power supply for the NOVA laser system at Lawrence Livermore Laboratory.

TABLE OF CONTENTS

PREFACE

Work performed by the Center for Electromechanics of The University of Texas at Austin for Lawrence Livermore Laboratory under Subcontract No. 1823209 is described. However, in the on going LLL-UT CEM program to design, fabricate, and test the half scale engineering prototype, (Purchase Order No. 3325309) design iterations have been made as new problems are discovered and solved. Therefore, some discussion of the engineering prototype is described in this report as required to illustrate design considerations that were not addressed by the point design, but are important to the design of the full scale system for NOVA.

LIST OF FIGURES

LIST OF FIGURES (cont'd)

LIST OF TABLES

I. INTRODUCTION

1.1 Background

The Center for Electromechanics of The University of Texas at Austin has proposed a new power source as a possible replacement for the large bank of capacitors now used to power the large lasers for inertial confinement fusion experiments. The proposed power source is a compensated pulsed alternator.

The compensated pulsed alternator, or compulsator, converts rotational mechanical energy directly into electrical energy, utilizing the principles of both magnetic induction and flux compression. The primary advantage of the power source is the economy and high energy density of inertial energy storage.

The alternator rotor serves as the flywheel of the device so that it is not necessary to transmit the full discharge torque via a coupling external to the machine. The high peak power rating of the device is obtained by minimizing the internal reactance of the armature winding by means of a stationary compensating winding, and by rating the system for pulsed duty.

The incentive for replacing capacitor banks with the pulsed alternator is to reduce the size and cost of the power source, and to increase its reliability. The basic high voltage energy storage capacitor is limited

to several kilojoules per unit. This basic unit is rather bulky due to the low energy density of the electric field as compared to the energy density of a magnetic field or a rotating mass. For example, the capacitor bank for a larger laser system (100 to 200 MJ) would contain tens of thousands of individual capacitors, while an inertial system of pulsed alternators would consist of tens of machines, occupying a much smaller space.

1.2 Summary of Work Performed

The Center for Electromechanics at The University of Texas at Austin has made a preliminary engineering design of a pulsed alternator to deliver 2.4 MJ of energy to a system of 96 parallel lamp circuits consisting of two lamps in series. The nominal impedance parameter K_o of the two series flashlamps is taken to be 225 Ω-amp$^{1/2}$. This preliminary design is referred to as the point design in this report. The preliminary alternator parameters were presented in a review held at Lawrence Livermore Laboratory, July 14, 1978. The work has been performed under Lawrence Livermore Subcontract Number 1823209, dated May, 1978.

In addition to the point design, the Center for Electromechanics has also continued the optimization and the revision of the prototype design under an add on to the above mentioned subcontract. The revision of the prototype design has incorporated some suggestions made at the July, 1978, design review and has been modified to match a lower impedance lamp with an impedance parameter K_o approximately equal to 180 Ω-amp$^{1/2}$ (for double lamp circuit, as specified by LLL after July, 1978).

To best match the flashlamps and to maximize delivered energy, the rotor diameter has been increased from 0.8 m to slightly larger than 1.0 m. The number of rotor conductors N_c has been reduced from 47 to 23. The performance is better for the smaller number of conductors because the internal impedance of the alternator varies as N_c^2 while the open circuit voltage varies linearly with N_c. The 23 conductor design has been found to be optimum for a flashlamp system with a peak current of 4.5 kA per lamp.

During the latter phases of the contract period, the Center for Electromechanics continued the engineering design of the full-scale prototype design and also began the design of the half-scale prototype. Several changes in the mechanical design have been made as deemed necessary or prudent by more detailed analysis. For example, the rotor winding conductors were originally to be machined from a thin copper shell. However, the eddy current losses of the air gap winding were found to be excessive and a stranded and transposed design conductor design has been substituted. An alternate design of the stator compensating winding support ring has also been suggested. These design features are discussed in detail in Section III of this report.

It has been found that the magnitude of the inductance variation of the armature windings is the single most important factor in determining the basic dimensions of the alternator to match a specified flashlamp load. The methods of calculating machine parameters to match a system of flashlamps and general scaling laws are presented in Section IV. It

is noted that the scaling laws used in the optimization study are preliminary and that experimental verification of the electromagnetic analysis is required before the engineering design of the full-scale prototype is attempted. In fact, recent calculations of armature inductance for the half-scale engineering prototype, coupled with earlier calculations for the point design, indicate that some scaling factors used in this report should be modified.

If manufacturing limitations and material availability are considered, it appears that a four pole machine with a 1.0 m diameter rotor is still a logical choice for the full-scale engineering prototype. It is anticipated that such a device would drive approximately 200 parallel flashlamp circuits, delivering approximately five megajoules to the load at a peak current of 4.5 kiloamps per lamp circuit.

The compensated pulsed alternator devices presented in the report have been specifically designed for the NOVA system and are not, therefore, necessarily suited for high repetition rate continuous duty applications. The machines should, however, be fully capable of meeting the proposed duty for NOVA. To reduce rotational drag and heat generation, the main fields of the alternators are pulsed and brushes are lifted except for the brief periods just prior to, during, and after the current discharge.

The compensated pulsed alternator will require some advances in rotating machine technology, primarily those advances associated with developing a compensated (low reactance) air gap winding in a magnetic

field with a higher frequency and peak flux density than is normally found in conventional rotating machinery. The problems to be overcome in this development program are summarized in Section V.

The Center for Electromechanics is continuing the work initiated under Subcontract Number 1823209 and described in this report. Under LLL Purchase Order 3325309 the Center for Electromechanics is to design, fabricate, and test a half-scale engineering prototype and to design a full-scale prototype pulsed alternator for the NOVA System. The testing phase of the program is to begin in April, 1979.

II. APPLICATION OF COMPENSATED PULSED ALTERNATOR TO FLASHLAMP LOAD

2.1 Electromagnetic Theory of Operation

2.1.1 Basic Theory

The compensated pulsed alternator is an electromechanical device which combines rotary flux compression with conventional alternator energy conversion. A schematic diagram of the machine is shown in Figure 1. The ciruit is represented by a sinusoidal voltage source V (t), a resistance R, and a variable inductance L. The resistance R is the sum of the generator resistance and the non-linear resistance of the flashlamp load. The circuit differential equation is given by

$$\frac{d}{dt}(Li) + \frac{R}{L}(Li) = V(t) \tag{1}$$

or $$\frac{d\phi}{dt} + \frac{R}{L}(\phi) = V(t) \tag{1a}$$

The solution to Equation (1a) is

$$\phi = \left[\phi_{initial} + \int_o^t V(t)dt \right] e^{-\int (R/L)dt} \tag{2}$$

where $\phi_{initial} = L_{max} i_{initial}$

The current may be expressed as

$$i = \frac{1}{L} \left(L_{max} i_{initial} + \int_o^t V(t)dt\right) e^{-\int R/L dt} \tag{3}$$

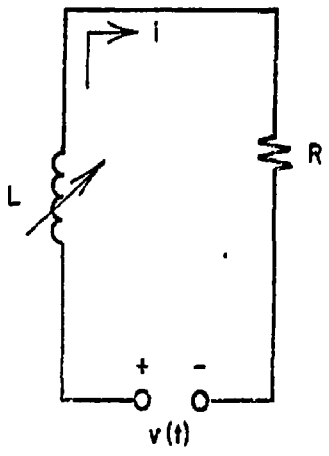

Figure 1: Rotating Flux Compressor Schematic

where R, L, and i are instantaneous values.

Sketches of resistance, inductance, and current waveforms are shown in Figure 2.

It is important to note that the second term in Equation 3, $\int_0^t V(t)dt$, is more important in determining the total energy transmitted to the load. As discussed in Section 2.3 the supplied alternator volt seconds are approximately equal to the circuit resistive volt seconds. The inductance variation or flux compression, primarily affects the pulse shape (amplitude and half width) rather than delivered energy.

2.1.2 Inductance Variation

The armature inductance L is an intermediate quantity which relates flux linkage λ to armature current i.

$$L = \lambda/i$$

In a pulsed high current device such as the compensated pulsed alternator, non-linear time varying effects of magnetic saturation and diffusion make it useful, analytically, to consider the inductance in terms of magnetic energy rather than flux linkages. The inductance is calculated by

$$L = \frac{2}{i^2} \int_{vol} \tfrac{1}{2}\vec{B}.\vec{H}\, d(vol) \qquad (4)$$

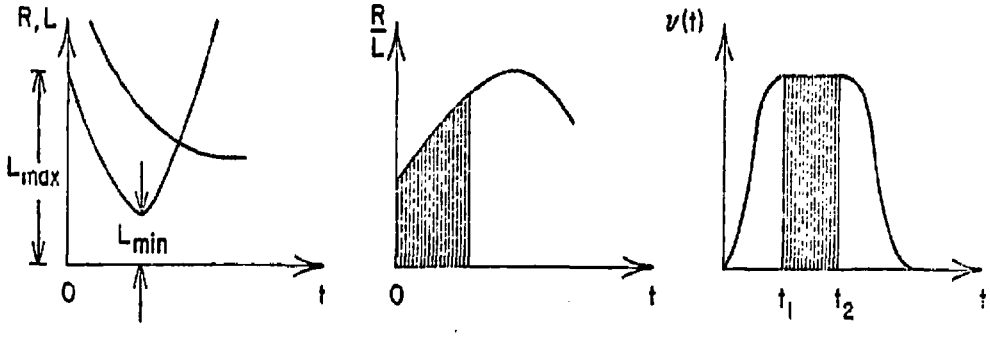

Figure 2: R, L, R/L and V as Functions of Time

The inductance variation is calculated by determining the armature flux distribution as a function of rotor position, armature current, and time, using a transient finite element method computer code. The magnetic energy W_m is calculated as

$$W_m = \sum_{i=1}^{N_{elements}} \left(1/2 \frac{B^2}{\mu_o \mu_r} \cdot Vol\right)_i$$

The initial armature current is established during the startup period during which the flashlamps are also preionized. At some time t_o the lamps are switched across the alternator terminals. At the moment of switching the rotor and stator (compensating) coils are displaced approximately 32 electrical degrees, and the armature flux is as shown in Figure 3.

Note that the direction of the flux lines in the air gap is radial. The ampere turns which generate the flux are located at the four uncompensated sectors, 32 electrical degrees each, which are distributed 180 electrical degrees apart. Since the flux lines are radial, the magnetic circuit has a relatively low reluctance and, therefore, a high inductance. Approximately 80 percent of the magnetic energy is stored in the air gap. The remaining 20 percent is stored in the rotor. The relative permeability of the rotor laminations is determined by the main field flux density and is approximately equal to 40. Since the volume of the rotor iron is much greater than the air gap, the energy stored in the rotor does influence the inductance calculation somewhat.

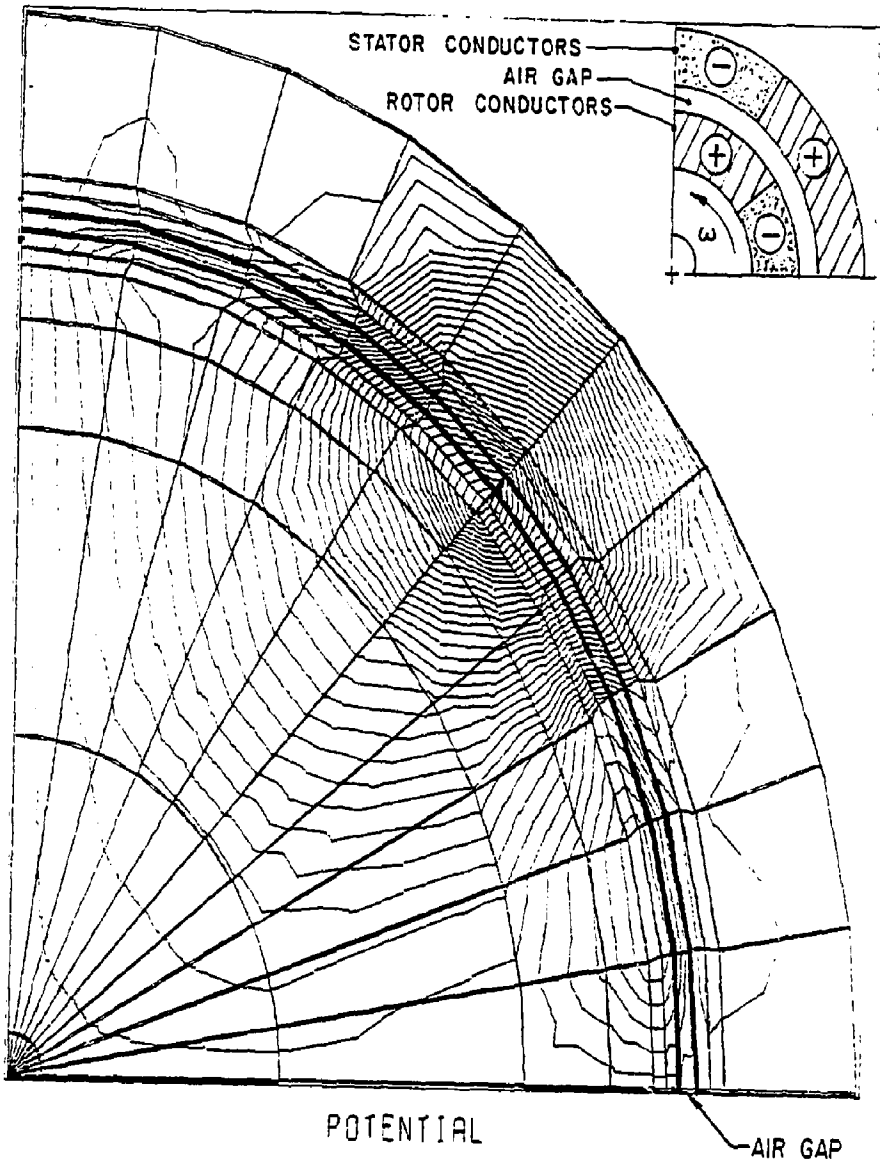

Figure 3: Flux Plot -- Coil Systems Displaced 32° (Electrical)

As the rotor spins during the pulse the angular displacement between the coils decreases and when the displacement reaches zero, the inductance is minimized. The armature flux distribution at the point of minimum inductance (maximum compensation) is shown in Figure 4. In this case the flux lines in the air gap are tangential to the periphery of the rotor, the length of the magnetic path proportional to the polar pitch τ. Since the reluctance of this circuit is greater, the corresponding inductance is smaller.

The variation of inductance of the point design pulsed alternator is shown in Figure 5. The variation in the inductance over the main pulse is approximately twenty to one.

To determine the ratio of L_{max}/L_{min} for another machine configuration, it is best to run the finite element code for that particular case. However, for comparing a large number of machines, this is not practical and a simple scaling law is required. The approximate scaling factor can be obtained by comparing the ratio of the magnetic flux density in the airgap at the maximum and minimum inductance positions. The magnetic flux density is inversely proportional to the air gap flux path length. Therefore, to determine (L_{max}/L_{min}) for machine A given (L_{max}/L_{min}) for machine B

$$(L_{max}/L_{min})_A = (\tau/g)_A^2 \,/\, (\tau/g)_B^2 \cdot (L_{max}/L_{min})_B \qquad (5)$$

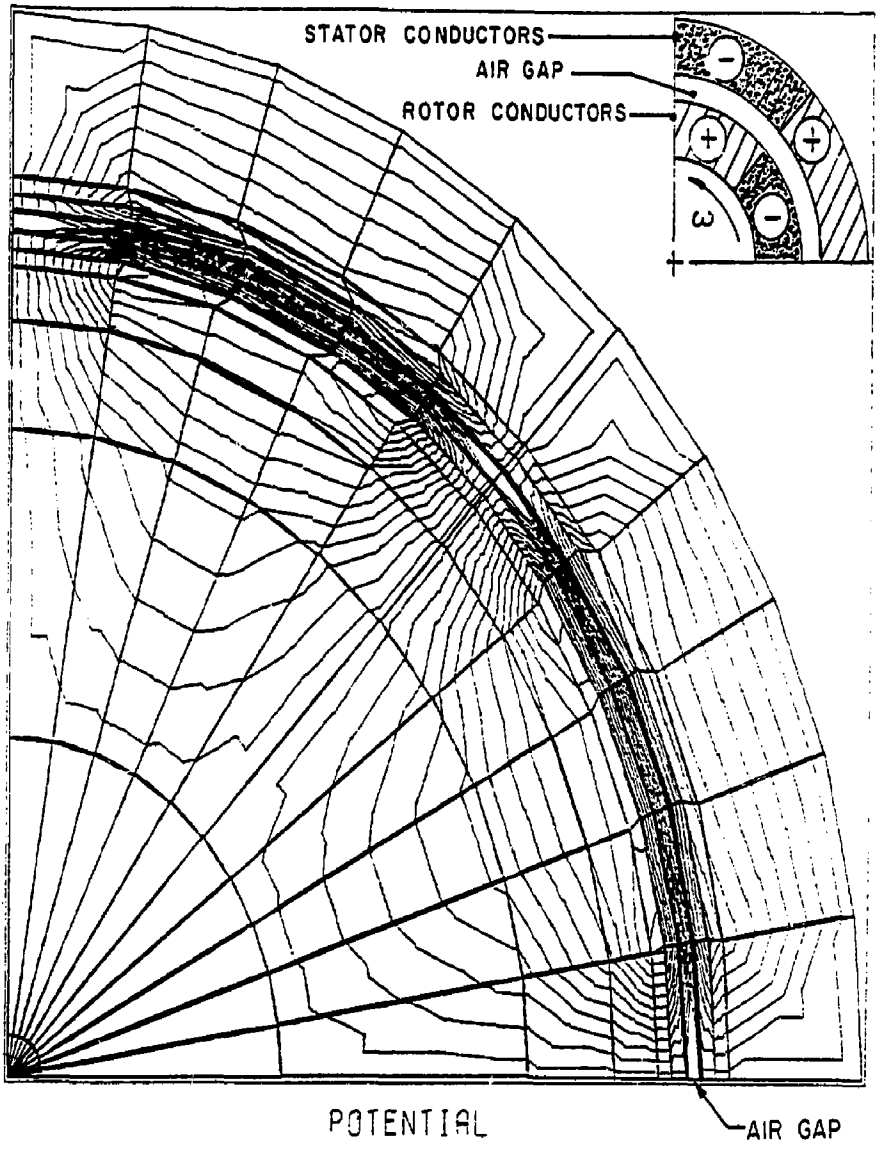

Figure 4: Flux Plot -- Coil Systems Displaced 0° (Electrical)

*Initial inductance rise from zero is due to proximity effects and does not occur if conductors are stranded and transposed.

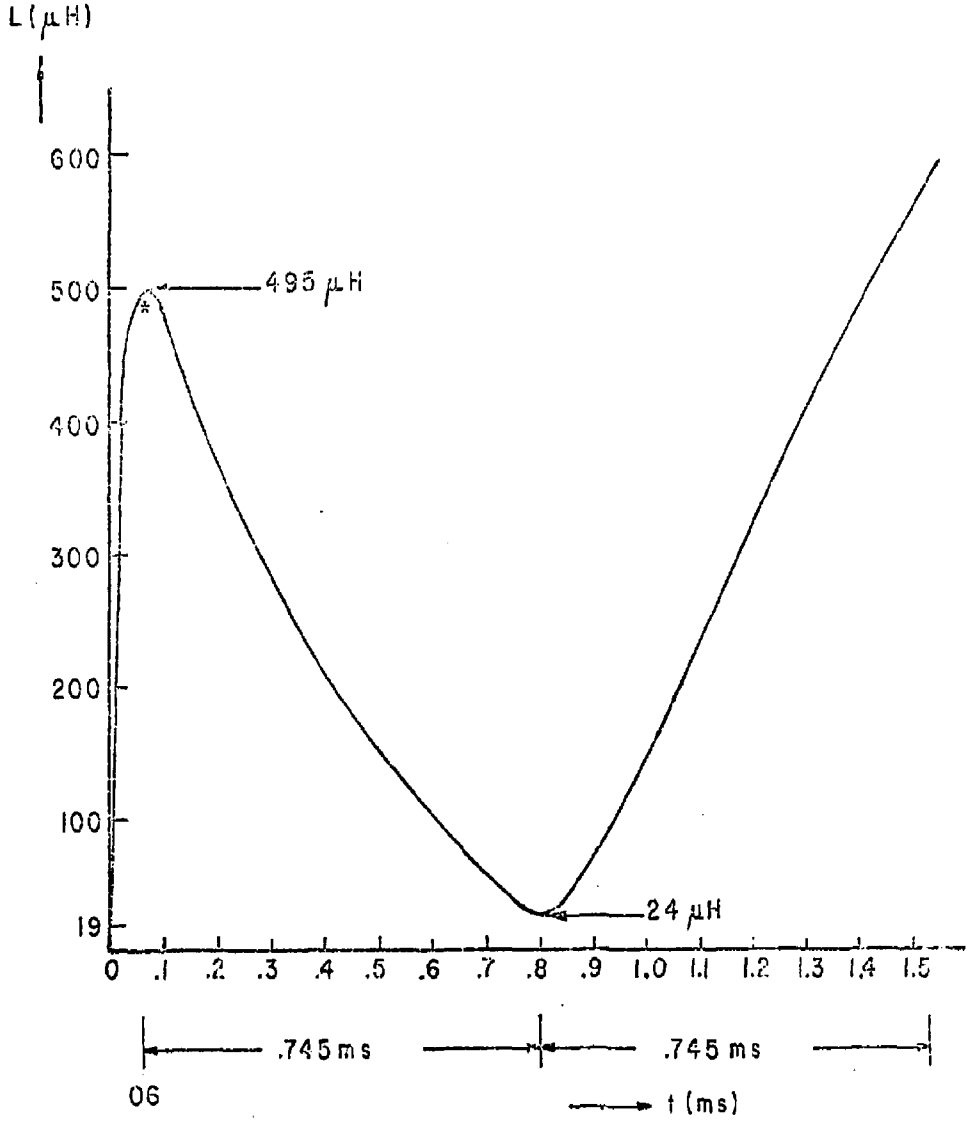

Figure 5: Armature Circuit Inductance Variation

Since the width of the air gap does not increase linearly with diameter, the inductance variation increases with diameter. However, the pole pitch τ is inversely proportional to the number of poles. Therefore, for a given diameter, the inductance variation is greatest for the machine with the fewest number of poles.

2.2 Flashlamp Power Supply Requirements

The behavior of the xenon flashlamps may be separated into two phases. These are 1) the initial streamer breakdown and arc growth to full bore and 2) the lamp current buildup and decay at full bore. The circuit requirements for each phase are different.

During the first phase, the lamps are highly resistive. A high voltage is required to initiate the breakdown. Two 44 in. long, 15 mm i.d. flashlamps connected in series typically require 33-34 kV for breakdown. With the conventional capacitor bank power supply, the high voltage for lamp triggering is obtained from pulse charging coaxial cables at an applied voltage of 20 kV. The lamps spontaneously breakdown as the open circuited cable voltage approaches double the applied voltage. After breakdown, a relatively small amount of energy input is required for arc growth to full bore. Two 44 in. long lamps in series require about 208 J. For proper lamp operation, the arc growth should proceed as rapidly as possible without damage to the lamp envelopes.

For current buildup at full lamp diameter, the lamps are much less resistive. During this phase, the current varies as $k_o i_L^{-1/2}$, where

k_o is the lamp impedance parameter and i_L is the lamp current. The parameter k_o is typically 180 Ω-$A^{1/2}$ for two 44 in. long, 15 mm i.d. lamps in series. Current buildup requires a moderate lamp voltage and a relatively large energy input. Two 44 in. long lamps in series need a voltage of about 16 kV and an energy absorption of about 25 kJ.

The flashlamp power supply system thus must rapidly furnish a small amount of energy at high initial voltage and subsequently furnish a large amount of energy at moderate voltage over a period of about 400-600 μsec.

2.2.1 PILC Circuit

A cost efficient flashlamp compulsator is a moderate voltage (~15 kV) machine with a discharge time of the order of the desired flashlamp current pulse (~400-600 μsec). The compulsator requires 1-2 msec to charge up to 5% of its peak load current from zero initial alternator voltage. Therefore, a small (208 J/series lamp pair), high voltage (20 kV), auxiliary capacitor bank must be used to breakdown and pre-ionize the flashlamps. Such an auxiliary capacitor bank has been proposed to check for proper lamp characteristics prior to the main pulse. This is the Pulse Ionization Lamp Check or PILC bank. If a PILC bank is to be used to check against flashlamp failures, its additional use for lamp breakdown with the compulsator should require very little additional cost.

2.2.2 Compulsator Current Initiation

The charging time of the compulsator effective inductance from zero current to a startoff current of 5% of its peak load current is fairly long due to the large values of its effective inductance and the small voltage prior to switching in the load. The charging time increases with increasing series armature resistance. Therefore, during the initial compulsator current buildup the external circuit resistance should be held to a minimum to reduce both the charging time and the resistive losses in the circuit.

2.2.3 Proposed Circuit Configurations

One suggested method[1] for effectively isolated startup of the compulsator and the flashlamps to the startoff current is the two switch circuit shown in Figure 6.

In this schematic, the compulsator is represented by the sinusoidal alternator voltage source V, the temperature dependent armature resistance R_{eff}, and the rotationally varying inductance L_{eff}. The PILC bank is represented by the capacitance C_p. The coaxial cables are represented by the $L_c C_c$ T network and the flashlamps by the current dependent resistance R_L. The elements S_1 and S_2 are switches.

In this system the PILC capacitor is initially charged to 16-20 kV. At time t = 0 the switch S_1 is closed and the PILC capacitor pulse

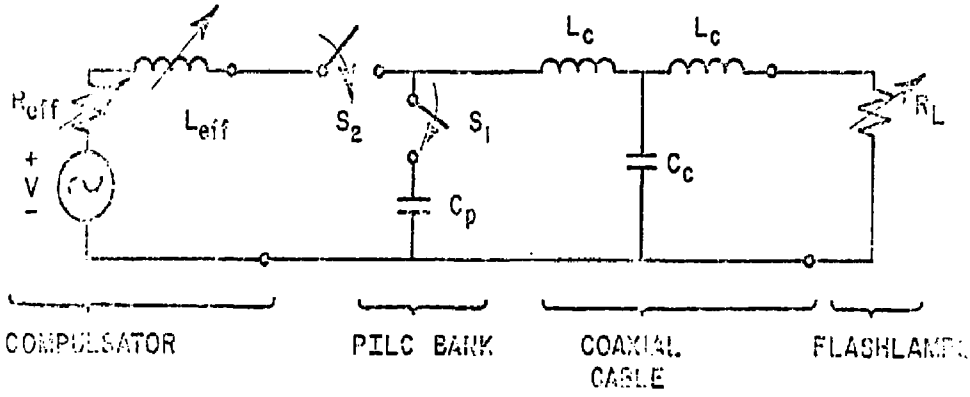

Figure 6: Schematic Diagram, Two-switch Circuit

charges the cable capacitance to the lamp breakdown voltage. The impedance of the lamps drop as energy is deposited in the lamps. At a time later the voltage on the PILC capacitor is reduced and the switch S_2 is closed, connecting the pulsed alternator to the circuit. The circuit analysis for this two switch circuit has been performed at Lawrence Livermore Laboratory. The Center for Electromechanics has done some circuit analysis for a two switch circuit in which the pulsed alternator is used to charge the PILC capacitor before the lamps are ionized. The disadvantage of this approach is that the alternator terminal voltage may be higher during the charging of the PILC capacitor than under load, making the design of the ground plane insulation and air gap insulation more difficult.

A second proposed method for isolated compulsator and flashlamp startup is the three switch circuit shown in Figure 7.

A crowbar or shunt resistor R_c and a switch S_3 have been inserted between the compulsator and the switch S_1 of the previous circuit. At some time, the crowbar switch S_3 is closed and the compulsator current builds up through the low resistance crowbar resistor. At some later time, the switch S_2 is closed and the pre-charged PILC capacitor pulse charges the cable capacitance C_c. The lamps break down and their current builds up to its start off value. At this time, the switch S_1 is closed and the compulsator then drives the lamp current through its desired evolution. Circuit analysis has shown that, after connection of the compulsator to the flashlamps, the current in the crowbar resistor

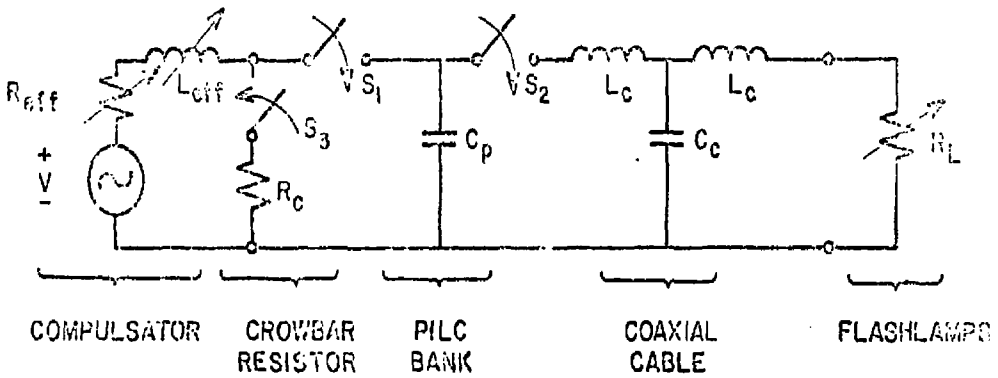

Figure 7: Schematic Diagram, Three-switch Circuit

naturally passes through zero without forced commutation. The use of a nonlinear, temperature dependent resistor for R_c should enhance the speed of this natural commutation. The three switch circuit analysis is described in detail in Appendix A.

Reference

[1]Carder, B., LLL.

2.3 Point Design Circuit Analysis

A detailed circuit analysis of the three switch circuit is described in Appendix A. The detailed circuit analysis model includes the effects of the breakdown and arc growth of the flashlamps and the capacitance of the coaxial cables and high current generator bus. If the initial breakdown and arc growth of the flashlamps are not included, a simple circuit model results. The reduced circuit model requires less computation time and yields sufficient accuracy to determine the sensitivity of peak current and delivered energy to changes in generator or flashlamp characteristics.

The schematic diagram of the reduced circuit model is shown in Figure 8. The following assumptions are made:

1. The flashlamps are broken down and pre-ionized by a separate source which is isolated from the alternator flashlamp circuit.

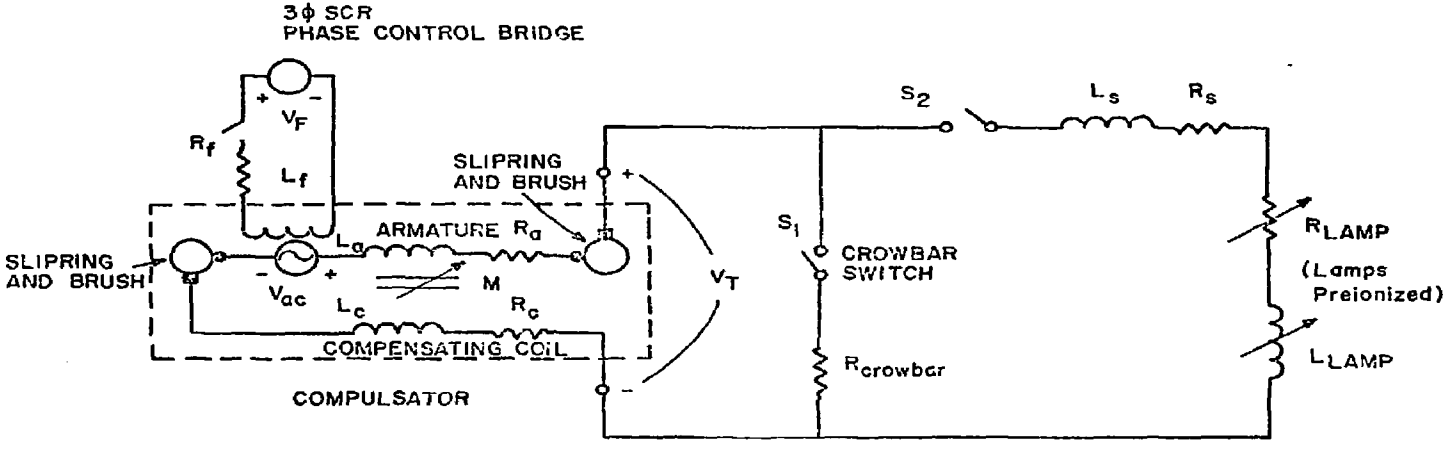

Figure 8: Reduced Three-switch Circuit Model

BIRD
UT-CEM
LLL
11-30-78

2. The flashlamp plasma fills the entire bore.
3. The resistance of each series connected flashlamp pair is given by

$$R \sim K_o i^{-1/2} \ \Omega$$

Where K_o is the impedance parameter of the flashlamp pair and i is the current per lamp circuit.

4. Switches are ideal.
5. Alternator rotational losses are negligible during the discharge pulse.

The effects of the variable inductance and conductor temperature rise of the armature circuit are included. The variation of rotor speed is considered in the alternator voltage calculation. However, the effect of armature reaction and the eddy current resistive losses in the rotor laminations and poles are not included.

It is assumed that the crowbar switch S_1 is closed at the time that the rotor winding links maximum field flux (zero voltage). The armature current rises slowly, but the rate of rise increases monotonically as the driving voltage increases and the inductance decreases. The current at the end of the startup phase is approximately five percent of the peak output current. At this time switch S_2 is closed and switch S_1 is opened. The current in the crowbar circuit is transferred to the flashlamps, which have been pre-ionized. The current continues to rise as the armature inductance decreases and the Blv voltage increases.

After the rotor winding passes the point of minimum inductance, the current decreases rapidly forming the spiked pulse shape. As the inductance continues to increase and the speed voltage reverses in polarity, the current is gradually driven through zero, and switch S_2 is opened. Typical circuit waveforms are shown in Figures 9-14.

The typical current and voltage values of the compensated pulsed alternator are listed in Table I. At early times during the startup phase, the alternator terminal voltage is small and the alternator speed voltage is used to overcome the large internal reactance of the machines. At t ~ 1.5 msec the flashlamps are switched into the circuit and the terminal voltage jumps from a hundred volts to over five kilovolts. The terms enclosed in the box of Table I indicate that period of the pulse that the variable inductance terms act as a net energy source rather than an energy sink. It should be noted that the peak terminal voltage under load is greater than the alternator speed voltage because of the effect of the variable inductance.

The system energy balance is listed in Table II. The inertial energy stored in the rotor at the beginning of the pulse is 38 MJ. As the generator is discharged, a fraction of this energy (4.8 MJ) is converted into i^2R losses in the generator and the flashlamps. Approximately 54 percent of the converted energy is delivered to the flashlamps, with the remainder distributed between the armature conductors and buswork. A significant fraction of the energy is temporarily stored

COMPULSATOR CURRENT VERSUS TIME

ENAR 624-134

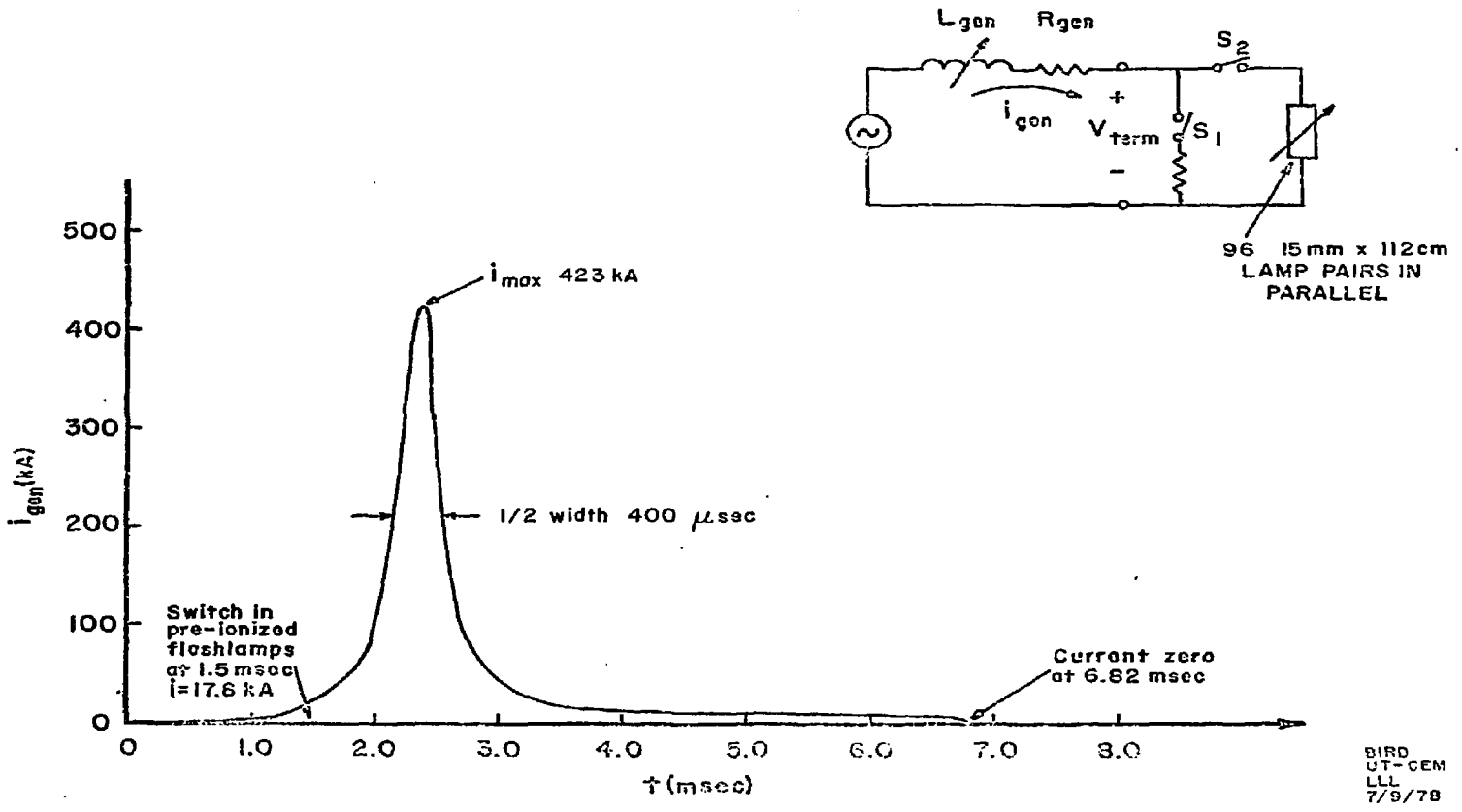

BIRD
UT-CEM
LLL
7/9/78

Figure 9: Typical Waveform, Current vs Time

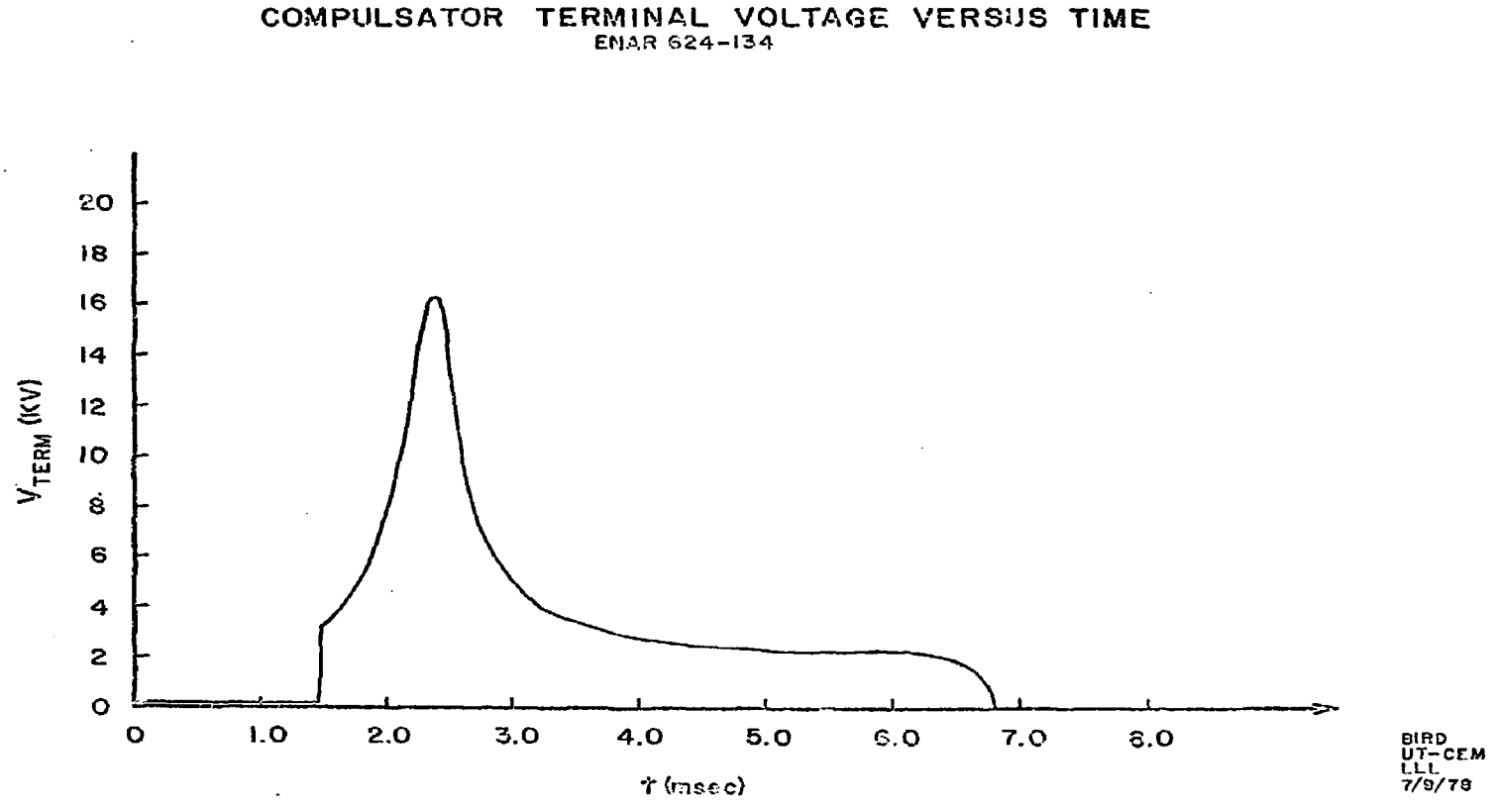

Figure 10: Typical Waveform, Terminal Voltage vs Time

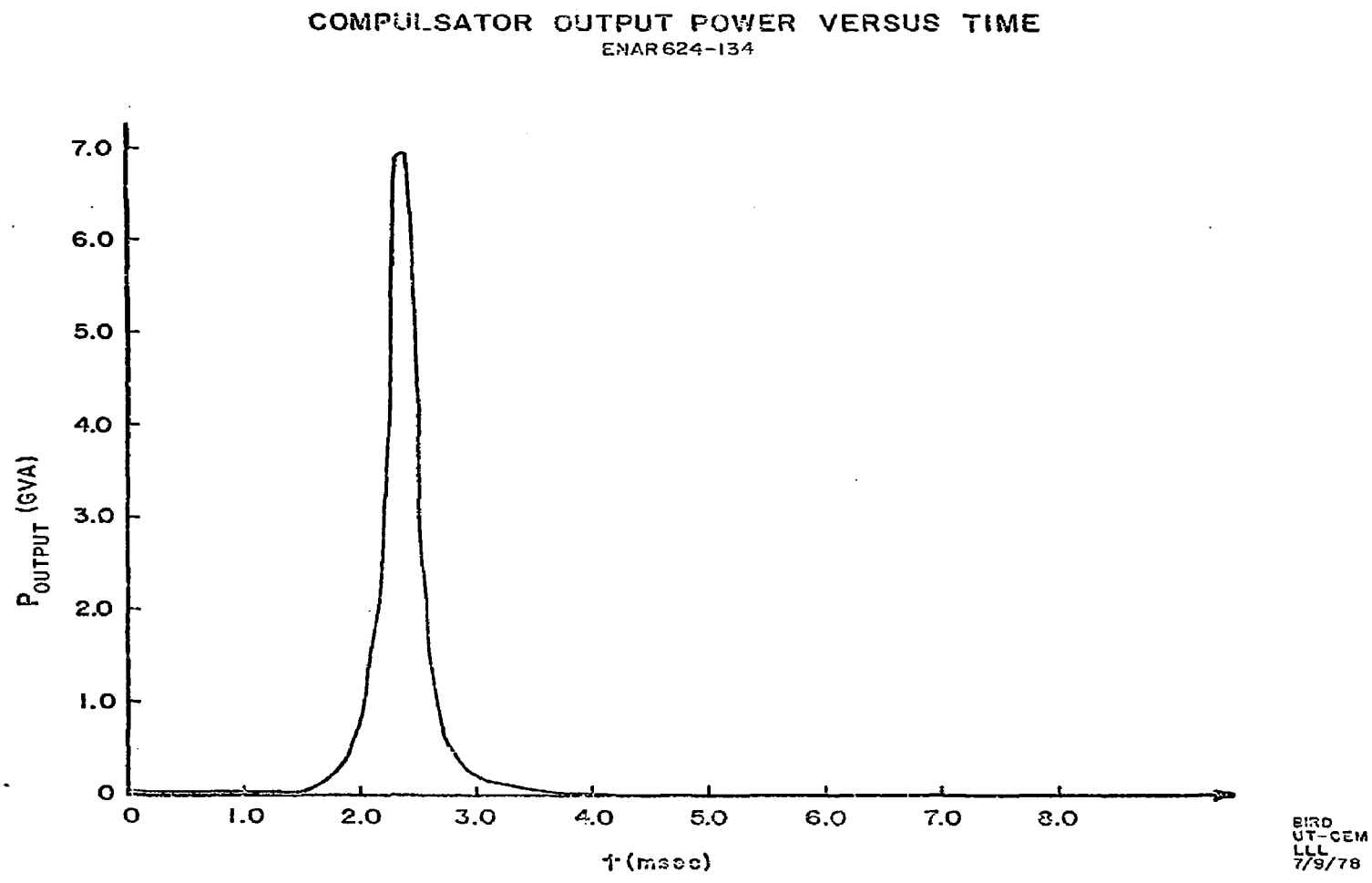

Figure 11: Typical Waveform, Output Power vs Time

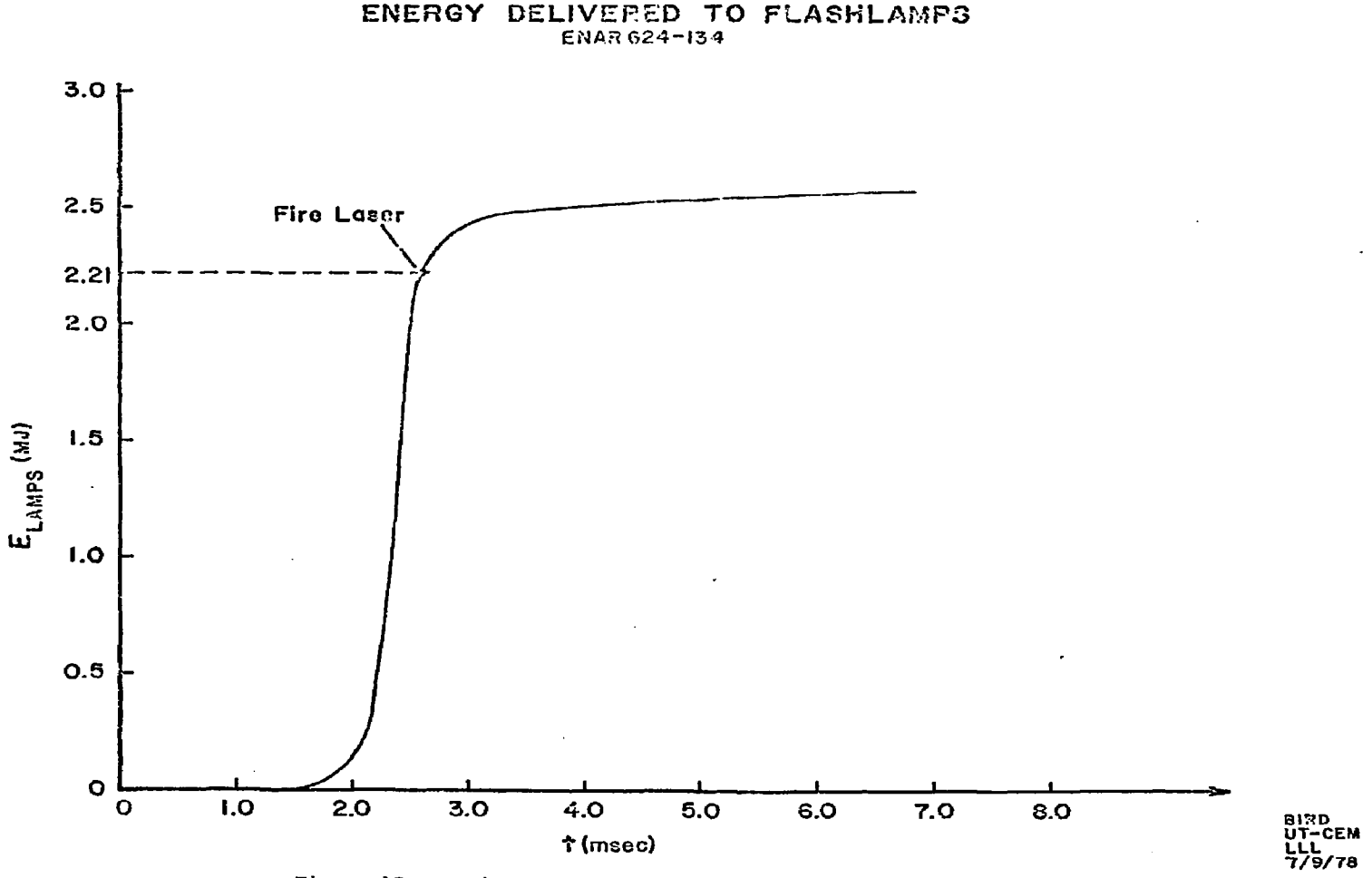

Figure 12: Typical Waveform, Energy Delivered to Flashlamps

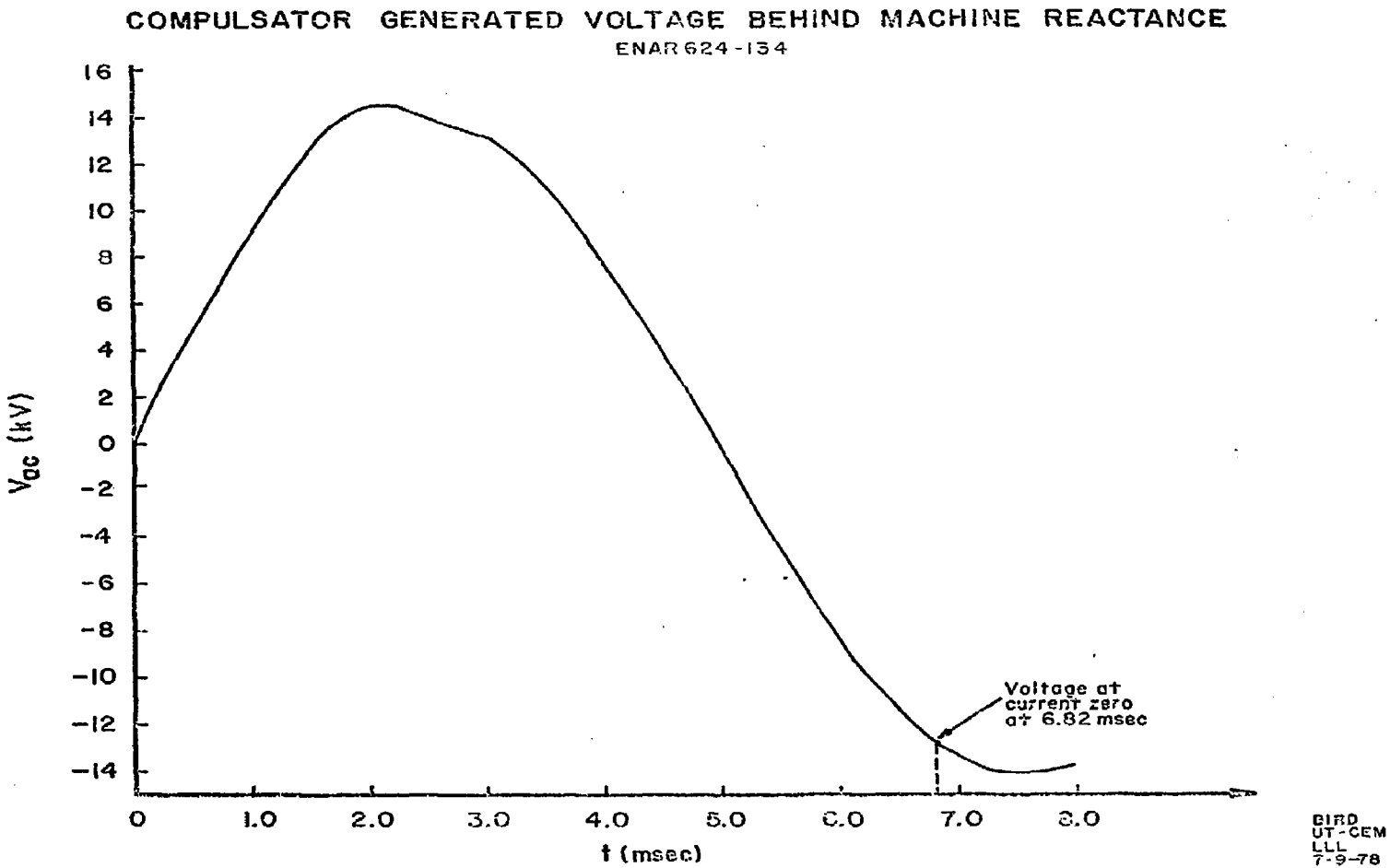

Figure 13: Typical Waveform, Generated Voltage Behind Machine Reactance

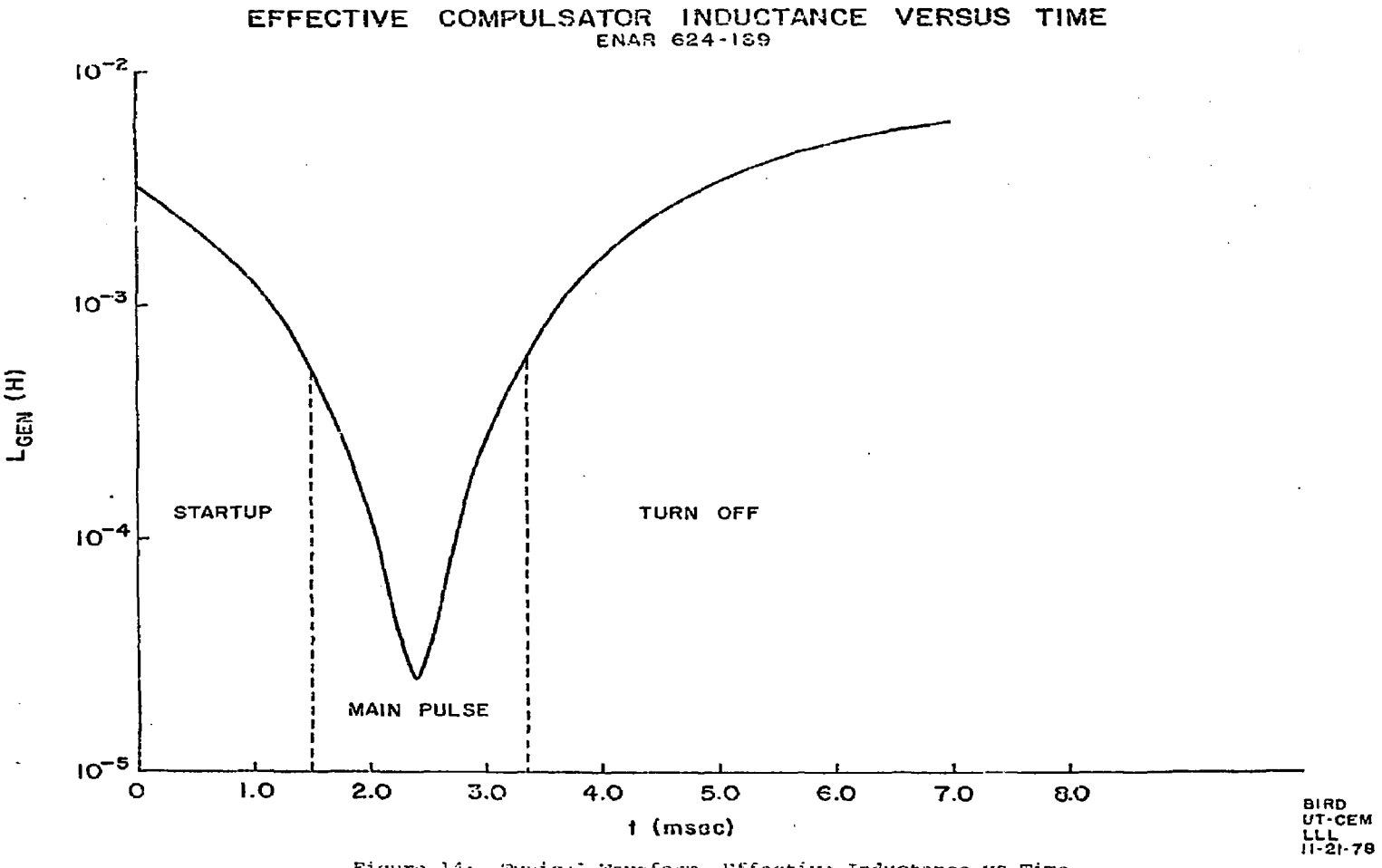

Figure 14: Typical Waveform, Effective Inductance vs Time

Table I

COMPULSATOR CURRENT & VOLTAGE VALUES

ENAR 624-134

t(sec)	i(amps)	$\omega(sec^{-1})$	$\dot{\omega}(sec^{-2})$	$(V_{ac}$	- i R_{gen}	- (volts) Li/dt	- $Id\dot{L}/dt$	- $V_{Term})$	T(N-m)
0	0	$3.288x10^{2}$	0	0	0	0	0	0	0
$5.000x10^{-4}$	$7.787x10^{2}$	$3.288x10^{2}$	$-1.709x10^{1}$	$4.044x10^{2}$	$2.645x10^{1}$	$5.352x10^{3}$	$-5.373x10^{2}$	$1.225x10^{0}$	$-1.211x10^{4}$
$1.000x10^{-3}$	$4.280x10^{3}$	$3.288x10^{2}$	$-2.113x10^{2}$	$9.167x10^{3}$	$1.454x10^{2}$	$1.368x10^{4}$	$-4.674x10^{3}$	$1.625x10^{1}$	$-1.497x10^{5}$
$1.494x10^{-3}$	$1.792x10^{4}$	$3.284x10^{2}$	$-1.678x10^{3}$	$1.246x10^{4}$	$6.089x10^{2}$	$3.044x10^{4}$	$-1.866x10^{4}$	$6.873x10^{1}$	$-1.189x10^{5}$
$1.834x10^{-3}$	$5.183x10^{4}$	$3.271x10^{2}$	$-7.459x10^{3}$	$1.394x10^{4}$	$1.762x10^{3}$	$4.558x10^{4}$	$-3.884x10^{4}$	$5.413x10^{1}$	$-5.205x10^{6}$
$1.934x10^{-3}$	$7.567x10^{4}$	$3.262x10^{2}$	$-1.248x10^{4}$	$1.422x10^{4}$	$2.574x10^{3}$	$5.284x10^{4}$	$-4.782x10^{4}$	$6.623x10^{1}$	$-8.843x10^{6}$
$2.014x10^{-3}$	$1.055x10^{5}$	$3.249x10^{2}$	$-1.940x10^{4}$	$1.437x10^{4}$	$3.593x10^{3}$	$5.884x10^{4}$	$-5.595x10^{4}$	$7.893x10^{1}$	$-1.375x10^{7}$
$2.094x10^{-3}$	$1.512x10^{5}$	$3.230x10^{2}$	$-3.068x10^{4}$	$1.445x10^{4}$	$5.160x10^{3}$	$6.373x10^{4}$	$-6.401x10^{4}$	$9.563x10^{1}$	$-2.174x10^{7}$
$2.194x10^{-3}$	$2.427x10^{5}$	$3.189x10^{2}$	$-5.264x10^{4}$	$1.442x10^{4}$	$8.338x10^{3}$	$6.292x10^{4}$	$-6.917x10^{4}$	$1.233x10^{2}$	$-3.730x10^{7}$
$2.294x10^{-3}$	$3.680x10^{5}$	$3.126x10^{2}$	$(-6.848x10^{4})$	$1.422x10^{4}$	$1.285x10^{4}$	$3.998x10^{4}$	$-5.397x10^{4}$	$1.536x10^{2}$	$-4.852x10^{7}$
$2.334x10^{-3}$	$4.079x10^{5}$	$3.099x10^{2}$	$-6.136x10^{4}$	$1.412x10^{4}$	$1.440x10^{4}$	$2.145x10^{4}$	$-3.781x10^{4}$	$1.611x10^{2}$	$-4.348x10^{7}$
$2.374x10^{-3}$	$(4.232x10^{5})$	$3.078x10^{2}$	$-4.367x10^{4}$	$1.404x10^{4}$	$1.512x10^{4}$	$-4.039x10^{2}$	$-1.694x10^{4}$	$1.626x10^{2}$	$-3.094x10^{7}$
$2.414x10^{-3}$	$4.059x10^{5}$	$3.065x10^{2}$	$-2.164x10^{4}$	$1.398x10^{4}$	$1.460x10^{4}$	$-2.121x10^{4}$	$4.801x10^{3}$	$1.571x10^{2}$	$-1.533x10^{7}$
$2.454x10^{-3}$	$3.610x10^{5}$	$3.060x10^{2}$	$-4.225x10^{3}$	$1.395x10^{4}$	$1.319x10^{4}$	$-3.668x10^{4}$	$2.283x10^{4}$	$1.462x10^{2}$	$-2.904x10^{6}$
$2.494x10^{-3}$	$3.033x10^{5}$	$3.060x10^{2}$	$4.791x10^{3}$	$1.394x10^{4}$	$1.117x10^{4}$	$-4.522x10^{4}$	$3.473x10^{4}$	$1.326x10^{2}$	$1.395x10^{6}$
$2.534x10^{-3}$	$2.469x10^{5}$	$3.063x10^{2}$	$7.414x10^{3}$	$1.393x10^{4}$	$9.130x10^{3}$	$-4.798x10^{4}$	$4.089x10^{4}$	$1.188x10^{2}$	$5.254x10^{6}$
$2.594x10^{-3}$	$1.787x10^{5}$	$3.067x10^{2}$	$6.342x10^{3}$	$1.390x10^{4}$	$6.643x10^{3}$	$-4.602x10^{4}$	$4.322x10^{4}$	$1.005x10^{2}$	$4.494x10^{6}$
$2.614x10^{-3}$	$1.609x10^{5}$	$3.068x10^{2}$	$5.629x10^{3}$	$1.389x10^{4}$	$5.992x10^{3}$	$-4.461x10^{4}$	$4.298x10^{4}$	$9.525x10^{1}$	$3.989x10^{6}$
$2.714x10^{-3}$	$1.005x10^{5}$	$3.073x10^{2}$	$2.700x10^{3}$	$1.377x10^{4}$	$3.752x10^{3}$	$-3.671x10^{4}$	$3.923x10^{4}$	$7.402x10^{1}$	$1.913x10^{6}$
$2.914x10^{-3}$	$5.124x10^{4}$	$3.075x10^{2}$	$5.827x10^{2}$	$1.335x10^{4}$	$1.917x10^{3}$	$-2.555x10^{4}$	$3.165x10^{4}$	$5.327x10^{1}$	$4.129x10^{5}$
$3.362x10^{-3}$	$2.310x10^{4}$	$3.076x10^{2}$	$-4.397x10^{1}$	$1.167x10^{4}$	$8.651x10^{2}$	$-1.527x10^{4}$	$2.252x10^{4}$	$3.557x10^{1}$	$-3.110x10^{4}$
$4.362x10^{-3}$	$1.179x10^{4}$	$3.075x10^{2}$	$-4.695x10^{1}$	$5.043x10^{3}$	$4.416x10^{2}$	$-6.278x10^{3}$	$8.150x10^{3}$	$2.529x10^{1}$	$-1.127x10^{4}$
$5.362x10^{-3}$	$9.747x10^{3}$	$3.075x10^{2}$	$4.437x10^{1}$	$-1.414x10^{2}$	$3.652x10^{2}$	$-1.212x10^{3}$	$-4.885x10^{3}$	$2.297x10^{1}$	$3.144x10^{4}$
$6.362x10^{-3}$	$8.127x10^{3}$	$3.076x10^{2}$	$2.392x10^{2}$	$-1.066x10^{4}$	$3.045x10^{2}$	$-4.575x10^{3}$	$-8.482x10^{3}$	$2.094x10^{1}$	$1.695x10^{5}$
$6.815x10^{-3}$	$2.425x10^{-1}$	$3.077x10^{2}$	$1.419x10^{-2}$	$-1.276x10^{4}$	$9.080x10^{-1}$	$-1.275x10^{4}$	$-1.942x10^{-1}$	$-8.977x10^{0}$	$1.006x10^{4}$

Table II

COMPULSATOR ENERGY BALANCE (JOULES)

ENAR 624-114

TIME	WO	WNAGL	WINT	$\int i^2 R_{arm} dt$ x(1)	$\int i^2 R_{comp} dt$ x(4)	$\int i^2 R_{bus} dt$ x(5)	$\int i^2 R_{lamp} dt$ x(6)	$\frac{1}{2} L_{off} i^2$ x(10)	EDAL
0	3.831×10^{7}	0	3.831×10^{7}	0	0	0	0	0	0
5.000×10^{-4}		6.974×10^{-2}	3.831×10^{7}	1.123×10^{0}	8.263×10^{-1}	1.796×10^{-1}	0	4.719×10^{2}	-4.173×10^{-7}
1.000×10^{-3}		2.106×10^{0}	3.830×10^{7}	5.680×10^{1}	4.179×10^{1}	9.084×10^{0}	0	1.008×10^{4}	-4.490×10^{-7}
1.494×10^{-3}		3.694×10^{1}	3.822×10^{7}	1.064×10^{3}	7.832×10^{2}	1.702×10^{2}	0	8.699×10^{4}	-4.210×10^{-7}
1.834×10^{-3}		3.090×10^{2}	3.792×10^{7}	8.153×10^{3}	5.998×10^{3}	1.303×10^{3}	4.452×10^{4}	3.205×10^{5}	-4.880×10^{-7}
1.934×10^{-3}		6.584×10^{2}	3.769×10^{7}	1.597×10^{4}	1.175×10^{4}	2.553×10^{3}	8.082×10^{4}	5.021×10^{5}	-1.490×10^{-7}
2.014×10^{-3}		1.280×10^{3}	3.740×10^{7}	2.867×10^{4}	2.108×10^{4}	4.579×10^{3}	1.302×10^{5}	7.170×10^{5}	-7.151×10^{-7}
2.094×10^{-3}		2.628×10^{3}	3.695×10^{7}	5.419×10^{4}	3.982×10^{4}	8.641×10^{3}	2.134×10^{5}	1.036×10^{6}	-4.917×10^{-7}
2.194×10^{-3}		6.773×10^{3}	3.602×10^{7}	1.294×10^{5}	9.490×10^{4}	2.055×10^{4}	4.098×10^{5}	1.626×10^{6}	-3.800×10^{-7}
2.294×10^{-3}		1.555×10^{4}	3.461×10^{7}	3.182×10^{5}	2.323×10^{5}	5.002×10^{4}	7.981×10^{5}	2.280×10^{6}	-9.239×10^{-7}
2.334×10^{-3}		1.913×10^{4}	3.403×10^{7}	4.420×10^{5}	3.217×10^{5}	6.903×10^{4}	1.021×10^{6}	2.402×10^{6}	-5.960×10^{-7}
2.374×10^{-3}		2.059×10^{4}	3.357×10^{7}	5.865×10^{5}	4.255×10^{5}	9.091×10^{4}	1.270×10^{6}	2.348×10^{6}	-5.215×10^{-7}
2.414×10^{-3}		1.894×10^{4}	3.328×10^{7}	7.326×10^{5}	5.297×10^{5}	1.127×10^{5}	1.517×10^{6}	2.114×10^{6}	-5.364×10^{-7}
2.454×10^{-3}		1.499×10^{4}	3.318×10^{7}	8.590×10^{5}	6.191×10^{5}	1.311×10^{5}	1.737×10^{6}	1.770×10^{6}	3.725×10^{-8}
2.494×10^{-3}		1.058×10^{4}	3.318×10^{7}	9.545×10^{5}	6.865×10^{5}	1.452×10^{5}	1.911×10^{6}	1.413×10^{6}	3.502×10^{-7}
2.534×10^{-3}		7.010×10^{3}	3.324×10^{7}	1.020×10^{6}	7.327×10^{5}	1.547×10^{5}	2.046×10^{6}	1.107×10^{6}	1.427×10^{-7}
2.594×10^{-3}		3.673×10^{3}	3.331×10^{7}	1.079×10^{6}	7.738×10^{5}	1.631×10^{5}	2.180×10^{6}	7.754×10^{5}	2.757×10^{-7}
2.614×10^{-3}		2.979×10^{3}	3.336×10^{7}	1.091×10^{6}	7.826×10^{5}	1.649×10^{5}	2.212×10^{6}	6.947×10^{5}	6.855×10^{-7}
2.714×10^{-3}		1.161×10^{3}	3.345×10^{7}	1.128×10^{6}	8.080×10^{5}	1.701×10^{5}	2.317×10^{6}	4.370×10^{5}	9.350×10^{-7}
2.914×10^{-3}		3.020×10^{2}	3.351×10^{7}	1.151×10^{6}	8.242×10^{5}	1.734×10^{5}	2.405×10^{6}	2.467×10^{5}	5.951×10^{-7}
3.362×10^{-3}		6.139×10^{1}	3.352×10^{7}	1.163×10^{6}	8.323×10^{5}	1.750×10^{5}	2.470×10^{6}	1.478×10^{5}	-2.617×10^{-7}
4.362×10^{-3}		1.598×10^{1}	3.351×10^{7}	1.168×10^{6}	8.363×10^{5}	1.758×10^{5}	2.516×10^{6}	1.057×10^{5}	-2.235×10^{-8}
5.362×10^{-3}		1.093×10^{1}	3.350×10^{7}	1.171×10^{6}	8.380×10^{5}	1.762×10^{5}	2.540×10^{6}	7.786×10^{4}	-8.661×10^{-8}
6.362×10^{-3}		7.596×10^{0}	3.351×10^{7}	1.173×10^{6}	8.395×10^{5}	1.764×10^{5}	2.561×10^{6}	2.484×10^{4}	1.676×10^{-7}
6.815×10^{-3}		7.770×10^{-16}	3.355×10^{7}	1.173×10^{6}	8.395×10^{5}	1.765×10^{5}	2.565×10^{6}	1.753×10^{-8}	1.567×10^{-7}

in the armature inductance. It is therefore essential to design the machine so that the inductive energy is not trapped by eddy currents in the rotor laminations and pole pieces.

A variety of cases have been studied to determine the sensitivity of system performance to changes in circuit parameters. The results of the case study are given in Table III. The values are given for two sets of resistance values. The first assumes fully penetrated conductors (stranded and transposed) and the values in parentheses for a higher resistance case (skin depth limited). The energy delivered to the flashlamps depends on armature resistance (depth of penetration and initial temperature of conductor), startup current (angular position and crowbar resistance), and alternator voltage (field flux and speed). The delivered energy for a given alternator is also very dependent on the lamp impedance parameter K_o. The point design alternator is optimized for a high impedance lamp (K_o ~ 272 or more).

The conclusion based on the sensitivity analysis is that the point design should deliver the necessary energy to the flashlamps provided that

1. $K_o \geq 225\ \Omega\ \text{amp}^{1/2}$
2. Initial conductor temperature $T_o \leq 20°C$
3. Open circuit voltage $V_{ac} \geq 14.7$ kV
4. Angular position $\theta_m(0)$ and speed N controlled within one percent
5. Crowbar resistance $\ll 0.15\ \Omega$

Table III

COMPULSATOR CIRCUIT ANALYSIS DATA - FULLY PENETRATED CASE (2.54 mm DEPTH OF PENETRATION)

RUN NUMBER	VARIABLE CHANGE	i_{max} (kA)	$t(i=i_{max})$ (msec)	E_{lamps} (MJ)	ΔT_{arm} °C
ENAR624-134 (136)	BASE CASE	423.2 (370.2)	2.374 (2.364)	2.565 (2.095)	32.95 (52.31)
139 (137)	T_0=40°C	414.0 (359.3)	2.374 (2.354)	2.483 (2.006)	33.93 (52.90)
140 (138)	T_0=60°C	405.1 (348.9)	2.374 (2.354)	2.405 (1.923)	34.78 (53.30)
142 (143)	SHORT CIRCUIT	622.4 (537.1)	2.394 (2.384)	0 (0)	80.99 (123.9)
148 (145)	k_0=178	460.3 (401.9)	2.374 (2.364)	2.317 (1.876)	39.58 (62.61)
149 (146)	k_0=250	404.1 (354.1)	2.374 (2.354)	2.655 (2.178)	29.88 (47.52)
150 (147)	k_0=272	387.9 (340.4)	2.364 (2.354)	2.714 (2.233)	27.40 (43.66)
155 (152)	CROWBAR R=0.15Ω	407.3 (356.9)	2.374 (2.364)	2.424 (1.988)	30.27 (48.15)
156 (153)	CROWBAR R=0.30Ω	393.1 (345.1)	2.374 (2.364)	2.301 (1.894)	27.99 (44.63)
157 (154)	CROWBAR R=0.75Ω	358.8 (316.4)	2.374 (2.364)	2.013 (1.672)	22.97 (31.38)
161 (159)	$\theta_m(0)=-\pi/4x0.95$	421.9 (369.1)	2.255 (2.245)	2.553 (2.086)	32.72 (51.96)
162 (160)	$\theta_m(0)=-\pi/4x1.05$	421.9 (369.1)	2.494 (2.484)	2.553 (2.086)	32.72 (51.96)
166 (164)	$\theta_m(0)=-\pi/4x0.99$	423.1 (370.2)	2.351 (2.341)	2.565 (2.095)	32.94 (52.30)
167 (165)	$\theta_m(0)=-\pi/4x1.01$	423.1 (370.2)	2.398 (2.388)	2.565 (2.094)	32.94 (52.29)
171 (169)	N=3140x0.99	424.7 (371.0)	2.399 (2.127)	2.610 (2.127)	33.64 (53.28)
172 (170)	N=3140x1.01	421.6 (369.4)	2.350 (2.340)	2.521 (2.063)	32.28 (51.36)
177 (174)	V_{ac}=15kvx0.98	413.4 (361.9)	2.374 (2.364)	2.472 (2.022)	31.30 (49.69)
178 (175)	x0.95	398.8 (349.3)	2.374 (2.364)	2.336 (1.914)	28.92 (45.93)
179 (176)	x0.90	374.4 (328.4)	2.374 (2.354)	2.116 (1.739)	25.21 (40.05)
182 (181)	139,177,166,172 (137,174,164,170)	403.1 (350.3)	2.326 (2.306)	2.353 (1.907)	31.59 (49.38)

WLB
UT-CEM
LLL
7/11/78

If the lamp impedance parameter differs significantly from the value given above, an alternator with a larger diameter rotor and fewer turns is recommended. The optimization technique is discussed in Section 4.2.

III. ELECTROMECHANICAL DESIGN OF THE COMPENSATED PULSED ALTERNATOR

3.1 Armature Windings

The armature circuit consists of two air gap windings connected in series opposing. The rotor winding is connected to the compensating (stator) winding and the alternator terminals via slip rings located at both ends of the shaft. The windings provide a variable armature inductance with angular position, with the minimum inductance occurring when the axes of the coils are aligned with the direct axes of the main field windings. The rotor and compensating winding conductors are wound in a continuous serpentine fashion as shown in Figure 15. The serpentine winding scheme was chosen to simplify the construction of the end turns by eliminating solder connections and current crossovers. Note that the end turns are supported by the rotor laminations and do not overhang the ends of the rotor. The end turns of the compensating winding are supported similarly.

Depending on the physical size of the alternator and the peak current, the conductors may or may not be set into slots. Any slots must be extremely shallow and the teeth need to be constructed of nonferromagnetic material or highly saturated ferromagnetic material to maintain a minimum inductance system. Irregardless, it will be necessary to rely on an adhesive bond to share the shear load, or to take the shear load entirely. The point design alternator windings are set into shallow slots. However, for a variety of reasons including material availability, fabrication and assembly techniques

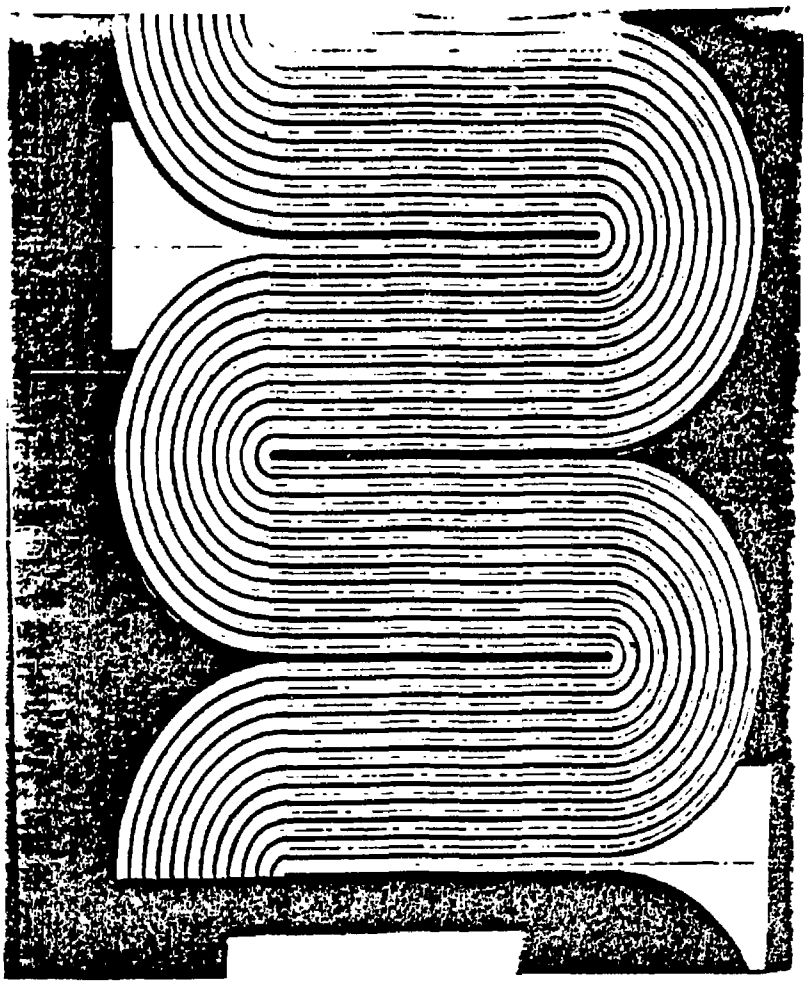

Figure 15: Serpentine Winding Design (Rotor and Compensating Conductors)

and the level of shear stress, the engineering prototype windings are not set in slots, and the full shear stress is taken by the adhesive bond.

Since the adhesive bond of the conductors to the rotor is crucial, it is necessary to load the bond in compression and shear and to avoid any tensile loading which can cause the bond to fail in a peel mode. Therefore, the periphery of the rotor is banded with a pre-tensioned glass or Kevlar fiber wrap, which is designed to maintain a compressive load on the bond at all speeds within the design speed range.

3.1.1 Conductor Design

In an air gap winding the rotor conductors are exposed to a high density (1.9 Tesla) relatively high frequency (120-180 Hz) magnetic field. Therefore, the rotor conductors must be constructed from an assembly of small diameter wires to reduce eddy current losses and to prevent a significant temperature rise in the conductors during the time that the main field windings are excited. The main field will be pulsed to reduce both core loss and eddy current loss, but it must remain at full strength for a time long enough to synchronize the speed and angular position of all alternators in the system. Based on the fundamental time constant of the field, it is anticipated that the field of the point design generator would be ramped to the peak level in 30 seconds, held constant for 60 to 120 seconds, and ramped down in 30 seconds. Since it is doubtful that any significant heat transfer will occur during the field pulse, an adiabatic heating process can be assumed to size the conductors. Using this assumption the temperature rise of the conductor is given by[1]

$$\Delta T = \frac{P_{ec} t}{mC_p} = \left(\frac{\pi \sigma \omega_e^2 B_o^2 d_w^4 \ell}{128 m C_p}\right) t \quad °C$$

where

σ	Electrical Conductivity (mho/m)
ω_e	Electrical angular frequency (sec^{-1})
B_o	Peak flux density (Tesla)
d_w	Wire diameter (m)
ℓ	Active wire length (m)
t	Elapsed time (sec)
m	Wire mass (kg)
C_p	Specific heat (joules/°C/kg)

Assuming that the field is energized for 60 seconds and the open circuit frequency is 180 Hz, the temperature rise of a #20 AWG copper wire is 96°C at a peak field level of 1.9 Tesla. Similarly a #30 AWG copper wire experiences a 9.4°C temperature rise. Therefore, #30 AWG basic wire size is recommended for the engineering prototype. If the frequency of the full scale machine is 120 Hz or less, a larger diameter wire can be substituted.

To prevent the buildup of circulating currents within a conductor, the assembly of small diameter insulated wires must be stranded and transposed so that each wire links the same flux. The stranded and transposed construction removes the limitation of depth of penetration of the discharge current into a solid conductor. Therefore, the winding resistance and inductance are more influenced by the physical dimension of geometrically scaled machines. The windings are formed of an array of type 8 Litz wire as manufactured by

New England Electric Wire Company. The type 8 Litz wire is a spiral flattened tube which is rolled into a rectangular cross section. The tube consists of multiple bundles of seven strand (six around one) insulated magnet wire. A sketch of one rotor conductor consisting of 13 type 8 Litz wires is shown in Figure 16.

Since the Litz wires are connected in paralled at the slip rings, it is important that each cut the same flux. Note that the serpentine winding forms a natural transposition: a wire that occupies the inside position of the main conductor width under the North poles, occupies the outside position under the South poles. Although this transposition is not perfect, it is anticipated that it will be adequate. Conceivably, each Litz wire could be terminated with its own slip ring and brush, providing a natural division for supplying multiple circuits from one alternator.

3.1.2 Turn-to-Turn Insulation

Each type 8 Litz wire is insulated with a linear wrap of glass filled epoxy tape 0.13 - 0.18 mm (5 - 7 mils) thick. If the voltages are uniformly distributed along the windings, the peak turn to turn voltage between adjacent conductors in the serpentine winding is given by

$$V_{T-T} = 4V_{Term}/N_c$$

Where V_{Term} is the peak terminal voltage and N_c is the number of rotor conductors. Depending on the peak voltage, it may be necessary to further insulate the conductors by wrapping the group of parallel Litz wires

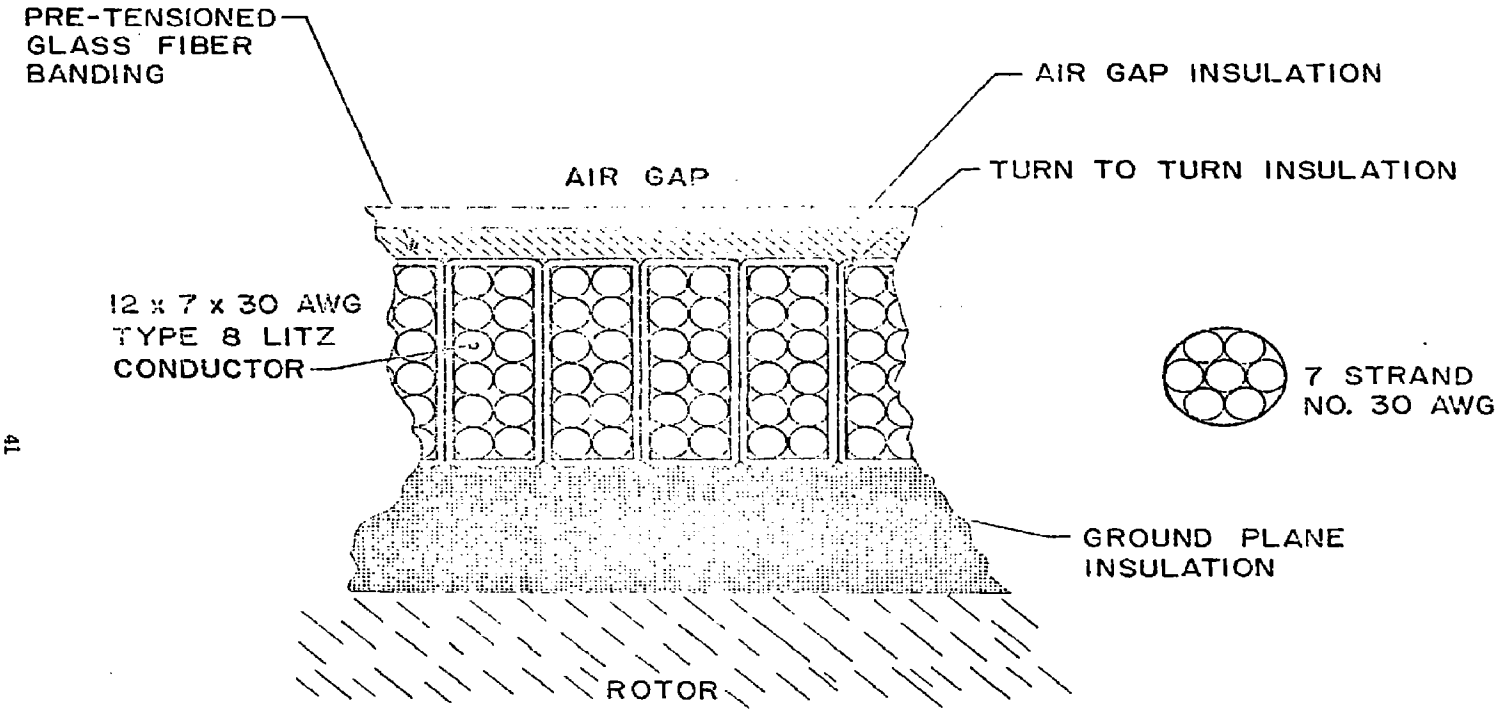

Figure 16: Rotor Conductor Detail

with a half lap wrap of glass/epoxy tape. To achieve long insulation life (20 years), the recommended maximum 60 Hz dielectric stress for glass/epoxy tape is 30 VPM RMS.[2] However, the stress can be increased if reduced life is acceptable. Dielectric stress-insulation life tests on the specific glass/epoxy system used are required.

3.1.3 Ground Plane Insulation

The rotor ground plane insulation serves two vital functions: one, to withstand the high voltages impressed on the windings, and second, to transfer the high forces (in shear) required to decelerate the rotor and shaft during discharge. Similarly, the stator ground plane insulation must transmit the reaction torque from the compensating winding to the poles and stainless steel pole supports. The ground plane insulation is a build of multiple half lap wraps of epoxy filled glass tape. The tape may be applied in a wet lay up with a VPI process to remove voids, or may be applied in B stage forms and cured under pressure. The thickness of the ground plane insulation is determined by the dielectric strength and required life of the glass/epoxy system. Other considerations are magnetic air gap mmf and interlaminar shear strength. Fortunately, the minimum inductance constraint does not influence the ground plane insulation design since the ground insulation is not located in the cylindrical gap between windings, as is the air gap insulation.

3.1.4 Rotor Bonding Wrap

The rotor windings will experience centrifugal forces due to the spin of the rotor. To keep the winding in contact with the rotor, a tensile load

is placed on the bond. The tensile stress is on the order of 1.7×10^6 N/m^2 (250 psi). Since the tensile strength of the bond is weak, especially if a crack is present, this situation cannot be permitted. Therefore, the periphery of the rotor is wrapped with pre-tensioned glass or Kevlar fiber banding tape. The required winding tensile stress on the Kevlar fibers is approximately $1.6 - 2.5 \times 10^8$ N/m^2 (25 ksi) after processing and curing. Glass-fiber banding of traction motor armatures is common practice and prestressed levels of 3×10^8 N/m^2 (45 ksi) after processing are typical.[3]

3.1.5 Air Gap Insulation

The radial separation of the rotor and stator winding is critical since the armature conductor spacing affects the magnitude of the minimum circuit inductance. Therefore, the thickness of the gap insulation must be minimized to obtain maximum performance. Since the gap insulation is not required to transmit large mechanical forces, it can be constructed of a mechanically weaker, higher dielectric strength material. The gap insulation should have superior arc and corona resistance. A long life system may consist of resin rich, mica tape. However, organic materials such as Kapton, a Du Pont polymide film, may prove satisfactory. The polymide materials have a substantially higher short time dielectric strength than mica paper.

Assuming that a corona suppression system is used so that the air gap does not carry the voltage stress, the stator gap insulation and the rotor gap insulation and banding must then take the dielectric stress. The thick-

ness and dielectric constant of the insulation must be chosen so that each layer of insulation shares the stress in the same fraction of its dielectric strength to avoid a successive series of breakdowns.

3.1.6 Corona Suppression

The mechanical clearance also must be minimized since it essentially determines the minimum inductance of the alternator for a given winding geometry. Mechanically, the winding clearance must be several times larger than the maximum displacement of the rotor caused by the worst case vibrational mode. The clearance must also be sufficiently large that assembly methods do not result in damage to the gap insulation. Finally, the gap must be sized so that windage losses are manageable.

For the dimensions assumed in the original point design, the voltage gradient across the gap exceeds the dielectric strength of air. As a result, the air will breakdown, transferring the electric stress to the gap insulation. This can be a severe problem if an electrical discharge burns a pin hole in the insulation, leaving a carbon track. Eventually, successive breakdown of layers would result in a power arc fault between the armature windings. There are multiple approaches to handling this problem:

1. Increase clearance of gap and reduce performance.
2. Run rotor in vacuum.

3. Run rotor in SF_6 or other atmosphere with higher dielectric strength.
4. Reduce voltage of machine by one half (one half turns). Drive twice as many single lamp circuits as double lamp circuits.
5. Incorporate a corona suppression system.
6. Trade increased mechanical clearance for reduced banding thickness.
7. Combination of above.

Obviously, each approach has advantages and disadvantages. One does not wish to derate the alternator performance by increasing the winding separation because of increased cost. Running the generator rotor in vacuum would require special seals and may be more difficult to cool without a gaseous heat transfer medium. Gases such as SF_6 may be incompatible with other materials and cause increased windage losses. Higher current generators would require multiple slip rings and additional brush gear as well as increasing the number of external switches and current sharing reactors.

The approach suggested at the July 14, 1978, design review held at Lawrence Livermore Laboratory was to develop a corona suppression system using semiconductive varnish or paint.

Semiconductive varnish is used to avoid discharges at the surface of the stator conductor insulation in conventional high voltage (up to 30 kV) rotating machines. The anti-discharge paint is applied to

eliminate superficial discharges at the slot exits and in the interstices between the main insulation of the conductor assembly, and the walls of the slots.[4]

In the compulsator, however, the armature conductors will be bonded to the rotor or stator with the glass/epoxy adhesive insulation system. It is not desirable to coat the surface of the conductor/ground plane interface because doing so will reduce the mechanical integrity of the bond. What has been suggested is to coat the gap insulation surfaces with a higher conductivity varnish which allows the flow of currents to average the dielectric stress placed on the gap, and thereby reduce the peak voltage stress seen by the gap. The specific resistivity of the varnish must be chosen so that the surface power density is below the threshold at which graphite powder in the varnish begins to carbonize. Thienpont and Sie[5] have observed that this threshold is approximately 0.3 W/cm^2 of steady state operation.

As a first pass consider the engineering prototype. At the 3600 rpm rated speed the peak voltage under load is 4.3 kV. The mechanical clearance is approximately 0.16 cm. Therefore, the peak voltage gradient is on the order of 27 kV/cm. At 50 percent overspeed (5400 rpm) this stress is increased to 45 kV/cm. Therefore, if the stress can be reduced by a factor of two, it may be possible to run in air with a pulsed field and low duty cycle. If corona does occur, the semiconducting paint will carry the stress over the surface of the part so that corona damage will be reduced. If the specific power density exceeds 0.3 W/cm^2, a powdered metal, or metal coated glass fiber, may be more applicable than a finely divided carbon compounding material.

3.1.7 Armature Winding Forces

There are three major forces which act on the armature windings during discharge. These forces are classified as follows:

1. Centrifugal forces due to rotor spin.
2. Normal electromechanical energy conversion (J x B forces).
3. Armature self field forces
   a. Radial magnetic pressure in air gap ($B^2/2\mu_o$)
   b. Variable reluctance torque ($1/2\ i^2 dL/d\theta$)
   c. End turn forces

Compared to the magnetic forces, the centrifugal forces on the conductors are inconsequential, provided that the banding fibers are pretensioned such that coil movement is eliminated and the rotor is properly balanced. Therefore, only the latter types of forces will be discussed here.

Magnetic pressure loads the armature windings and insulation radially in compression during the main current pulse. The magnetic pressure is approximated by

$$P = B^2/2\mu_o = \mu_o H^2/2 = \mu_o K^2/2 \qquad N/m^2$$

where K is the effective surface current density of the armature windings.

$$K = N_p N_{cp} I_a / (2\pi r) \quad A/m$$

where N_p is the number of poles, N_{cp} is the number of conductors per pole, I_a is the armature current and r is the rotor radius.

The magnetic pressure is of the order of 42 MPa (6 ksi) under normal operation, but may approach 90 MPa (13 ksi) under short circuit conditions. If the conductors are evenly distributed around the rotor periphery, the magnetic pressure is a factor only on the conductors and insulation, since the forces are balanced. However, if the conductors are not evenly distributed, but are lumped into four belts as shown in Figure 17, significant side loads will be placed on the rotor and bearings. The magnetic force on the current belt with the missing conductor will be 8 to 16 percent less than the forces acting on the other belts, and the rotor will be forced toward the weakest pole. Magnetic damping will reduce the magnitude of this force, but lateral rotor displacement must be anticipated. The problem with evenly distributing the windings is that the minimum center to center spacing and conductor width is determined by the minimum bend radius of the conductors. To achieve the equivalent cross-sectional area of a lumped conductor design, the width of the Litz bundles must be increased, resulting in a larger effective air gap and in a higher inductance winding.

The J x B force of the armature current crossed with the applied magnetic field results in a torque which must be transmitted across the insulating bond. The inertia of the rotor and shaft is approximately 95 percent of the total inertia so that essentially all of the torque must be transmitted. The average shear stress on the bond is given by

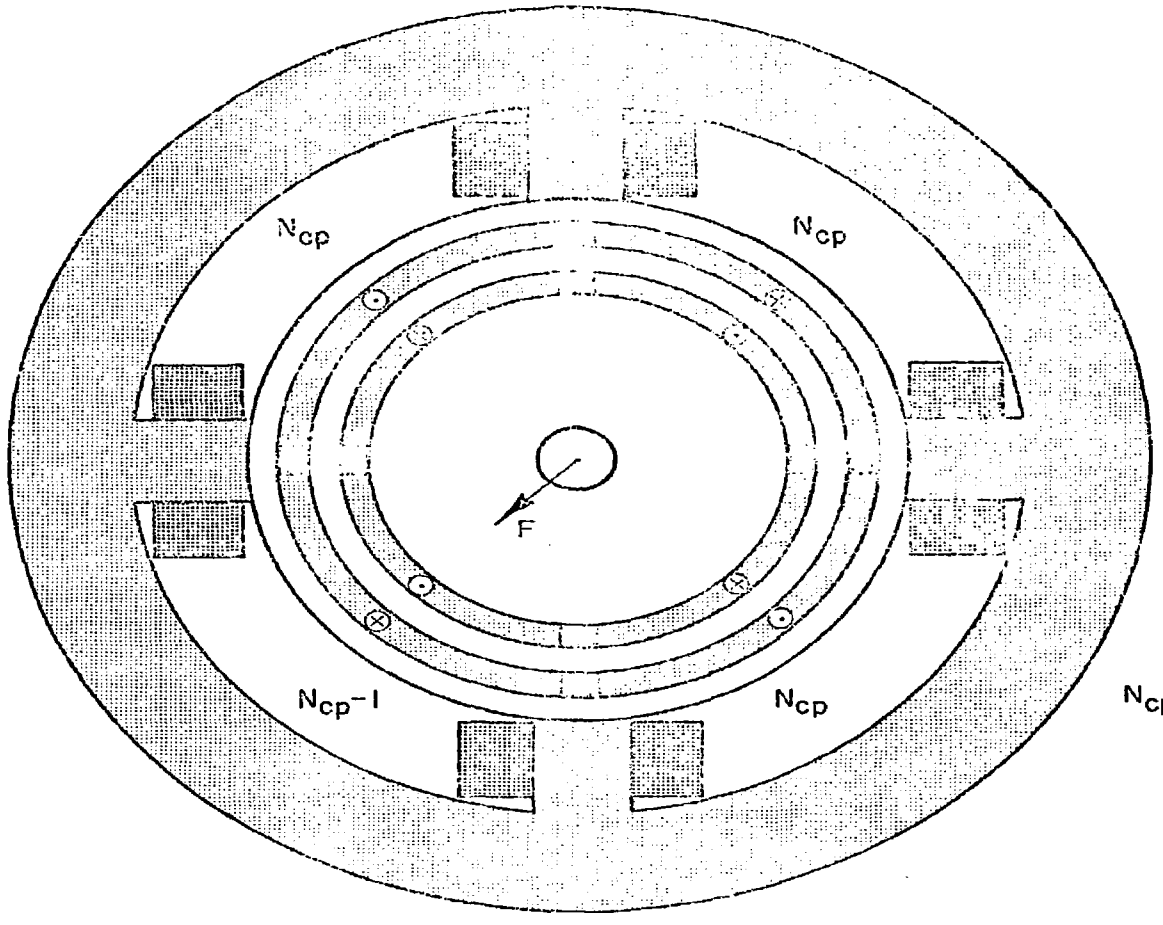

N_{cp} – Nominal Numbe of Conductors per Pole

$$\tau = 2V_{ac} I_a / (\pi \omega_m D^2 L)$$

Where V_{ac} is the peak ac voltages, I_a is the armature current, ω_m is the rotor angular velocity, D is the rotor diameter, and L is the rotor effective length. For the point design the average shear stress due to the J x B force is about 10 MPa (1520 psi) under normal load.

The usual alternator electromechanical energy conversion action, however, accounts for only a third or so of the peak mechanical torque. The mechanical work required to overcome the change in inductance and increase in stored magnetic energy is substantial. For example, for the point design, the peak discharge torque results in an average shear stress of 29 MPa (4370 psi). Under fault conditions the average shear stress may be as high as 50 MPa (7280 psi). It should be noted that the point design was optimized for a lamp system with a higher impedance constant than is now expected to be used for NOVA. A better design is the four pole 1.02 meter rotor diameter machine (Case A) described in Section 4.2. This machine has fewer turns than the point design alternator, but approximately the same ampere turn product. The peak mechanical torque is increased by approximately forty percent due to an increased mechanical clearance and higher alternator J x B forces. The average shear stress is reduced to 20 MPa (2900 psi), however, because of the increased diameter and active length of the rotor.

The shear stress placed on the bond is approximately equal to the average shear stress if the windings are distributed as shown in

Figure 17. If the windings are placed in slots as done in the point design and shown in Figure 17A, the shear stress on the bond is reduced because some of the load is transferred to the steel teeth. The stress on the bond in the point design is reduced approximately 30 percent in the toothed rotor configuration, based on finite element calculations of the stress distribution. However, slots are not necessarily desirable because the available area for conductors is reduced. The factor is important since the required Litz construction further reduces the fraction of the periphery covered by copper.

One encouraging factor is the positive effect of a combined compressive and shear loading on the ultimate shear strength of the insulation and bond. The ground plane insulation is loaded in compression by magnetic pressure at the time of maximum shear stress. This time is slightly before the time of peak current. For the point design the peak torque occurs when the current is approximately 87 percent of the peak value. Therefore, the compressive load at that time is 76 percent of maximum or 32 MPa (4.6 ksi). The shear strength of typical epoxy/glass insulation proposed for this application (Hexcel F159 system) improves significantly under combined compressive and shear loading. Grumman and Princeton have conducted tests of various epoxy/glass systems for the development of large toroidal field coils for tokamak experiments.[6]

Based on the improved machine design (Case A), the expected shear stress on the adhesive bond is approximately 20 MPa (2900 psi) under normal conditions. The magnetic pressure which loads the insulation in

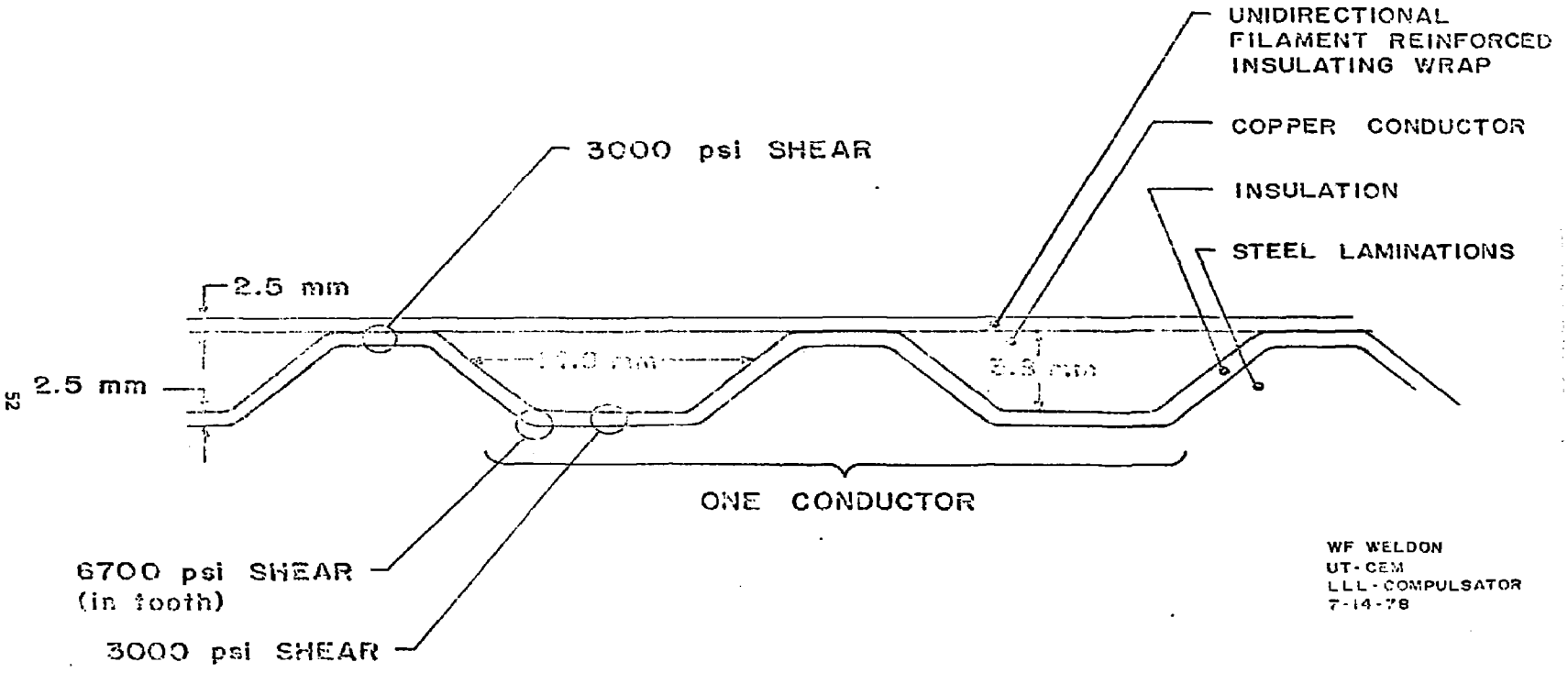

Figure 17A: Slotted Rotor Winding Distribution

compression will improve the shear strength of the insulation. The maximum shear stress under fault loading will approximately double both the shear stress and the compressive stress on the insulation system. The shear stress under fault approaches the 48 MPa (7000 psi) ultimate shear strength of the Hexcel 159 system at 82°C as determined by the Grumman/Princeton tests under combined loading. Considering all of the construction and performance advantages of the smooth rotor air gap winding scheme, the adhesive insulation design appears to be the proper approach. However, extensive testing and development of the proper winding techniques will be required to obtain a design with mechanical integrity.

Due to its own field, a conductor bent in a circular arc to form an end turn will try to straighten. This force is highest on the inner most conductors of the armature windings adjacent to the coil axes. The end turns also experience axial forces, since a portion of the end turns are within the active length of the rotor. In fact, the relative axial position of the pole and end turns represents a compromise between generated voltage and axial forces on the conductors, which are taken in additional tension of the shaft. The axial forces on each end turn of the point design is approximately 4.6×10^5 N, which add a tensile stress of 126 MPa (18.2 ksi) on the shaft.

Finally, the terminal conductors of the rotor and compensating winding cause another asymmetry in the radial magnetic pressure distribution. The forces on the ends of the rotor are not colinear, and the net effect is to skew the rotor and bearing axes. To reduce the magnitude of these

forces, the terminal conductors are flared to reduce the average surface current density. The force is inversely proportional to the width of the conductor. For the point design, the force is approximately ten percent of the force due to the unevenly distributed rotor winding.

References

[1]James L. Kirtley, Jr., "Design and Construction of an Armature for an Alternator with Superconducting Field Winding," Doctoral Dissertation, Massachusetts Institute of Technology, August, 1971.

[2]Hugo Lauroesch, General Electric Company, personal communication.

[3]E. C. Appleby, "Glass-Fiber Banding of Traction-Motor Armatures," Paper Number 58-A-173, The American Society of Mechanical Engineers, Annual Meeting, New York, N. Y., November 30 - December 5, 1958.

[4]J. Thienpont and T. H. Sie, "Suppression of Surface Discharges in the Stator Windings of High Voltage Machines."

[5]Ibid.

[6]C. Burke, "Development of High-Mechanical Strength Electrical Insulations for Tokamak Toroidal Field Coils," Prodeedings Seventh Symposium on Engineering Problems, Knoxville, Tennessee, October, 1977, p. 1513. (Also See: C. Burke - Grumman Aerospace Corporation, Coil Integrity Insulation Mechanical Screening Interim Test Report, RDAC 11.B.4-2, Report No. EP-D-016, December 13, 1977.)

3.2 Stator Reaction Torque Frame

Point design features include provision for a stator reaction torque frame consisting of a stainless steel support ring (slotted, like the rotor), the pole pieces, and the backiron. The complete frame functions in such a manner that it has sifficient strength to withstand the discharge torque of the return conductor when the compulsator is discharged.

Manufacturing the stainless steel support ring as shown in Figures 30, 31, and 32 of Section 4.2 accomplishes the following:

The thin segments, which are positioned under the pole faces, minimize the magnetic air gap.

Thick segments of the ring are positioned between the poles, where they serve the dual roles of (1) transmitting discharge torque from the support ring to the pole pieces and (2) acting as a pressure vessel which prevents the existing magnetic pressure from pushing the return conductor away from the rotor conductors.

Welding the "ears" of the ring to the sides of the pole pieces produces a continuous hoop of material which is at least the thickness of the "ear." As a result, hoop strength is not limited by the thinner segments under the pole faces. Magnetic pressure causes the support ring to push against the pole pieces, which are in turn pushed against the thick and heavy backiron. The combined strength of this support ring-pole piece-backiron frame is sufficient to withstand the magnetic pressure that is present. Hence, the stator ring does not need to be self sustaining as a pressure vessel, but sufficiently thick to avoid distortion from the discharge torque.

3.3 Rotor and Shaft

Significant dimensions of the shaft and rotor are:

Shaft - 0.254 m (10 in.) diameter
3.19 m (125.6 in.) length
Rotor - 0.76 m (30.0 in.) outside diameter
2.41 m (94.9 in.) length

Two of the basic considerations included in design of the shaft and rotor involve eddy current losses and shaft stiffness.

Eddy currents must be kept to a minimum, in order that machine efficiency will not be degraded to an unacceptable level. To accomplish this objective, machine design includes provisions for shrink-fitting

individually-insulated ferromagnetic steel laminations to a 304 stainless steel shaft. With the laminations thus insulated from each other, eddy current losses will be reduced to an acceptable level. Use of 304 stainless steel in the shaft will preclude piping of magnetic flux into undesired areas.

Shaft stiffness must be sufficient to withstand possible severe vibrations at critical frequencies, a problem which is accentuated when the magnetic field is energized. A relatively large four-per-revolution forcing function may exist due to any runout on the rotor and the resulting attraction of the runout to the poles as the rotor rotates. Since the stiffness of the shaft alone is not sufficient to keep the first critical frequency above operating speed, machine design includes provisions for clamping the rotor laminations together by means of two large Belleville springs which are loaded with a nut on the shaft. The resulting configuration allows the load to be applied at the outer edge of the laminations where it is needed.

Experimental data[1] indicates a minimum required pressure of 0.414 MPa (60 psi). This is based on the fact that a substantial reduction in the length of a core is observed up to 0.276 - .414 MPa (40-60 psi) and a much smaller reduction with increasing pressure beyond this point. However, further considerations require a much higher loading. As long as the laminations remain in compression, the assembly is considerably stiffer than if the laminations experience a tensile load due to bending and come apart. This is very similar to a preloaded bolt. Therefore, by assuming the load applied by the Belleville springs is uniformly

distributed at the midsection of the rotor, the required applied load to maintain compression in the laminations for a given dynamic loading can be calculated. For example, if the dynamic loading is equal to the weight of the rotor, the required spring force is 2.80×10^5 N (63,000 lbs.). The effective flexural stiffness of the assembly is more difficult to estimate, since the physical properties are anisotropic and unknown. However, if a packing factor of 95% is assumed (with epoxy filling the remaining 5%), and with the steel having a modulus of elasticity 30 times that of the epoxy, the effective axial stiffness is reduced to approximately 60 percent of that of solid steel, or 1.51×10^{10} N/m (86×10^6 lb./in.).

Reference

[1]Walker, Rogers, Jackson, "Pressing and Clamping Laminated Cores," Proceedings of IEEE, Volume III, No. 3, March 1964, pp. 565-576.

3.4 Bearings

Three types of bearings have been considered for the prototype COMPULSATOR:

a) hydrostatic,

b) rolling element, and

c) tilting pad hydrodynamic.

For reasons which are discussed below, the tilting pad hydrodynamic bearings have been chosen for the final design.

Of the three types, the hydrostatic bearings are unquestionably the most complex and expensive - but they are also the most versatile, offering minimum friction at all speeds, excellent stiffness independent of speed, the highest degree of damping of the three types, and (after design, fabrication and installation) a far greater range of "tuneability" than either of the other types. Although they do require high pressure oil supply systems, such systems are well within the state of the art, and the Center for Electromechanics has experience in their design and operation from two machines presently in use in the laboratory. If the construction of the engineering prototype were done without thought to later production machines, it is probable that the hydrostatic bearing would be selected. However, considerations of cost, fabrication requirements, and back-up oil supplies (in case of pump failure) for a large quantity of bearings have led to the choice of a different type of bearing.

The second type of bearing considered was the rolling element bearing. Rolling elements are lower in basic unit cost than either of the other two options, but that advantage is offset by more precise installation requirements and by the requirement for regular spectrographic oil analysis and/or signature analysis procedures necessary to predict possible bearing failure. Although the rolling element bearing is less demanding in lubrication requirements, the fact that they still require a supply and scavenge system does little to simplify the lubrication system. Other concerns in using rolling element bearings include the following: They offer no damping; they would be required to run at a DN number (bearing diameter x RPM) in the upper range of accepted practice; and they offer little protection against unexpected overloads which permanently damage such bearings.

The third bearing option considered (and the one finally chosen) was the hydrodynamic tilting pad bearing. These bearings are production items operating well within their rated loads and speeds, and they are available from many manufacturers. One such manufacturer, Waukesha Bearing Corporation, has been contacted and a specific design identified. Waukesha has not experienced any problems with pad instabilities on any bearings they have built, but it is known that such instabilities (if experienced) could be corrected in unidirectional bearings by trimming the pads so that they are slightly asymmetrical. Other advantages of this type of bearing include the following: They are self-aligning in both the axial and circumferential directions, hence requiring less stringent and less costly manufacturing techniques; they have damping and squeeze film protection against overloads; and whirl instabilities are uncommon.

Our major concern in using a tilting pad bearing is the transition of the critical speed from super- to sub-critical when the magnetic field is energized. Such a transition is due to the change in the load the bearing experiences and the fact that the load capacity (hence the stiffness) of the bearing is highly nonlinear with eccentricity ratio. Therefore, when the bearing is essentially unloaded (except for small dynamic loads), it will operate supercritically; as the magnetic field is energized, however, the rotor is pulled to one side and the bearings become loaded, causing the bearings to pass through their critical frequency into the subcritical regime. The vibrations generated could possibly affect the alignment of the laser amplifiers; however, this potential problem can be avoided by partially energizing one field coil at startup, thus loading the bearing and allowing subcritical operation at all times.

Three main issues were considered in our selection of the bearing option:

a) tradeoff between stiffness and damping offered by the various types;

b) degree of confidence in the analytical technique available for predicting the performance of the bearings; and

c) liklihood, manner, and consequences of a bearing failure with rotors storing tens of magajoules of energy. (This latter was the primary factor in our decision.)

Based on these issues, tilting pad hydrodynamic bearings are considered to offer the best compromise for a production machine. (It should also be noted that all rotating electrical machines of any substantial power rating use hydrodynamic bearings.)

The radial bearings that we have selected run on a 25.4 cm (10 in.) shaft, with an average oil temperature of 57°C (135°F), a viscosity of 150 SSS at 38°C (100°F), and a diametral clearance of 0.38 mm (0.015 in.). At the operating speed of 3600 RPM each bearing has a load capacity of 48,900 N (11,000 lbs.) and a loss of 18.6 kW. A resistance temperature detector embedded in the babbit of one land monitors the bearing temperature.

One advantage of the Waukesha design is that the pad is mounted on a hardened steel button which allows for considerable axial misalignment. This could prove to be a significant advantage, due to the unknown direction of the loads which the rotor will experience when the field is energized. The design also allows for the clearance to be adjusted by placing shims beneath the button.

The thrust bearing we have selected is a double-sided (capable of taking loads in both directions), retained pad, 30.5 cm (12 in.) diameter, tilting pad thrust bearing. At the operating speed of 3600 RPM the bearing has a maximum load capacity of 133,500 N (30,000 lbs.) and a loss of 29.8 kW (40 hp). A load cell and a resistance temperature detector placed on the loaded side will monitor bearing loads and temperatures. If desired, an oil film can be provided under the pads at startup by incorporation of a hydrostatic lift (or by other means that are available).

As previously mentioned, the rotor will be pulsed toward one of the poles when the magnetic field is energized. An equivalent negative magnetic spring constant was calculated and found to be about 1.75×10^{8} N/m (1.0×10^{6} lb./in.). The rotor attains a force equilibrium when the force exerted by the bearing equals that of the magnetic field. Based on the bearing operating data furnished by Waukesha, the rotor should reach equilibrium at an eccentricity ratio of about 0.71 in the bearing (see Figure 18), which is a quite acceptable minimum film thickness of 7.37×10^{-2} mm (0.0029 in.). This additional load capacity of the bearing is needed as a safety factor against any uncalculable forces which may exist during the discharge. The same is true for the thrust bearing: Normal loading is the weight of the rotor, 9320 kG (20,500 lbs.), and the additional load capacity is needed for additional forces which can be generated during the discharge.

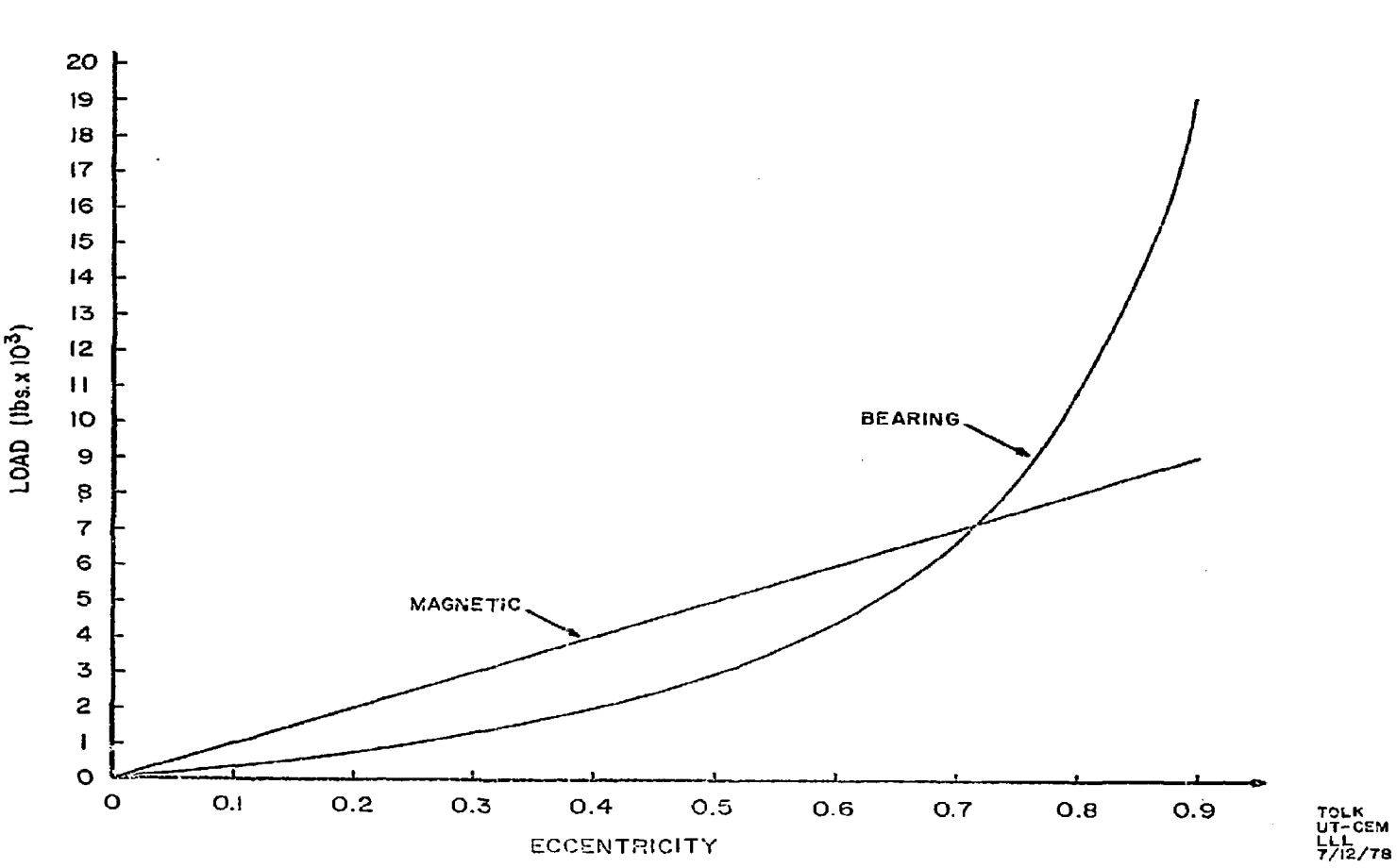

Figure 12: Bearing Forces

3.5 Applied Magnetic Field

3.5.1 Magnetic Circuit Topology

The magnetic circuit of the compensated pulsed alternator is shown in Figure 19. The field conductors are wound around salient poles which are bolted to the stator back iron, which is constructed of hot rolled steel plate or cast steel. The rotor is constructed as an assembly of several thousand 29 guage (0.356 mm) M-19 nonoriented electrical sheet steel laminations which are clamped together at high pressure 6.9 MPa (1000 psi) and press fit onto a 304 stainless steel shaft. The configuration most closely resembles that of a compensated direct current motor or generator without interpoles. The armature current is collected by a slip ring at each end of the rotor rather than a single commutator, however. This topology has been pursued for a variety of reasons:

1. The armature circuit consists of both a rotor winding and a series compensating winding on the stator. Since armature current must be carried by slip rings irregardless of the location of the field winding, there is no incentive to put the field windings on the rotor because of current collection.

2. The field windings are designed for a much higher duty cycle than the armature windings; hence, they are of heavier section. The centrifugal forces on field windings would therefore be much larger in magnitude than the centrifugal forces on the

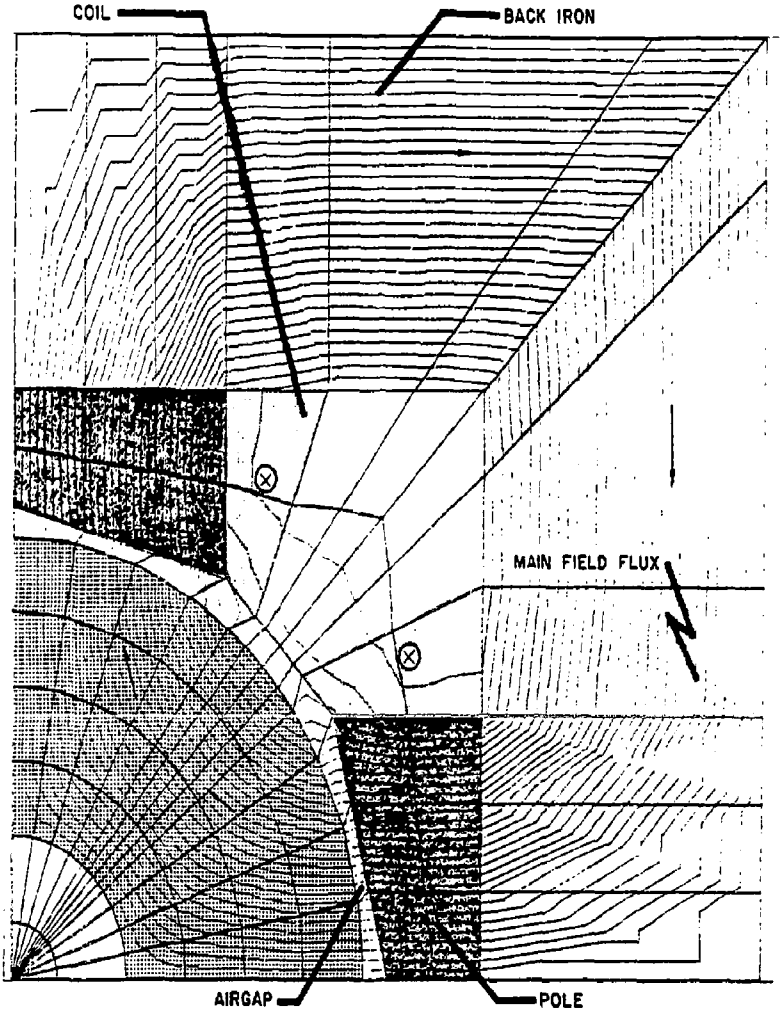

Figure 19: Main Field Magnetic Circuit

armature conductors. A deep slotted rotor configuration would be required which could force a reduction in maximum air gap flux density and possibly, rotor tip speed.

3. The volume of rotor iron is less than the volume of stator iron. Therefore, magnetic core losses are reduced.

The primary disadvantage of the topology is that the laminated rotor is less stiff mechanically and has a lower natural frequency than a solid rotor.

One tradeoff that has not yet been addressed quantitatively is the design of the stator (salient poles or non-salient poles). However, it is felt that the average air gap magnetic flux density of the salient pole design is greater than that of the non-salient case for the same magnetomotive force. Other considerations include mechanical assembly problems and the ability to transfer large mechanical forces when the compensating coil and field windings are located in close proximity.

3.5.2 Air Gap Flux Distribution

Neglecting the effects of armature reactions and eddy currents, the steady state solution for the air gap magnetic flux distribution can be obtained using a finite element method computer code. Due to the presence of highly saturated iron in both the rotor and poles, it is important to consider the non-linear characteristics of both the rotor lamination material and stator material. A typical air gap magnetic

flux distribution for a four pole compensated pulsed alternator with a smooth rotor periphery and smooth pole faces is plotted in Figure 20. The pole faces are assumed to be bored concentric to the rotor diameter. No additional machining of the pole faces to modify the flux distribution is anticipated. Note that the flux distribution is neither a perfect sinusoid nor an ideal square wave.

It is useful to represent the air gap flux density as an infinite series of sinusoids for the purposes of calculating the open circuit voltage and estimating core loss. Then, the air gap flux density is given by

$$B_{gap}(\theta_m) = \sum_{n=1}^{\infty} B_n \cos(nN_p\theta_m/2)$$

where θ_m is the mechanical angle in radians, N_p is the number of poles, and B_n is the magnitude of the flux density of the nth space harmonic. The maximum flux density B_{max} is given by

$$B_{max} = B_{gap}(\theta_m=0) = \sum_{n=1}^{\infty} B_n$$

The relative values of B_n to the maximum flux density B_{max} are listed in Table IV.

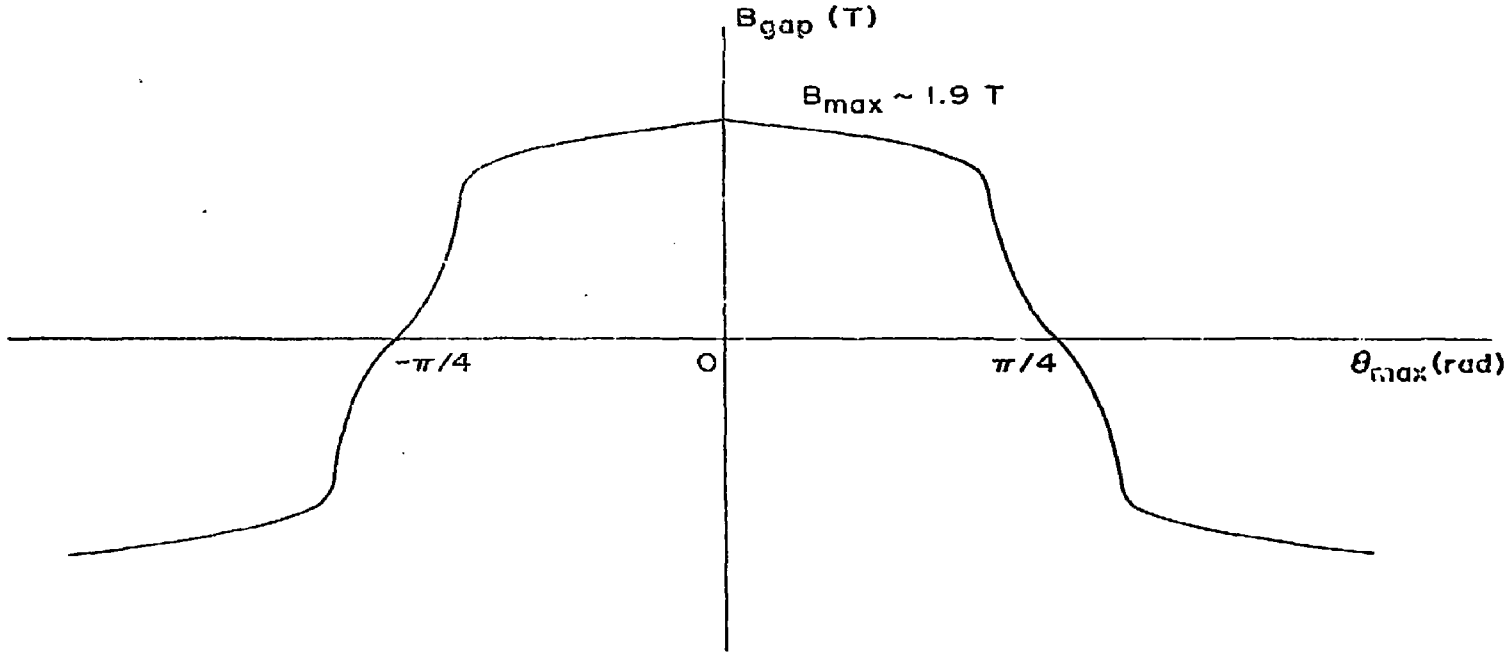

Figure 20: Air Gap Magnetic Flux Distribution

TABLE IV: APPLIED FIELD HARMONIC CONTENT

n	$\alpha_n = B_n/B_{max}$
1	1.146
3	-0.210
5	0.058
7	0.014
9	-0.029
11	0.033
13	-0.021
15	0.010
17	-0.001

3.5.3 Open Circuit Voltage Waveform

The open circuit voltage waveform can be calculated using the air gap flux density data from the previous section and the spatial distribution of the rotor winding. As an example consider the rotor conductor distribution shown in Figure 21. The open circuit voltage generated is given by

$$V_{oc}(\theta_m) = N_p B_{max} l_{eff} v \sum_{n=1}^{\infty} \sum_{k=0}^{(N_{cp}-1)/2} \alpha_n \cos[nN_p(\theta_m \pm k\Delta\theta)/2]$$

N_{cp} odd

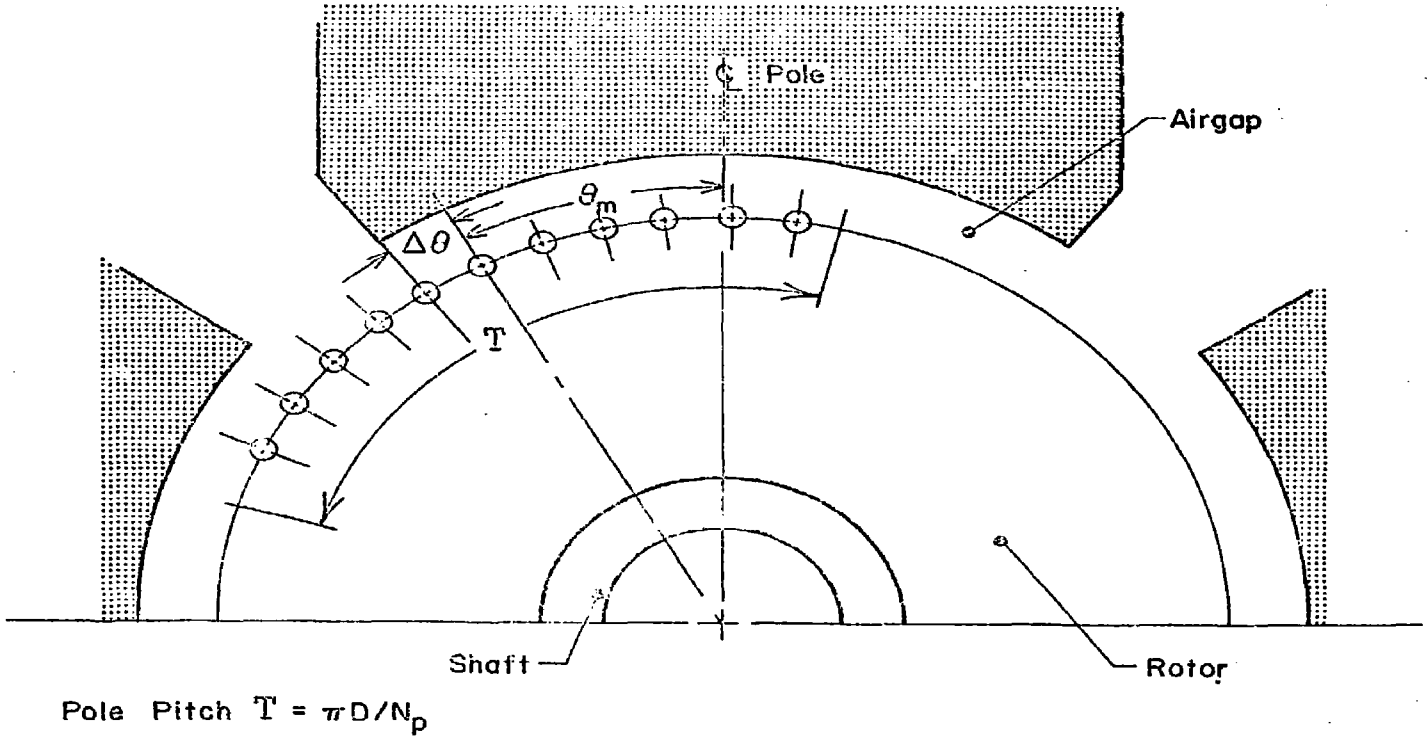

Figure 21: Rotor Winding Layout (Per Pole) for [illegible] le Voltage Calculation

where l_{eff} is the active length of the rotor winding, N_p is the number of poles, N_{cp} is the number of conductors per pole, θ_m is the mechanical angle of the center of the belt of conductors, $\Delta\theta$ is the angular centerline spacing of the conductors, v is the rotor tip speed, and α_n is the relative amplitude of the nth harmonic.

For a four pole machine with equally distributed conductors over the pole pitch, the previous equation is reduced to

$$V_{oc}(\theta_m) = N_p B_{max} l_{eff} v \sum_{n=1}^{\infty} f_n \alpha_n \cos(2n\theta_m)$$

where f_n is an averaging factor given by

$$f_n = [1 + \sum_{k=1}^{(N_{cp}-1)/2} 2 \cos(2k_n \Delta\theta)]/N_{cp}$$

Values of f_n are listed in Table V for the case where N_{cp} is equal to eleven.

TABLE V: AVERAGING FACTOR f_n FOR N_{cp}=11

n	f_n
1	0.64
3	-0.22
5	0.31
7	0.01

For the values given in Tables IV and V the peak open circuit voltage of the pulsed alternator is

$$(V_{oc})_{peak} = V_{oc}(\theta_m = 0) = N_p N_{cp} B_{avg} l_{eff} v$$

where $B_{avg} = (\sum_{n=1}^{\infty} \alpha_n f_n) B_{max} \sim 0.79\ B_{max}$

3.5.4 Magnetomotive Force Calculation

To achieve the maximum performance per unit mass of material, the peak air gap flux density is chosen to be 1.9 Tesla, which is 25 to 90 percent larger in magnitude than the operating flux density of conventional machinery. With the pulsed duty anticipated for NOVA, it is possible to run the field at higher excitation and core loss levels than is done under steady state conditions.

The dimensions of the rotor and poles are constrained so that the nominal flux density in those materials is less than 1.9 Tesla. The back iron is sized more conservatively at 1.6 Tesla. The pole width and back iron thickness are adjusted to account for additional flux due to leakage. Depending on the level of excitation, the leakage flux may represent twenty to thirty percent of the total flux per pole.

Each field winding supplies the magnetomotive force to drive the flux per pole across the magnetic air gap and to provide the mmf drops in the rotor laminations, the poles, and the back iron. Although a

flux plot is used to verify the final value, a good estimate of the ampere turns required per pole can be made by a hand calculation:

$$N_f I_f \sim \frac{1.9}{\mu_o}\left[g + \frac{h_p}{\mu_{rp}} + \frac{l_r}{\mu_{rr}}\right] + \frac{1.6\ell_s}{\mu_o \mu_{rs}}$$

where g is the magnetic air gap, h_p is the radial pole height, l_r and ℓ_s are the effective path lengths of the rotor and stator flux, μ_o is the permeability of free space, and μ_{rp}, μ_{rr}, and μ_{rs} are the relative permeabilities of the pole, rotor, and stator material. The magnetomotive force per pole required for the point design pulsed alternator is 8.1×10^4 amp-turns.

3.5.5 Field Coil Construction

The field windings are constructed of water cooled copper conductors which are wound in a double pancake fashion. Cooling passages are arranged in parallel, and electrical connections are made in series. The conductors are wound in a saddle shape around the main poles and the stainless steel torque ring. The number of turns of the pancake coils is chosen to achieve an overall coil shape which minimizes the height of the pole and, hence, the volume of the stator iron for a specified cross-sectional area.

The field coils of the point design are sized for steady state operation with a 25°C coolant temperature rise. The average current density over the gross coil area is about 5.5×10^6 A/m^2. This design is conservative, perhaps too much so when the pulsed duty of the coil

is considered. The gross current density of the field coils of the engineering prototype is 5.5×10^6 A/m^2 based on a 40°C steady state temperature rise of the coolant. The higher value is used for the scaling studies included in this report. The peak current density in the copper is 11.6×10^6 A/m^2, a specific power of 260 Watts/kg. This compares to 22 Watts/kg for conductors cooled by natural convection and radiation and 33 Watts/kg for systems cooled by forced convection (air).[1]

The hollow copper conductors are insulated with epoxy filled fiberglass tape. The tape thickness is determined by heat transfer considerations rather than dielectric stress.

3.5.6 Field Time Constant

The poles and back iron of the stator are not laminated in the present designs of the pulsed alternator. Therefore, the response time of the main field is determined by the fundamental decay time of eddy currents in the solid steel pieces. The time constant is a function of the resistivity, relative permeability, and dimensions of the stator iron, and the effective length of the air gap. Using the method given by Rüdenberg[2] the fundamental time constant of the full scale point design pulsed alternator is approximately eight seconds. This time constant is the sum of the time constant of the step response of the iron and the ordinary time constant of the field coil proper.

References

[1]Anaconda Co., "Publication C-25," Eleventh Edition, Anaconda American Brass Company, Waterbury, Connecticut, 1971, P. 41.

[2]Rüdenberg, Transient Performance of Electric Power Systems, MIT Press, Cambridge, Massachusetts, May 1970, pp. 106-116.

3.6 Brushes

The machine configuration includes two 0.5 m (19.7 in.) slip rings, one at each end of the rotor, which have a rotational speed of 3140 rpm. Each set of brushes is required to operate at a surface velocity of 82 m/sec and to carry a total peak current of 423 kA.

3.6.1 Surface Velocity

The slip ring surface velocity of 82 m/sec should pose no problems. Brush manufacturers advertise several grades of brushes capable of continuous operation at that velocity. The mechanical duty for the alternator is even less demanding in this respect since the brushes will be lifted off the slip ring between pulses.

Considerations which have resulted in the decision to lift the brushes between pulses include the following:

a) The motoring system will be required to supply torque to overcome brush drag only during the actual pulse.

b) Brush debris accumulation is reduced; hence, brush life is increased.

c) Heating from brush drag is reduced.

3.6.2 Current Collection

The set of brushes for each of the two slip rings will be required to carry a peak current of 423 kA. Depending on the total number of brushes that will be included in the final design, each individual brush will be required to carry 5-10 kA. This appears to be within existing pulsed brush technology.[1]

Brushes have been tested successfully at 5 kA per brush at these and higher speeds for longer pulses than will be experienced with this machine,[2] and experience at the Center for Electromechanics has shown that pulse length is important in determining current-carrying capacity: The shorter the pulse, the higher the current capacity. The 5 MJ homopolar generator in the CEM laboratory has been operated at currents as high as 15 kiloamps per brush on the shaft slip ring and 5.2 kiloamps per brush on the rotor, with a discharge time of 0.7 sec under a staged fault from half speed.[3] The generator is routinely run at 2.9 kiloamps/brush on the rotor and 6.5 kiloamps/brush on the shaft slip rings during resistance welding experiments.

3.6.3 Heating

There are two sources of heat at a brush interface:

a) Coulomb heating, which is generated mechanically by the sliding interface, and

b) Joule heating, which is generated electrically by the interface voltage drop.

Mechanical power (Coulomb heating), P_m, and electrical power (Joule heating), P_e, generated at the interface can be calculated respectively as

$$P_m = \int \mu N V_s \, dt$$

$$P_e = \int I^2 R \, dt$$

where

μ = coefficient of friction

N = normal force on brush

V_s = surface velocity

dt = differential time element while brush is in contact with rotor

I = current

R = effective interface resistance

dt = differential time element while current flows

If the brush material and slip ring material remain unchanged and N is kept within a small range of values for a set of tests, it is reasonable to assume that μ and R will remain essentially constant. P_m and P_e can be represented as

$$P_m' = V_s \Delta T$$

$$P_e' = \int I^2 \, dt$$

where ΔT is the amount of time the brush is in contact with the rotor and P_e' is integrated from the beginning to the end of the current pulse.

Figure 22 shows a plot of P_m' vs P_e' for data gathered at the Center for Electromechanics for Morganite CM1S (sintered copper-graphite) brushes operated on a steel slip ring. Using the following conservative estimates, a compulsator brush data point has been generated and plotted on that figure which shows that the point of operation of the compulsator brushes is well within the limits of the experimental data:

$\Delta T = 0.75$ sec

$V_s = 94$ m/sec

$I = 10$ kA

$\int dt = 0.0005$ sec (step function)

The surface phenomena at the brush-slip ring interface is far more complex than implied by this analysis. However, this analysis does allow a comparison between the duty of the pulsed alternator brushes and existing experimental data.

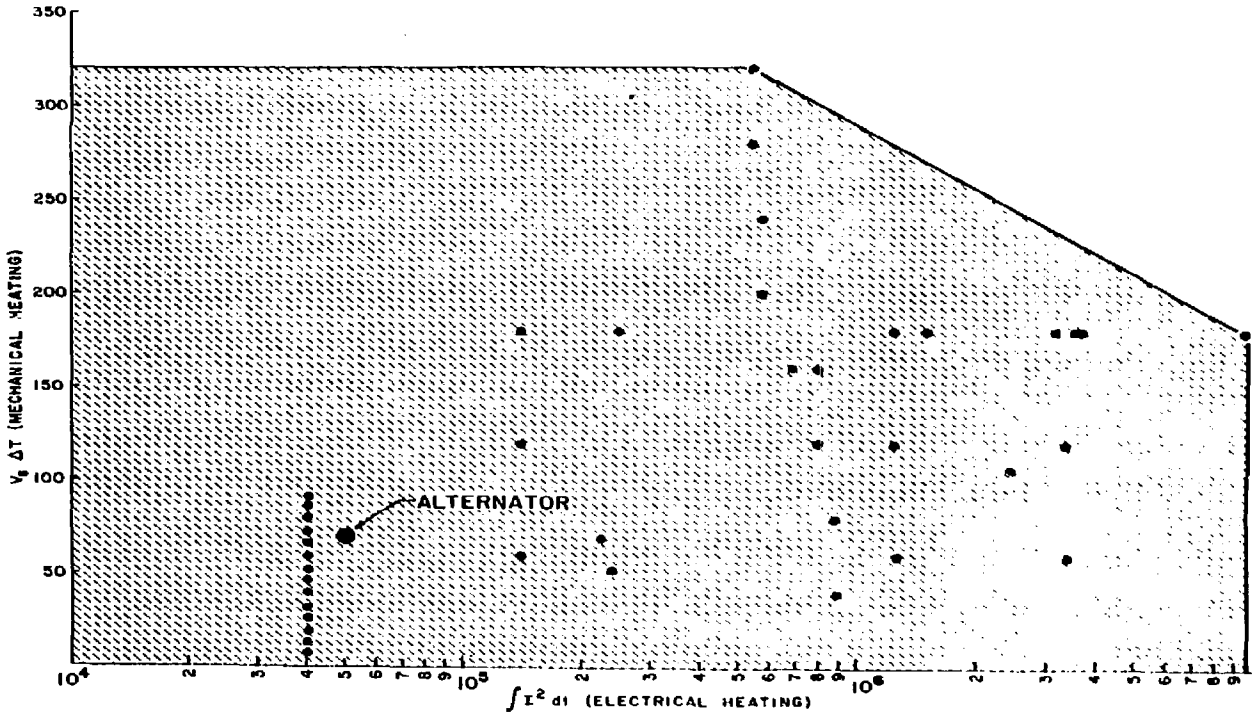

Figure 22: Brush Heating

References

[1] I. R. McNab, "Pulsed High Power Brush Research," Proceedings of the 23rd Holm Conference on Electrical Contacts, November, 1977.

[2] M. Brennan, et al., "Test Data On Electrical Contacts at High Surface Velocities and High Current Densities for Homopolar Generators," Proceedings of the Seventh Symposium on Engineering Problems of Fusion Research, October, 1977.

[3] R. C. Swanson, Editor, "Progress Report Number 1, Homopolar Motor-Generator Research for Inertial Energy Storage," Internal Report, June, 1975.

3.7 Pulsed Alternator Loss Analysis

The primary pulsed alternator losses must be considered to determine the pulsed rating of the machine itself and to specify the rating of the prime mover and auxiliary cooling system. The major alternator losses include:

1. Core loss
2. Stray eddy current loss
3. Armature copper loss
4. Bearing and seal friction
5. Windage
6. Brush friction and contact drop
7. Field copper loss

3.7.1 Core Loss

The core loss is the sum of the hysteresis loss and eddy current loss in the rotor laminations proper plus the interlaminar eddy current loss. The core loss is difficult to calculate precisely and is often determined by experiment. However, it is possible to make a conservative estimate by assuming a purely alternating magnetic field and extrapolating manufacturers' core loss data.

The rotor laminations are subjected to both alternating and rotating magnetic fields. The magnetic field at the outer radius is primarily rotational since the flux density is essentially constant in magnitude,

but varies in direction from tangential to radial as the material passes beneath a field pole. At the inner radius the flux density in the laminations is alternating, as the direction remains tangential and the magnitude is variable. The magnetic field at intermediate radii consists of both alternating and rotating components. The core losses for the two conditions differ in magnitude as illustrated in Figure 23.[1] At high flux densities the alternating field core loss is greater, and since alternating field test data is available, it is used to estimate the loss.

The alternating core loss P_c at 1.9 Tesla, 120 Hz is extrapolated using the equation[2]

$$P_c = K_h B^{1.6} f + K_e B^2 f^2 \text{ Watts/kg} \quad (1)$$

where the constants K_h and K_e are determined from published hysteresis and eddy current data for 29 gauge M-19 nonoriented electrical steel sheet at 1.5 Tesla, 60 Hz. As shown in Section 3.5 the air gap magnetic field is not sinusoidal, and the presence of higher harmonics will increase the core loss. The estimated core loss for the full scale point design alternator is 21.4 Watts/kg of which 20 percent is attributable to the third harmonic.

The laminations are coated with C-3 or C-5 core plate to increase the interlaminar resistance and to reduce interlaminar eddy current losses. The estimated interlaminar loss is 0.7 Watts/kg or three percent of the main core loss. Therefore, the total is about 22 Watts/kg (10 Watts/lb.).

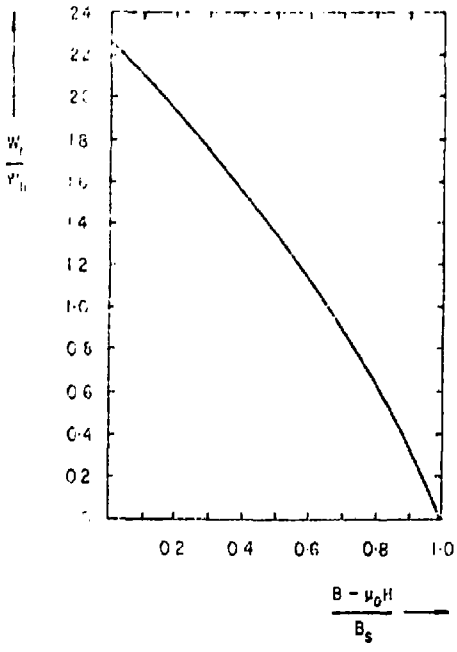

Figure 23: Ratio of Rotational to Alternating Hysteresis Loss for Various Materials

Since the core loss results in a large drag on the motoring system and consequent temperature rise of the laminations, the field is pulsed to full strength after the machine has been accelerated to full speed. The core loss for the 7,400 kg rotor at 3600 rpm is 165 kW (220 hp). However, this is a conservative number used to size the motoring system for the prototype. It is proposed to measure the actual core loss on initial testing and to size the prime mover for the full system accordingly.

3.7.2 Stray Eddy Current Loss

Alternating magnetic fields will also induce eddy currents in the shaft, rotor clamping washers and other conductive materials on the rotor. The shaft eddy current loss is approximately 5.4 kW and the washer eddy current losses total 5.8 kW at full speed. If the rotor periphery is slotted, high frequency eddy currents will also be generated in the pole faces due to the ripple in the air gap flux distribution caused by the presence of ferromagnetic teeth. The pulsation and pole entry losses caused by the teeth are reduced, however, if the slots are shallow so that the magnetic air gap of the main field is large compared to the slot depth.

3.7.3 Armature Copper Loss

The armature winding copper losses are generated by the main transport current, eddy currents caused by rotating in the main field

air gap, and circulating currents due to imperfect transposition of the stranded cables.

The basic stranded wire diameter is sized so that the temperature rise of the conductor due to eddy current heating is about ten percent of the temperature rise due to the discharge current pulse.

The resistance of the Litz conductors per se is essentially equal to the dc resistance because losses due to skin and proximity effects in the copper itself are minor. However, eddy currents are induced in the rotor laminations, stainless steel ring, and other conductive material which is linked by the armature flux. These transformer coupled resistances will tend to dampen the output current pulse.

The i^2R loss in the rotor and compensating winding conductors is slightly less than the energy delivered to the flashlamps. Since the radial dimension of the windings is reduced to minimize system inductance, the armature conductors are smaller in cross section than in conventional machinery and therefore have a relatively small heat capacity. Therefore, the temperature rise per pulse in the copper is significant, being 32°C for normal conditions and as high as 80°C under fault conditions. It is suggested that fault protection devices be provided in the external circuitry which are capable of clearing the fault at the first or second naturally occuring current zero to limit the peak conductor temperature rise.

It is not practical to predict the circulating current loss caused by imperfect transposition of the stranded conductors. These losses will be determined during the test program of the prototype generator. It is not anticipated that these losses will be unmanageable.

3.7.4 Bearing and Seal Friction

The thrust and journal bearings recommended for the pulsed alternator are hydrodynamic tilting pad bearings. The viscous drag for a given bearing geometry depends on the lubricant viscosity and film thickness (load) and rotational speed. These losses are published by the manufacturers. Typical loss curves for journal bearings and thrust bearings are shown in Figures 24 and 25.[3] The full speed bearing losses for the point design alternator total 67 kW (89 hp).

Only one seal is required in the vertical shaft configuration with the hydrodynamic bearings. It is proposed that the seal at the bottom of the upper journal bearing be a stovepipe type seal as opposed to a rubbing seal such as the split ring carbon type. The rotational seal drag is negligible compared to the bearing drag.

3.7.5 Windage

The mechanical clearance between the rotor and stator is reduced to minimize armature circuit inductance. With such a small gap it may not be feasible to cool the alternator by circulating gas axially down the annular gap. The windage loss increases rapidly with axial

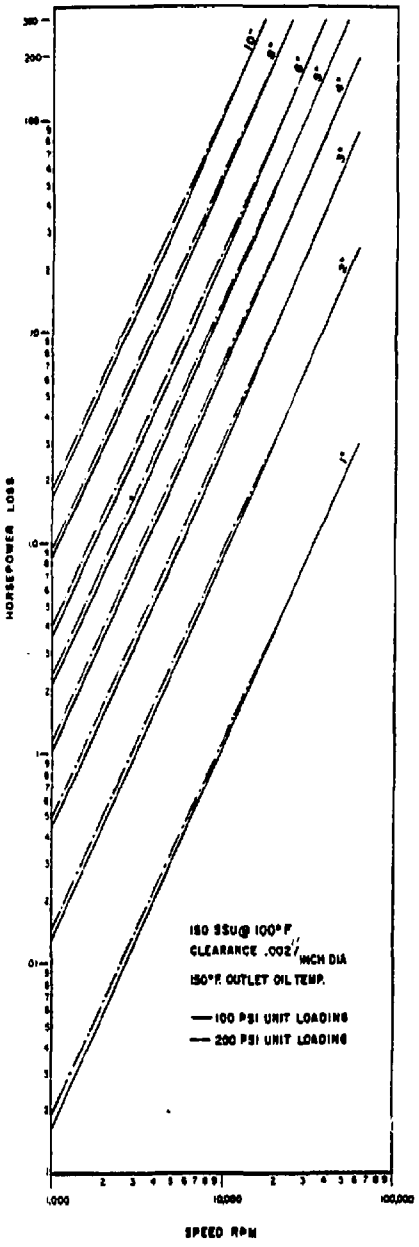

Figure 24: Typical Journal Bearing Loss Curve

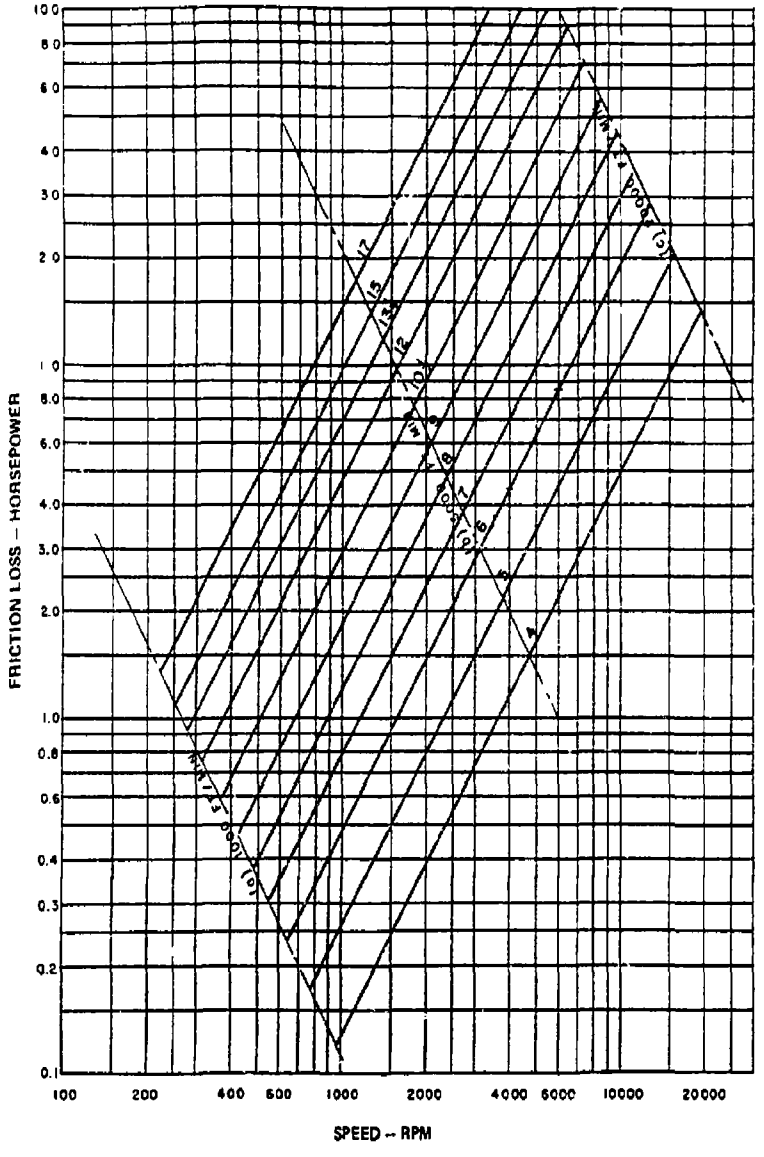

Figure 25: Typical Thrust Bearing Loss Curve

flow. It is assumed that the gas in the annular gap will not be circulated to reject rotor losses, but will only be used as a heat transfer medium to reject the losses to the liquid cooled stator. The windage loss for zero axial flow P_w is given by[4]

$$P_w = M\omega_m = C_f' \pi r^4 L \gamma \omega_m^3 \quad \text{Watts} \tag{2}$$

Where C_f' is an empirical loss coefficient and the other variables are defined as follows:

Windage drag torque	M	(N-m)
Rotor radius	r	(m)
Rotor length	L	(m)
Gas Density	γ	(kg/m^3)
Angular velocity	ω_m	(Sec^{-1})

The calculated windage loss for the full scale prototype alternator is 19.2 kW (26 hp) at 3600 rpm.

3.7.6 Brush Losses

The armature current is collected at each end of the rotor by a set of sintered copper graphite brushes. The brushes are run on copper slip rings which are mounted on the steel nuts which clamp the rotor laminations. If it is assumed that the brushes are loaded against the slip ring with a normal force of 0.01 N/amp[5] and that the coefficient

of friction is 0.2, the calculated brush drag is 160 kW (214 hp) at 3600 rpm. Since the brush drag is significant compared to the motoring power and because it is desirable to limit the peak temperature rise of the brush, the brushes will be lifted except for a brief interval each cycle. The pneumatically operated brushes will be lowered 100-200 msec prior to each pulse and lifted 200-500 msec after the current has been interrupted.

The peak electrical loss due to contact resistance is estimated to be 420 kW based on a one volt double contact voltage drop for copper graphite against copper. From a heating standpoint, however, the electrical loss is small compared to the mechanical loss because of the narrow current pulse width.

3.7.7 Field Copper Loss

The calculated peak field copper loss for the full scale prototype alternator is 60 kW per pole based on an average coil current density of 3.8×10^6 A/m^2. If the average current density is increased to 5.5×10^6 A/m^2 to reduce iron and copper cost, the peak power is increased to 90 kW per pole. The optimum design current density depends on the relative cost of materials, the cost of the field power supply, and the cooling system.

3.7.8 Alternator Loss Summary

The peak and average pulsed alternator losses are summarized in Table VI. The average values are based on one pulse per 15 minutes.

It is assumed that the field is energized for one minute and that the brushes are loaded against the slip rings for one second per pulse. The other mechanical losses are assumed to be continuous, and the generator is designed to run continuously at full speed if unexcited. However, the generator may be brought to rest between pulses in normal operation. If so, the average mechanical losses will be reduced.

Table VI: Pulsed Alternator Loss Analysis

Parameter	Peak Loss (kW)	Average Loss (kW)
Core Loss	163	11
Stray Eddy Current Loss	11	0.8
Armature Eddy Current Loss	3	0.2
Bearing Drag	67	67
Windage	19	19
Brush Friction	160	0.2
Total Rotational Losses	423	98
Armature i^2R	6×10^6	2.2
Field i^2R	240	16

References

[1]Carl Heck, Magnetic Materials and Their Applications, (New York: Crane, Russak and Company, 1974), p. 55.

[2]Pender, Del Mar, Electrical Engineers' Handbook, Electric Power, 4th edition, John Wiley, Sons, Inc., New York, 1949, pp. 3-21, 22.

[3]Catalog W-2A, Tilting Pad Journal Bearings, p. 16; and catalog W-3A, Tilting Pad Thrust Bearings, p. 23; Waukesha Bearings Corporation, Waukesha, Wisconsin.

[4]General Electric Company, Heat Transfer and Fluid Flow Data Books, General Electric Company, Schnectady, N.Y., Section G408.5, July 1969, pp. 1-3.

[5]I. R. McNab, "Pulsed High Power Brush Research," Proceedings of the Holm Conference on Electrical Contacts, Illinois Institute of Technology, Chicago, Illinois, November 1-3, 1977.

3.8 Motoring System

The prime mover is designed to accelerate the alternator rotor from rest to full speed in a period of several minutes. The prime mover must supply the torque to overcome the rotor inertia and rotational losses of the alternator. To minimize the required torque, the alternator field is either de-excited or weakly excited during spin up. Once the alternator rotor is at full speed, the accelerating torque can be applied to offset the increased core loss and armature eddy current loss when the field coils are fully excited.

Since more than one alternator will be required for NOVA, it will be necessary to synchronize the speed and angular position of each rotor to a master reference to insure that the multiple flashlamp circuits are driven simultaneously. Because the magnetic core loss will vary from unit to unit and the fundamental time constant of the main field flux is ten(s) of seconds, the rotors must be synchronized at full field. The brush friction loss is comparable in magnitude to the magnetic core loss. However, the brushes are seated against the slip ring only 100 to 200 msec prior to triggering the discharge circuit. The inertia of the rotor is sufficient to maintain rotor speed within a fraction of a percent during the time that the brushes are activated.

The rotor experiences a rapid deceleration during the discharge pulse. The peak discharge torque acting on the full scale prototype is 4.9×10^7 N-m for the normal discharge and 8.3×10^7 N-m under short circuit. The shaft coupling must be designed to transmit the torque required to decelerate the inertia of the prime mover or must be protected by a torque limiting mechanism in the drive train. If the effective inertia of the prime mover is one percent of the total system inertia, and the torque is not limited, the peak power that must be transmitted by the coupling is 180 MW.

3.8.1 Prime Mover Power Requirement

The torque required of the prime mover is equal to the accelerating torque plus the sum of the rotational losses.

$$T_{app}(\omega_m) = I\dot{\omega}_m + \Sigma T_{loss}(\omega_m) \text{ N-m}$$

The loss torque is plotted as a function of angular velocity in Figure 26 for three cases: field de-excited, fully excited, and fully excited with brush drag. The full speed loss torque for the three cases are 230 N-m, 700 N-m, and 1120 N-m, respectively.

The horsepower rating of the prime mover depends on its torque speed characteristic and the motoring duty cycle. As an example, consider a 300 hp variable speed dc motor drive designed for constant torque operation. The motor has a base speed of approximately 1800 rpm. Therefore, a 2:1 speed increaser is required. The motor drive will deliver 590 N-m at the alternator shaft continuously and is capable of providing 150 percent torque (890 N-m) at the alternator shaft for one minute. The motor will accelerate the load to full speed against bearing and windage losses in approximately ten minutes and will hold the speed against the losses for the time that the field is pulsed. The rotor will decelerate slightly during the brief interval that the brushes are actuated prior to discharge.

3.8.2 Prime Mover Candidates

The motoring system used to drive the full scale prototype pulsed alternator should have the following characteristics:

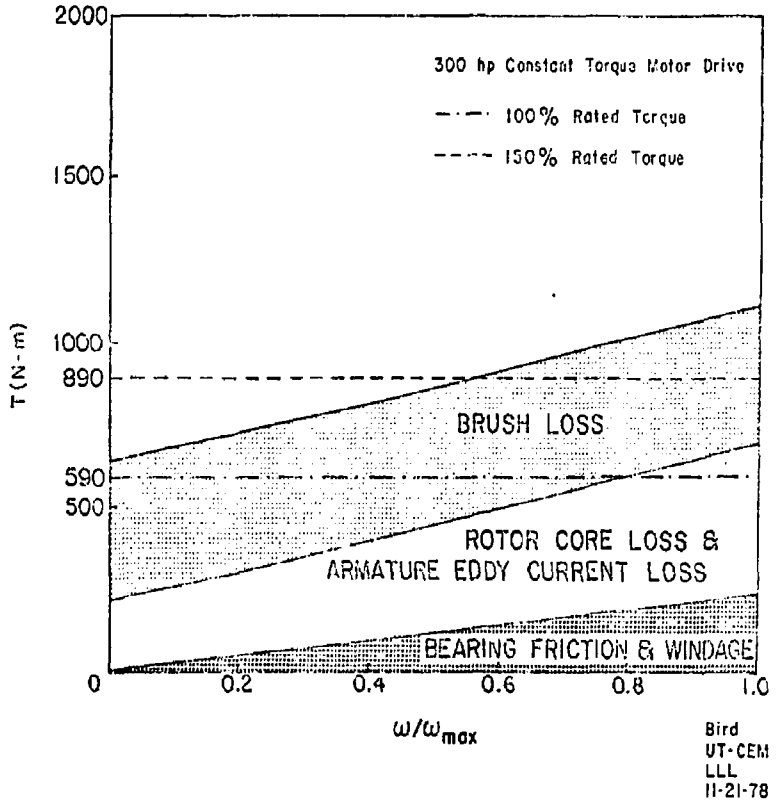

Figure 26: Loss Torque as a Function of Angular Velocity

1. Rated power $\geq$ 225 kW (300 Hp)
2. Rated speed 3600 rpm (no speed increaser)

   1800 rpm (2:1 speed increaser)
3. Momentary overload $\geq$ 150% for one minute
4. High starting torque and thermal capacity to accelerated high inertia load (I = 780 joule-sec^2)
5. Ability to withstand shock loading
6. Speed control $\pm$ 1%
7. Position control $\pm$ 0.5%

The angular position and speed control requirements are reasons to consider a synchronous motor drive. However, the high starting torque and thermal capacity requirements pose difficult problems for a conventional synchronous drive with a cage type damper winding. The problems can be overcome if the cage winding is replaced with a wound rotor winding and slip rings. An external resistor could then be inserted in the wound rotor circuit to increase starting torque and absorb the i^2R loss associated with accelerating an inertial load. The synchronous motor must develop a high pull in torque at small slip and must have a pull out torque larger than the combined loss torque of the fully excited compulsator. The number of poles of the alternator must be a multiple of the number of poles of the synchronous motor to insure that the angular position of the alternator rotors are properly synchronized. The position of the rotor can be further adjusted by trimming the field voltage of the synchronous motor.

A second approach is to use a variable speed motor drive. A dc system is proposed rather than an ac system because of cost. Although the dc motor is more expensive than the ac induction motor, the cost of the controlled rectifier dc motor drive is much less than the cost of a variable frequency ac inverter drive. Since the base speed of dc motors in the 300 horsepower range is 1750 rpm or less, it is necessary to use a timing belt or gear drive to increase the speed. Care must be taken, however, to protect the motor drive from shock loading during the alternator discharge. The speed and angular position of the rotor are controlled by a digital shaft encoder/tachometer feedback signal which is used to regulate the armature and field currents of the dc motor.

Another scheme is to use a steam turbine as a prime mover.[1] This approach may be best for a continuous duty system. An anticipated problem for pulsed duty is the requirement to vent high pressure steam between pulses. One suggested control scheme is to couple a small synchronous machine to each shaft.[2] The armature windings of the synchronous machines are connected to the same bus, and the power to each machine is monitored. If the net power is positive the synchronous machine is running as a motor and the torque of the main prime mover must be increased. If the net power is negative, the synchronous machine is running as a generator and the torque of the prime mover must be decreased.

It will be necessary to gain operating experience with the full scale prototype alternator and complete an extensive study of the motoring system alternatives before selecting the prime mover for NOVA. From

a system standpoint, there is some incentive to better match the speed of the pulsed alternator to the speed of the available prime movers in the 300-1000 horsepower range. One example presented in the scaling study results is a 6 pole, 1800 rpm pulsed alternator designed to drive lower impedance lamps. This machine has a wider current pulse and has the highest ratio of delivered energy to stored energy. Although the 6 pole design may pose a problem for a synchronous motor drive, the reduced speed would allow a direct coupled dc motor drive.

References

[1]Bruce Carder, Lawrence Livermore Laboratory, personal communication.

[2]W. C. Duesterhoeft, The University of Texas at Austin, personal communication.

3.9 Point Design Parameters

The parameters of the compensated pulsed alternator point design are listed in Table VII. The alternator is designed to deliver 2.4 MJ to a system of 96 parallel circuits consisting of two 1.5 cm x 112 cm xenon flashlamps connected in series.

End view and side view cross-sections of the prototype pulsed alternator are shown in Figure 27 and Figure 28. An end view of the compulsator bearing support is shown in Figure 29. The prototype

Table VII

COMPENSATED PULSED ALTERNATOR

PROTOTYPE DESIGN PARAMETERS

July 11, 1978

Number of Poles	4.0×10^{0}	Nominal Number Rotor Conductors/Pole	1.20×10^{1}
Discharge Speed (rpm)	3.14×10^{3}	Conductor Cross Section-Rotor (m^2)	9.61×10^{-5}
Open Circuit Voltage (volts)	1.50×10^{4}	Active Length of Conductor (m)	1.78×10^{0}
Open Circuit Frequency (Hz)	1.05×10^{2}	Average Length of End Turn (m)	4.94×10^{-1}
		Mass of Conductors-Total (kg)	9.24×10^{1}
Peak Current (amps)	4.23×10^{5}		
Peak Terminal Voltage (volts)	1.63×10^{4}	Conductor Cross Section-Stator (m^2)	1.31×10^{-4}
Peak Output Power (watts)	6.84×10^{9}	Length of Conductor (m)	1.78×10^{0}
Energy Delivered to Load (joules)	2.47×10^{6}	Average Length of End Turn (m)	5.01×10^{-1}
Inertial Energy Stored (joules)	3.83×10^{7}	Mass of Conductors-Total (kg)	1.27×10^{2}
Peak Reaction Torque (N-m)	4.85×10^{7}		
Fractional Speed Change per Pulse	6.41×10^{-2}	Stainless Steel Support Ring Diameter (m)	8.17×10^{-1}
		Mass of Stainless Steel Support Ring (kg)	1.18×10^{3}
DC Armature Resistance at 20°C (ohms	3.40×10^{-2}		
Minimum Armature Inductance (Henries)	2.5×10^{-5}	Magnetic Air Gap (m)	2.54×10^{-2}
Rotor Winding Temperature Rise per Pulse (°C)	3.30×10^{1}	Peak Gap Field Flux Density (T)	1.09×10^{0}
Stator Winding Temperature Rise per Pulse (°C)	2.36×10^{1}	Ampere-Turns/Pole	8.14×10^{4}
		Field Power-Pulsed (watts/pole)	5.94×10^{4}
Peak Fault Current (amps)	6.22×10^{5}	Mass Field Coil-Total (kg)	2.05×10^{3}
Peak Fault Reaction Torque (N-m)	8.26×10^{7}		
		Radial Pole Height (m)	1.75×10^{-1}
Rotor Diameter (m)	8.06×10^{-1}	Axial Pole Length (m)	1.65×10^{0}
Rotor Length (m)	2.41×10^{0}	Circumferential Pole Width (m)	4.68×10^{-1}
Slip Ring Diameter (m)	5.00×10^{-1}	Mass of Pole Pieces-Total (kg)	3.59×10^{3}
Shaft Diameter (m)	2.54×10^{-1}		
Shaft Length (m)	3.19×10^{0}	Mass bearing Supports (kg)	2.17×10^{3}
Mass Rotor Laminations (kg)	7.41×10^{3}	Mass of Armature Insulation (kg)	7.11×10^{1}
Mass Shaft (kg)	1.91×10^{3}	Mass of Clamping Washers (kg)	4.11×10^{2}
		Mass of Other Components (kg)	1.99×10^{2}
Outer Dimension Stator Iron (m)	1.68×10^{0}	Estimated Total Mass (kg)	4.31×10^{4}
Inner Dimension Stator Iron (m)	1.05×10^{0}		
Stator Back Iron Thickness (m)	3.13×10^{-1}	Estimated Height of Assembled Generator (m) (Without Prime Mover)	3.25×10^{0}
Mass Stator Iron (kg)	2.37×10^{4}		

WLB 11 July 1978

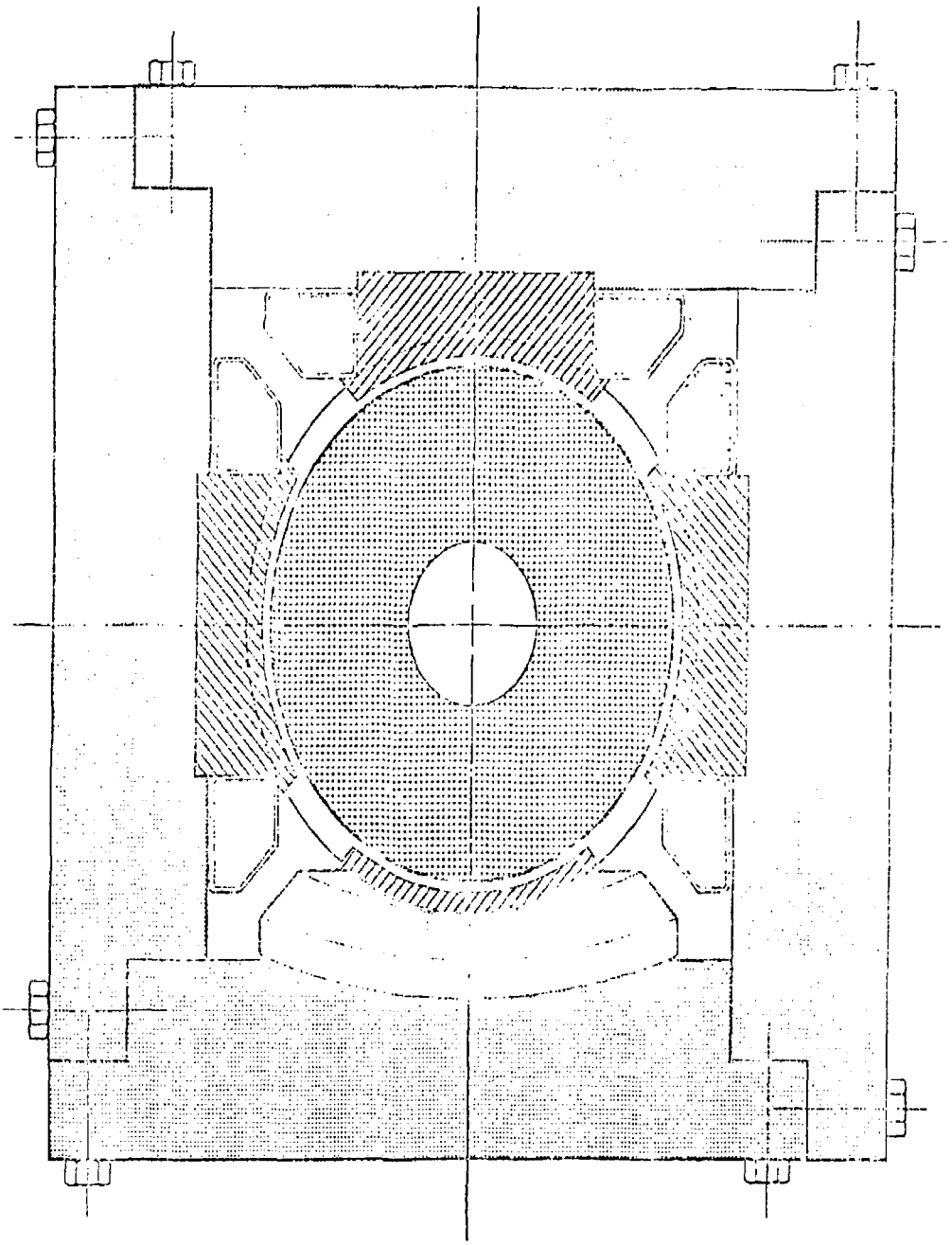

Figure 27: End View Cross-section, Prototype Pulsed Alternator

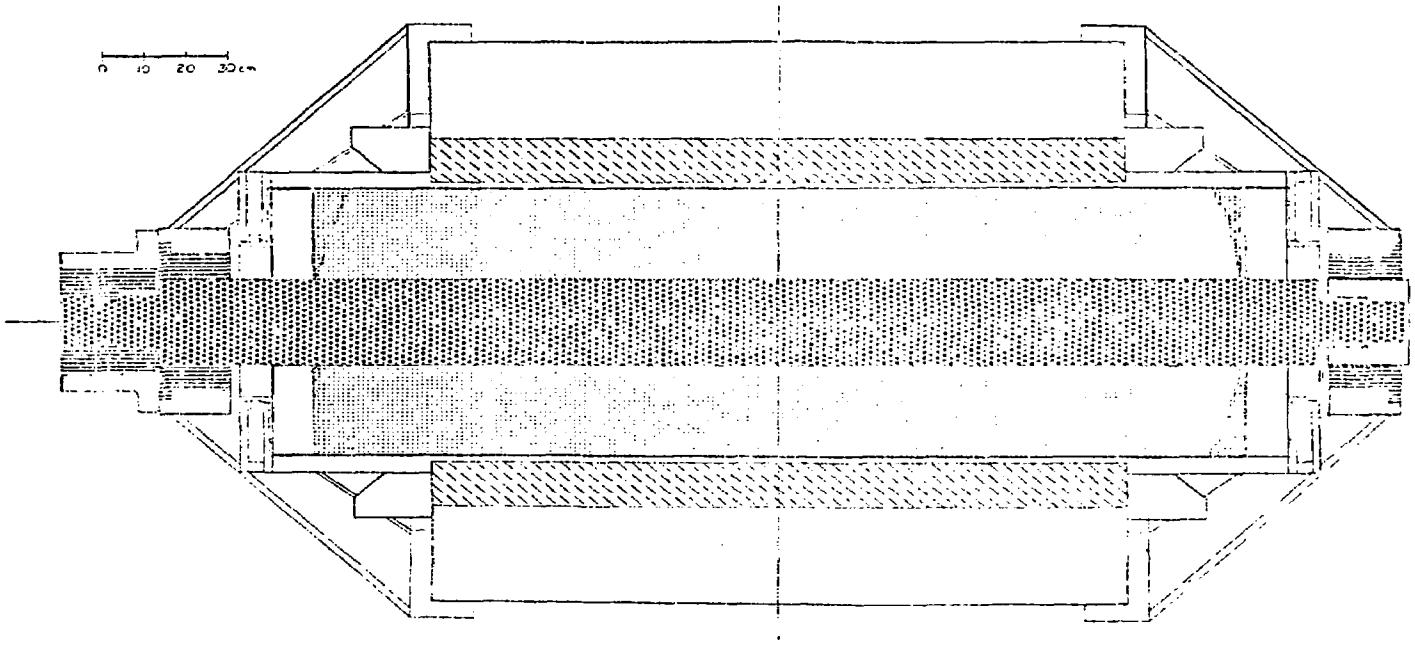

Figure 28: Side View Cross-section, Prototype Pulsed Alternator

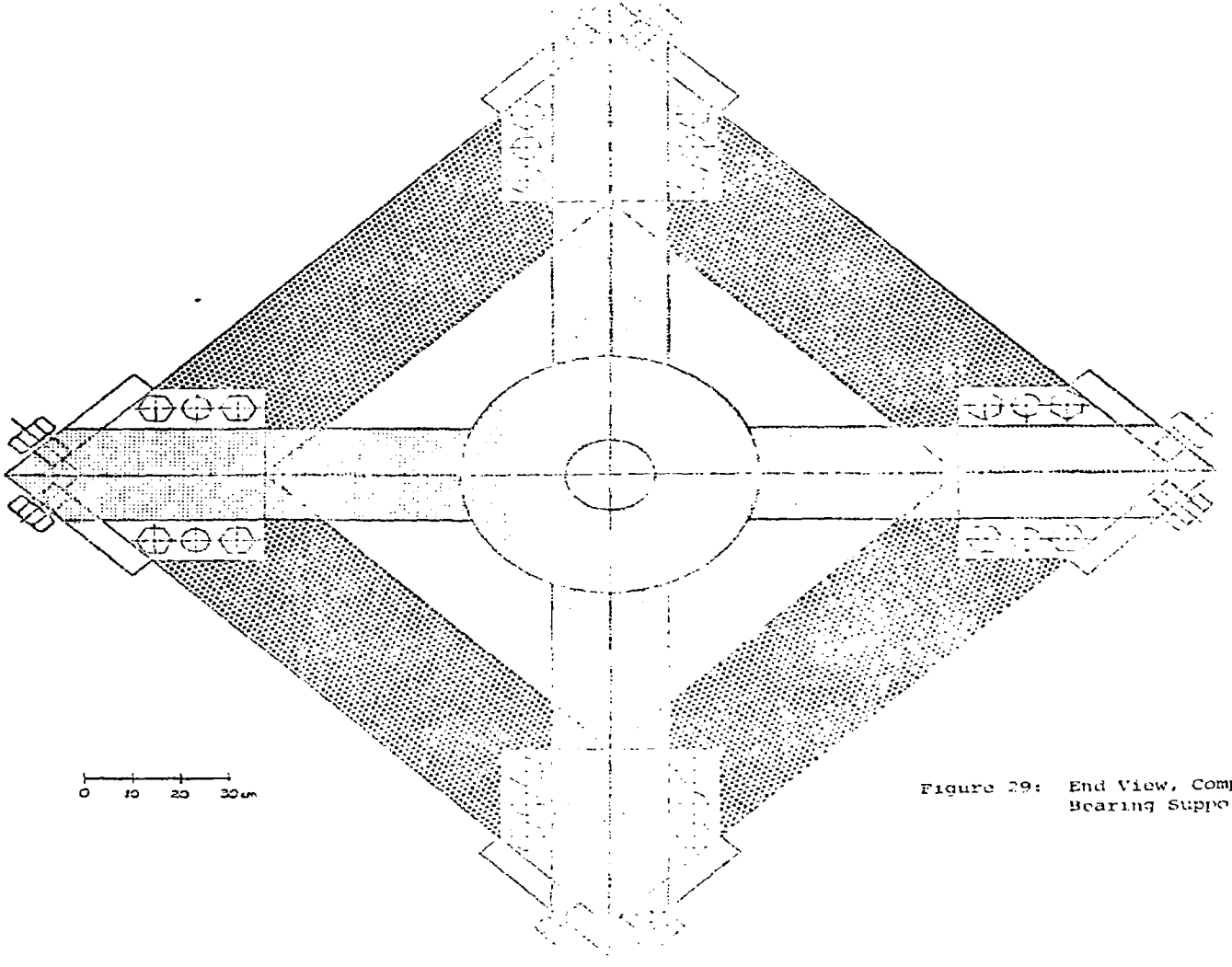

Figure 29: End View, Compulsator Bearing Support

machine back iron is shown as rectangular, since the lead time of a cast steel yoke does not fit into the desired project schedule, and it is, therefore, necessary to fabricate the stator from plate. The continuous ring configuration is preferred for the production units, however, because it is much more rigid mechanically and less costly.

Several design changes recommended for the full scale prototype are as follows:

1. Increase the diameter and reduce the angular velocity of the rotor to better match flashlamp impedance.
2. Reduce the number of turns of the rotor winding for the lower voltage load and to optimize alternator output.
3. Reduce the dielectric stress on the mechanical air gap.
   a. Increase mechanical clearance between rotor and stator.
   b. Reduce the thickness of the banding wrap to maintain the same conductor spacing (keep performance level).
   c. Cover periphery of rotor and inner diameter of stator with semiconductive surface to suppress corona.
4. Optimize the magnetic circuit design to minimize system cost.
   a. Increase gross current density of field windings.
   b. Reduce radial dimension of back iron.
5. Reduce eddy current drag of armature conductors by replacing solid conductors with stranded and transposed conductors.

IV. SYSTEM OPTIMIZATION AND SCALING STUDY

4.1 Scaling Laws and Algorithms

The general procedure used to match the compensated pulsed alternator to a flashlamp load is as follows:

1. Calculate the inductance variation with angular position as a function of rotor diameter.
2. Calculate angular velocity of rotor as a function of diameter to obtain proper peak current and pulse width.
3. Select radius and angular velocity for maximum rotor tip speed.
4. Calculate the number of rotor conductors to match voltage to load.
5. Determine the number of lamp circuits driven by the alternator (circuit analysis).
6. Calculate field power and back iron dimensions.
7. Determine cost per joule delivered.
8. Repeat for different number of poles or other generator parameter.

4.1.1 Inductance Variation

It is assumed that the armature circuit inductance may be expressed by

$$L(\theta_m) = L_{min} + \Delta L \left[1 - \cos(N_p \theta_m/2)\right] \qquad (1)$$

where L_{min} is the minimum inductance of the circuit at $\theta_m = 0$, θ_m is the angular position of the axis of the rotor winding relative to the axis of the stator winding, and N_p is the number of poles. If θ_o is the mechanical angle at the time $t = t_o$ that the flashlamps are switched across the machine terminals then

$$L(\theta_o) = L_{min} + \Delta L \left[1 - \cos(N_p \theta_m/2)\right] = (A_k + 1)L_{min} \qquad (2)$$

where

$$A_k \triangleq L_o/L_{min} - 1 = (L_o - L_{min})/L_{min}.$$

It will be shown that the peak amplitude and pulse width of the discharge current are primarily functions of the factor A_k.

4.1.2 Current Waveshape

At any time during the discharge pulse the sum of the inductive volt-seconds and resistive volt-seconds of the circuit is equal to the volt-seconds supplied by the alternator.

$$\int V_{ac}\,dt = \int iR_{ckt}\,dt + \int d(Li)$$

It has been observed from circuit analysis that for times $t \geq t_o$ (the time that the flashlamps are switched across the alternator terminals),

the resistive volt-seconds are approximately equal to the source volt-seconds.

$$\text{i.e. } \int_{t_o}^{t} V_{ac}\,dt \sim \int_{t_o}^{t} iR_{ckt}\,dt$$

Therefore, the armature flux linking the rotor winding is essentially constant. That is,

$$d/dt(Li) \sim 0.$$

If flux is conserved, then the discharge current is a function of the angular position of the rotor winding and is given by

$$i(\theta_m) = (A_k + 1)i_o / \left\{1 + A_k\left[1 - \cos(N_p\theta_m/2)\right] / \left[1 - \cos(N_p\theta_o/2)\right]\right\} = L_o i_o / L(\theta_m). \qquad (3)$$

Using the above equation for discharge current, and assuming a constant angular velocity ω_m, the current pulse half width is given by

$$t_{1/2} = \frac{4\cos^{-1}(1-f/A_k)}{N_p\omega_m} \quad \text{sec} \qquad (4)$$

where

$$f = 1 - \cos(N_p\theta_o/2)$$

and A_k and θ_o are as defined in Section 4.1.1.

4.1.3 Rotor Angular Velocity and Diameter

Using the equation for the discharge current given above, the energy delivered to a system of flashlamps can be calculated by

$$W = \int_{t_o}^{t_F} I^{3/2}(K_o)_{eff}\,dt \quad \text{joules}$$

where W is the total energy delivered to the lamps, I is the total current, and $(K_o)_{eff}$ is the effective lamp impedance given by

$$(K_o)_{eff} = K_o n_s n_p^{-1/2} \quad \Omega\text{-amps}^{1/2}.$$

The terms n_s and n_p are the number of lamps in series per circuit and the number of parallel circuits, respectively. K_o is the impedance constant of an individual flashlamp. To the first approximation the angular velocity of the rotor is assumed to be constant and is given by

$$\omega_m \sim \frac{2|\theta_o|S\, I^{3/2}(K_o)_{eff}}{W} = \frac{2|\theta_o|S\, i_L^{3/2}K_o}{w_L}$$

where S is a constant of integration dependent on the factor A_k and initial angle θ_o, i_L is the individual lamp current, and w_L is the delivered energy per flashlamp.

As an example, consider the following case:

$\theta_o = -0.294$ rad

$N_p = 4$

K_o = 90 Ω-amp$^{1/2}$

i_L = 4500 amp

w_L = 12.5 kJ (25 KJ per lamp pair)

The factor S, angular velocity ω_m, and maximum rotor radius r_{max} are listed in Table VIII for various values of A_k.

Table VIII: Rotor Angular Velocity and Radius

A_k	S'	ω_m (sec^{-1})	r_{max} (m) (V = 150 m/sec)
14	0.26	326	0.46
19	0.22	284	0.53
24	0.20	254	0.59

The approximate rotor diameter is determined by plotting the angular velocity ω_m and diameter of the rotor as a function of A_k and selecting the case which results in the maximum tip speed subject to spin stress constraints. For the scaling laws used in this study, the match for the four pole alternator occurs at a rotor radius of 0.5 m for K_o ~ 90 Ω-amp$^{1/2}$. The optimum diameter depends on the lamp impedance, and is larger for flashlamps with lower impedance.

4.1.4 Scaling Laws

The following assumptions have been made for the scaling study to size the pulsed alternator power supply for NOVA:

A. Lamp Characteristics

1. $K_o \sim 90\ \Omega\text{-amp}^{1/2}$ (one 1.5 cm x 112 cm xenon flashlamp)
2. $n_s = 2$ (two lamps in series per circuit)
3. $i_L = 4500$ amp
4. $w_L = 12.5$ kJ

B. Alternator Parameters

1. Rotor length to diameter ratio $(\ell/D) \sim 3$
2. Average length of conductor for impedance calculation (per conductor) $\ell_c \sim D\left[\left(\frac{\ell}{D}\right) - \pi/N_p(1 - \pi/4)\right]$
3. Average length of conductor for voltage calculation (per conductor) $\ell_a \sim f_1 D\left[\left(\frac{\ell}{D}\right) - \pi/N_p\right]$ $\qquad f_1 \sim 0.93$
4. Maximum air gap flux density $B_{max} \sim 1.9$ Tesla
5. Ratio of pole arc to pole pitch $f_2 \sim 0.75$
6. Average air gap flux density $B_{avg} \sim f_2 B_{max}$
7. Rotor tip speed $v \leq 150$ m/sec
8. Peak open circuit voltage $(V_{ac})_{peak} \sim 12.1$ kV
9. Number of rotor conductors N_c

$$N_c \sim \frac{(V_{ac})_{peak}}{B_{avg}\ell_a v}$$

10. Fraction of rotor periphery covered by conductor $f_3 \sim 0.56$

11. Effective width of rotor conductor $(W_\theta)_r$

$$(W_\theta)_r = \pi f_3 D/N_c$$

12. Effective thickness of stranded and transposed conductor $(t_{eff})_R$ for resistance calculation

$(t_{eff})_R \sim 3.2 \times 10^{-3}$ m (independent of radius)

13. Effective thickness of stranded and transposed conductor $(t_{eff})_L$ for inductance calculation

$(t_{eff})_L \sim 5.6 \times 10^{-3}$ m (independent of radius)

14. Conductivity of copper conductor at 20°C

$\sigma \sim 98\%$ IACS $= 5.6 \times 10^7$ mho/m

15. Effective width of stator conductor $(W_\theta)_s = f_4(W_\theta)_r \quad f_4 \leq 1.25$

16. Angular position of rotor

$\theta_m(t = 0) = -\pi/N_{poles}$ (Close crowbar switch t = 0)

$\theta_m(t = t_o) = -1.18/N_{poles}$ (Switch lamps into ckt at $t = t_o$)

17. Mechanical clearance $g_{mech} \sim 3.9 \times 10^{-3} \times D$ m

18. Rotor banding wrap thickness $t_{wrap} \sim 1.3 \times 10^{-3}$ m (independent of radius)

19. Stator air gap insulation $(t_{ins})_{gap}$ 6.4×10^{-4} m

20. Effective air gap for armature inductance calculation g_{eff}

$$g_{eff} \sim \left[2/3(t_{eff})_L + g_{mech} + (t_{ins})_{gap} \right]$$

21. Minimum armature inductance L_{min}

$$L_{min} \sim \frac{\mu_o}{\pi} N_c^2 (\ell_c/D) g_{eff} f_5 \qquad f_5 \sim 1.4$$

22. $L(\theta_o) \sim L_{min}(A_k + 1)$

23. $A_k \sim f_6 f_7$**

**See Section 4.2

f_7 - volume rotor iron/volume of air gap

f_6 - 0.79 based on finite element flux plots

24. Inner Diameter of rotor laminations r_i

$D_i - D(1 - f_2 f_8 \pi/N_p)$

f_8 - 1.16

25. Total radial thickness of stainless steel ring t_{ss}

$t_{ss} - 6.9 \times 10^{-2} \frac{(N_c I)^2}{D}$ m

26. Radial thickness of stainless steel ring under pole $(t_{ss})_p$

$(t_{ss})_p = f_q t_{ss}$ f_q 0.27

27. Ground plane insulation thickness $(t_{ins})_{ground} - 2.5 \times 10^{-3}$ m

28. Effective air gap for main field g_f

$g_f - \left[2(t_{ins})_{ground} + 2(t_{eff})_L + (t_{ss})_p + t_{wrap} + (t_{ins})_{gap} + g_{mech} \right]$

29. Field magnetomotive force $(NI)_f$

$(NI)_f - \mu_o B_{max} g_f + f_{10}$ x (mmf drop in back iron and rotor)

f_{10} - 2 (factor of safety)

30. Leakage flux per pole ϕ_ℓ - 25% useful flux per pole ϕ_u

31. Total flux per pole $\phi_t - 1.25\ \phi_u$

32. Back iron flux density 1.6 Tesla (μ_r - 260) $\mu = \mu_r \mu_o$

33. Maximum pole flux density 1.9 Tesla (μ_r - 78) $\mu = \mu_r \mu_o$

34. Gross field coil current density J_f - 5.5×10^6 A/m^2

35. Field coil conductor 2.54 cm square with 1.6 cm round coolant passage

36. Field coil construction - double pancakes with saddled ends

37. Shaft diameter $D_s \sim f_{11} D$

$f_{11} \sim 0.32$

38. Shaft wall thickness $t_{shaft} \sim f_{12} D_s$

$f_{12} \sim 0.2$

39. For $D_s < D_i$ - assume 50% web $D_s < D < D_i$

40. Bus and coaxial cable impedance

$$R_{Bus} \sim 5.1 \times 10^{2}/I + 1.82 \times 10^{-1}/N_{ckts}$$

$$L_{Bus} \sim 4.9 \times 10^{-2}/I + 8.2 \times 10^{-6}/N_{ckts}$$

4.2 Scaling Study Results

Using the scaling laws presented in Section 4.1, conceptual designs of four, six, and eight pole compensated pulsed alternators have been made for the flashlamps to be used in SHIVA/NOVA. The four pole design, Case A, is based on a rotor limiting tip speed of 150 m/sec. The six pole design, Case B, is based on a 1.2 m rotor diameter, which is possibly an upper limit for a single lamination sheet steel width. The eight pole design, Case C, is based on a 120 m/sec tip speed limit for a segmented rotor. Cases D and E are included to compare six and eight pole machines at the same rotor tip speed as the four pole machine. Finally, Case F is included to compare the performance of the six pole machine at a lower speed to the base case. The reduced speed would perhaps be more compatible with an electric motor drive.

The performance figures for these cases are listed in Table IX, and design dimensions for the three base case machines are given in

Table IX: Alternator Performance Summary

Parameter/Case	A	B	C	D	E	F
Number of Poles	4	6	8	6	8	6
Rotor tip speed (m/sec)	150	126	120	150	150	112
Rotor diameter (m)	1.02	1.20	1.45	1.50	1.92	1.20
Angular velocity (sec^{-1})	294	211	166	200	157	188
Inductance factor A_k**	17.6	15.1	13.4	16.9	15.3	15.1
Estimated half width (μsec)	469	471	479	469	473	>471
Open circuit voltage (kV)	10.3	11.4	9.0	8.1	14.9	10.1
Peak lamp voltage (kV)	11 9	11.9	11.9	11.9	11.9	11.5
Peak Current (kA)	865	887	1120	1880	2720	790
Number of lamp circuits	198	203	259	430	615	195
Peak lamp current (kA)	4.37	4.37	4.34	4.36	4.42	4.06
Energy to flashlamps (MJ)	4.94	5.08	6.49	10.8	15.4	4.88

**See Section 4.2.1

Parameter/Case	A	B	C	D	E	F
Actual half width(μsec)	493	494	502	496	487	557
No. of rotor conductors	23	23	15	11	15	23
Armature resistance (mΩ)	8.5	8.7	3.7	1.9	3.7	8.7
Minimum inductance (μH)	8.6	9.2	4.3	2.4	5.0	9.2
Rotor conductor temp rise (°C)	25	19	8.9	12	29	17
Armature i^2R loss (MJ)	2.6	2.7	1.9	2.8	11	2.4
Bus i^2R loss (MJ)	0.4	0.5	0.6	1.0	1.4	0.4
Estimated rotor inertia ($J\text{-}sec^2$) (laminations only)	2440	4980	11,700	15,600	47,700	4980
Final speed/initial speed (%)	96	96	97	98	98	95
Energy delivered/energy stored (%)	4.7	4.6	4.0	3.4	2.6	5.5

Table X. Cross sectional end views of the rotor and stator assemblies are shown in Figures 30, 31, and 32.

4.2.1 Scaling Performances

The magnitude and waveshape of the alternator current depends on the inductance variation. The non-linearity of the iron coupled with diffusion effects make calculation of the inductance variation difficult. At the time of this study the calculation has been performed using a transient finite element computer code, but only for the point design alternator. The inductance variation for machines of different diameter and different numbers of poles has been estimated using the scaling laws given in Section 4.1. While the minimum inductance may be estimated rather easily, the magnitude of the maximum inductance is more difficult to predict.

The scaling coefficient f_7 used in this study is equal to the ratio of the volume of the effective air gap to the volume of the laminated rotor. This ratio varies as (D/g_{eff}), with a weaker dependence on the number of poles. Recently, however, the finite element computer code has been used to calculate the inductance variation for the half-scale engineering prototype. Based on the two computer analyses for the July, 1978, point design and the half-scale engineering prototype, it appears that the inductance variation scales as

$$(L_{max}/L_{min}) \propto \left(\frac{\pi D/N_D}{g_{eff}}\right)^2$$

Table X: Alternator Parameter Summary

Parameter/Case	A	B	C
SS ring O.D. (m)	1.20×10^{0}	1.36×10^{0}	1.56×10^{0}
SS ring thickness (m)	7.66×10^{-2}	6.89×10^{-2}	3.88×10^{-2}
SS ring thickness at pole (m)	2.09×10^{-2}	1.88×10^{-2}	1.06×10^{-2}
SS ring length (m)	3.02×10^{0}	3.58×10^{0}	4.35×10^{0}
SS ring mass	4.54×10^{3}	5.25×10^{3}	4.67×10^{3}
Rotor O.D. (m)	1.02×10^{0}	1.20×10^{0}	1.45×10^{0}
Effective air gap (m)	4.05×10^{-3}	4.74×10^{-3}	5.76×10^{-3}
Magnetic air gap (m)	4.30×10^{-2}	4.16×10^{-2}	3.44×10^{-2}
Lamination I.D. (m)	3.28×10^{-1}	6.50×10^{-1}	9.50×10^{-1}
Lamination mass (m)	1.72×10^{4}	2.16×10^{4}	2.52×10^{4}
Shaft O.D. (m)	3.23×10^{-1}	3.79×10^{-1}	4.60×10^{-1}
Shaft wall thickness (m)	6.48×10^{-2}	7.58×10^{-2}	9.21×10^{-2}
Shaft length (m)	4.80×10^{0}	5.39×10^{0}	6.29×10^{0}
Shaft mass (kg)	1.94×10^{3}	2.98×10^{3}	5.12×10^{3}
Web mass (kg)	0	3.00×10^{3}	9.15×10^{3}
Inertia Rotor & Shaft (joules-sec^2)	2.50×10^{3}	5.48×10^{3}	1.45×10^{4}
Inertial Energy Store (J)	1.08×10^{8}	1.21×10^{8}	1.99×10^{8}

Parameter/Case	A	B	C
Armature conductor mass (kg)	5.79×10^{2}	8.08×10^{2}	1.20×10^{3}
Armature insulation mass (kg)	6.66×10^{1}	9.10×10^{1}	1.26×10^{2}
Pole width (m)	8.03×10^{-1}	6.19×10^{-1}	5.00×10^{-1}
Pole height (m)	1.79×10^{-1}	2.85×10^{-1}	2.59×10^{-1}
Pole length (m)	2.10×10^{0}	2.75×10^{0}	3.52×10^{0}
Back iron I.D. (m)	1.56×10^{0}	1.83×10^{0}	2.02×10^{0}
Back iron O.D. (m)	2.51×10^{0}	2.57×10^{0}	2.67×1^{0}
Back iron & pole mass (kg)	6.05×10^{4}	7.36×10^{4}	9.24×10^{4}
Field MMF/pole (A-t)	1.05×10^{5}	1.08×10^{5}	8.4×10^{4}
No turns/pole	28	28	24
Field current (A)	3.76×10^{3}	3.86×10^{3}	3.50×10^{3}
Field power/pole (W)	1.14×10^{5}	1.35×10^{5}	1.11×10^{5}
Field coil copper mass (kg)	2.81×10^{3}	4.76×10^{3}	6.35×10^{3}
Total mass (kg)	$>8.76 \times 10^{4}$	$>1.09 \times 10^{5}$	$>1.39 \times 10^{5}$
Relative Cost	1.0	1.18	1.13

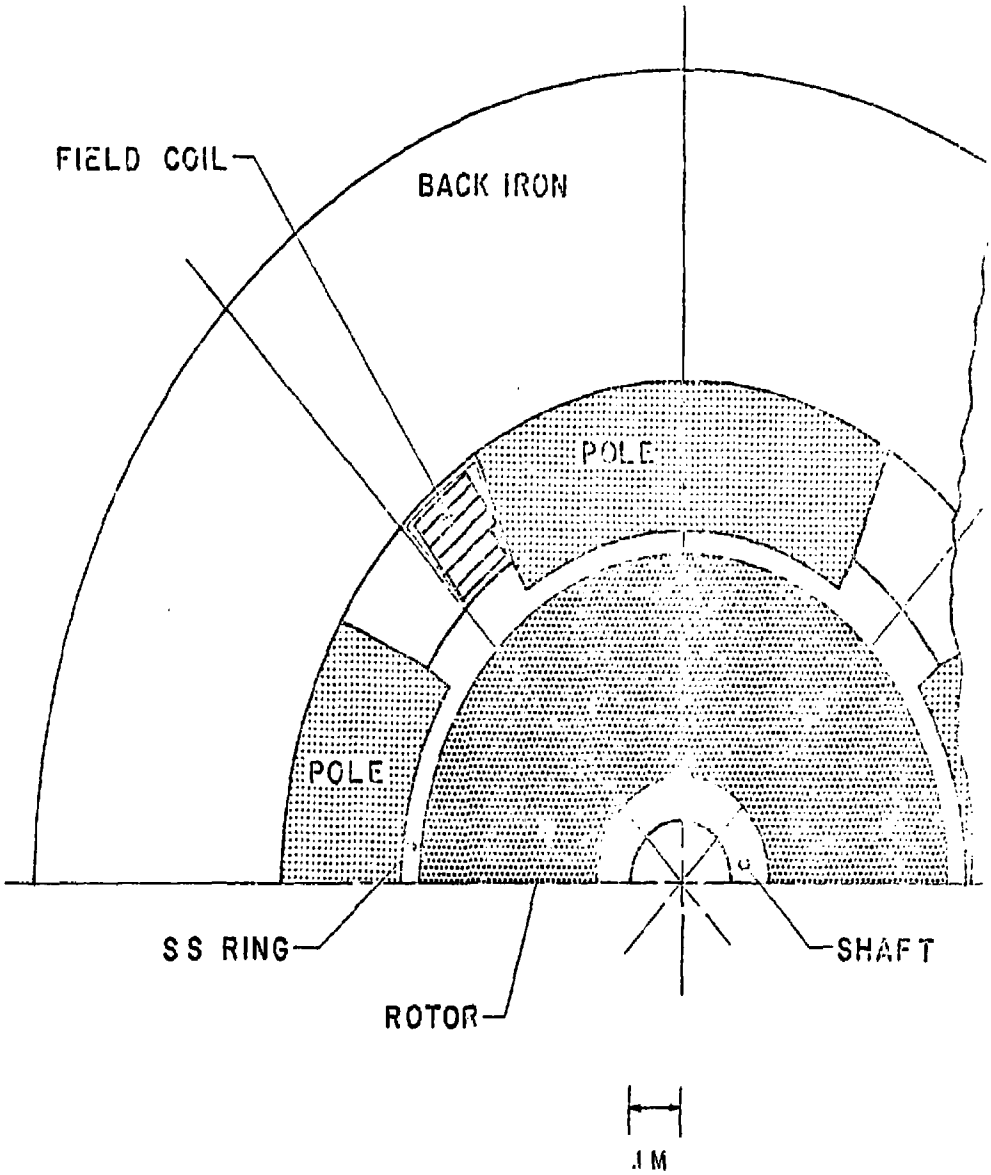

Figure 30: Case A., Four-pole Design

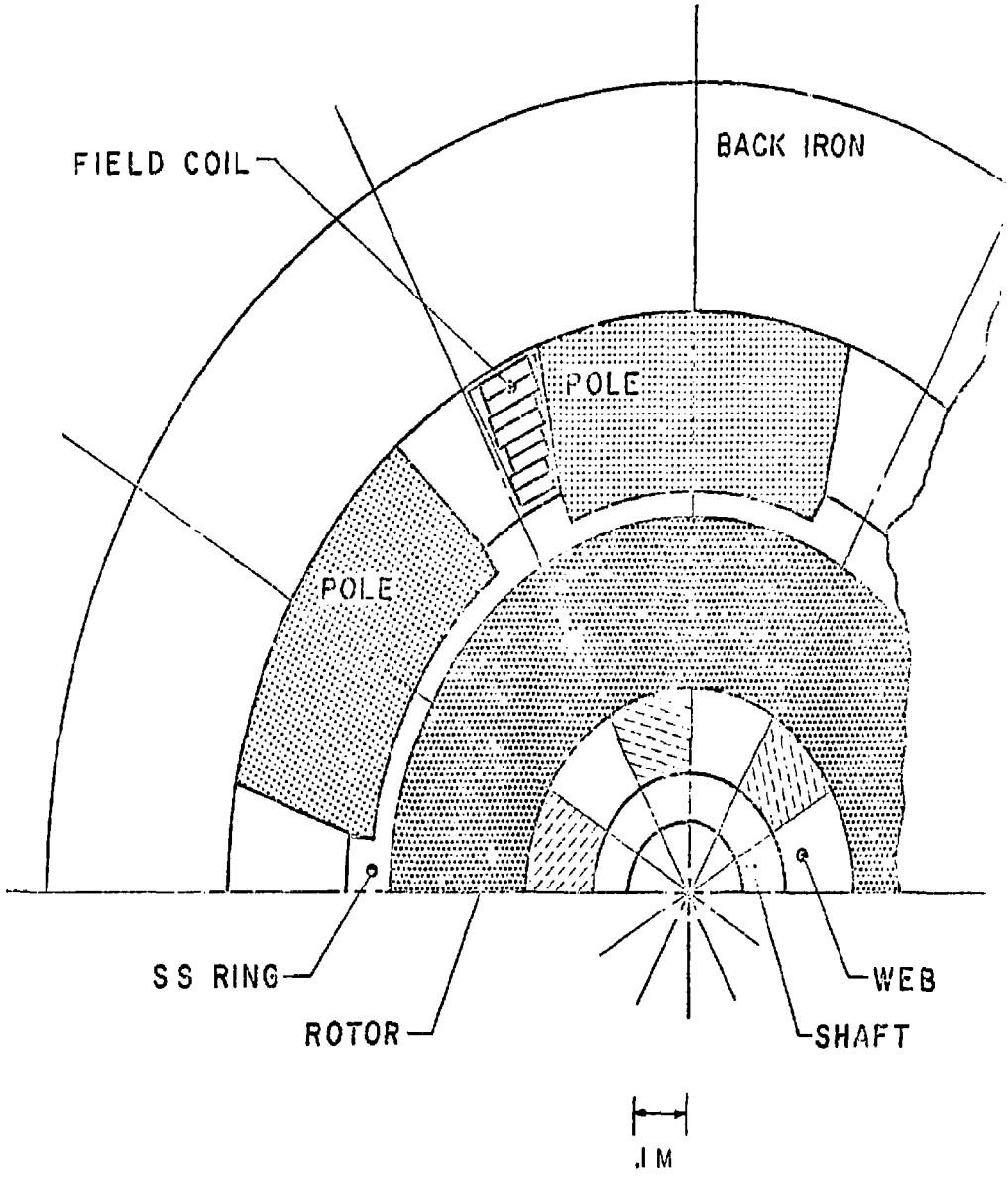

Figure 31: Case B, Six-pole Design

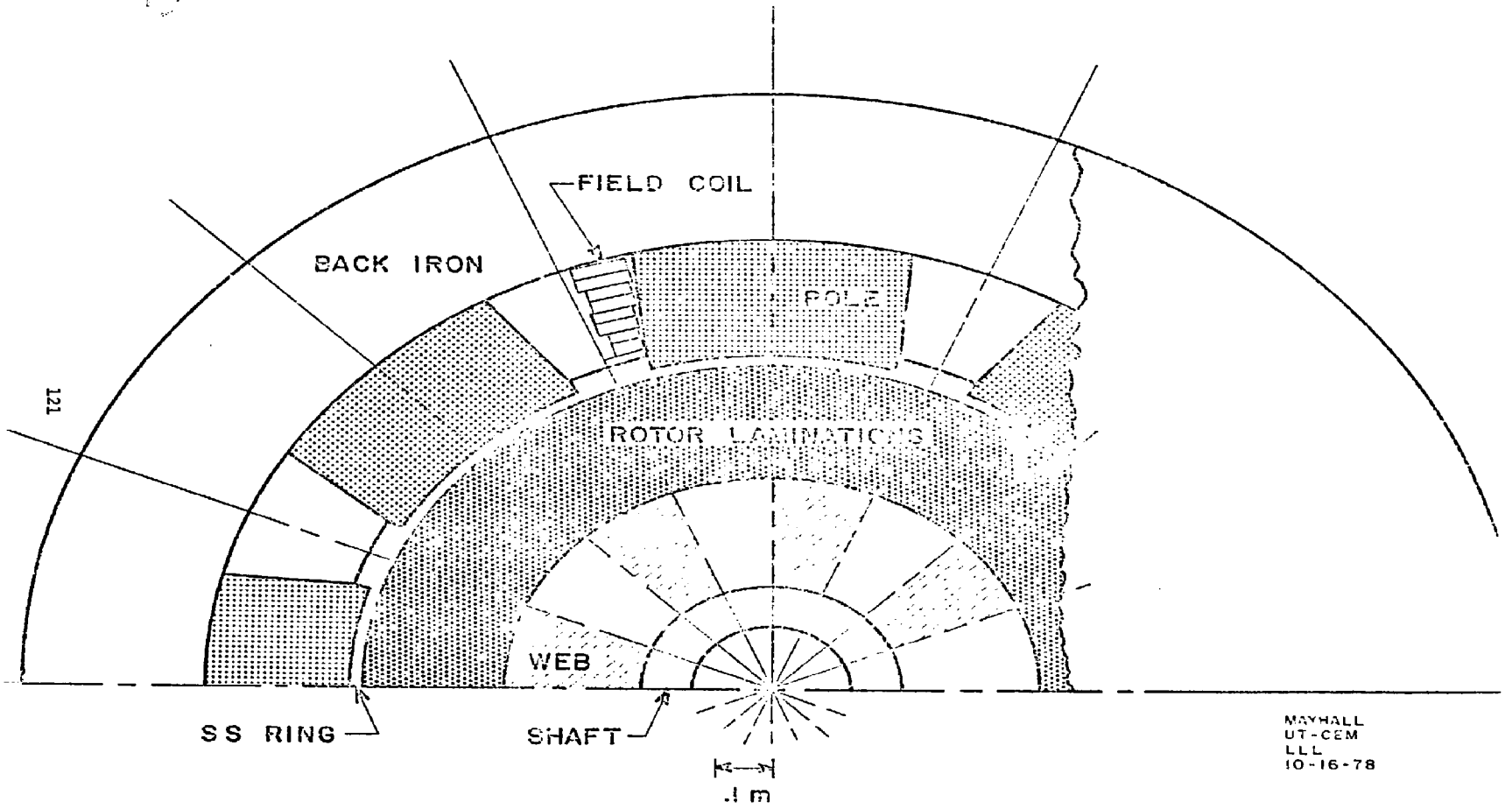

121

Figure 32: Case C, Eight-pole Design

as discussed in Section 2.1. The effect of this scaling factor change in sizing the six and eight pole alternators is discussed in the November, 1978, monthly progress report under LLL Purchase Order 3325309. It is, therefore, recommended that the six and eight pole machine performance described in Table IX not be considered as final, since the peak current and pulse width will be altered. However, the energy delivered should be representative.

4.2.2 System Costs

Using the design parameters of Cases A, B, and C, the relative cost of the three designs were calculated based on $/kg and $/kW figures based on budgetary cost estimates for the point design and engineering prototype alternators (Table XI). To account for economy of scale, it is assumed that the actual costs do not increase linearly with scale, but as the 0.8 power.

Table XI: Relative Alternator Costs

(Materials, Manufacture, and Assembly)

Item/Case	A	B	C
No. Units	10	10	8
Engineering	.03	.03	.04
Controls & Instrumentation	.02	.02	.02
Back Iron and Poles; Rotor Web	.13	.15	.19
Stainless Steel Ring	.17	.19	.17
Rotor Laminations	.18	.22	.25
Shaft	.04	.05	.08
Bearings & Accessories	.13	.17	.22
Brushgear	.01	.02	.02
Field Coils	.04	.06	.08
Field Supply	.04	.06	.07
Armature Conductors	.02	.02	.03
Armature Insulation	.01	.01	.01
Prime Mover	.18	.21	.31
Total Percent	100.00	121.00	149.00
Cost (joule delivered) (normalized)	1.0	1.18	1.13

4.3 Conclusions

A four pole, 1.0 meter diameter rotor, pulsed alternator with 23 conductors on the rotor and compensating winding appears to be a good match to a flashlamp system specified as follows:

Lamp Impedance Constant K_o - 90 Ω-amp$^{1/2}$

Peak lamp current - 4.5 kA

Number of lamps in series - 2

Energy per lamp - 12.5 kJ

Number of parallel lamp circuits - 198

Delivered energy - 4.95 MJ

The machine may require several design features not incorporated in the point design:

1. Stranded and transposed armature conductors
2. Corona suppression system
3. Multiple slip rings for independent lamp circuits
4. Smooth rotor and stator surfaces without slots

V. SUMMARY OF AREAS REQUIRING FURTHER WORK

Development of the compensated pulsed alternator will require several advances in rotating machine technology. The major issues to be resolved during the evolution of a pulsed power source for driving flashlamps for NOVA are listed in the following sections.

5.1 System Design

1. Develop a startup scenario to establish initial current in the alternator, pre-ionize the flashlamps, and couple the alternator to the load.
2. Design the circuit switches (ignitrons or sparkgaps) to reliably interrupt the alternator current at the first available current zero.
3. Design a circuit protection device to interrupt machine current in the event of a failure of the primary switch. The protection device must not cause an unacceptable voltage transient across the alternator terminals.
4. Design a fast, multiple circuit, high current busbar to carry current from alternator to switch headers.
5. Design emergency oil supply.

5.2 Alternator Design

1. Determine the validity of scaling laws and algorithms used to predict alternator performance, particularly the inductance variation.

2. Evaluate the effects of stator pole saliency or non-saliency on inductance variation.
3. Develop an air gap winding design using stranded and transposed armature conductors.
4. Design slip rings for multiple circuit alternators and provide means for proper current division between circuits and brushgear.
5. Develop a high mechanical strength ground plane insulation system with good corona endurance properties.
6. Design a corona suppression system to reduce the dielectric stress across the mechanical air gap.
7. Determine optimum lamp current and pulse width.
8. Design a shock absorbing coupling to protect prime mover from sudden deceleration of alternator rotor.
9. Determine best method of preloading journal bearing by adjusting field ampere turn distribution.
10. Define prime mover for full-scale prototype and develop speed and angular position synchronization system.
11. Design liquid-cooled stator to reject machine losses for 15-minute-repetition-rate duty cycle.

APPENDIX A

Detailed Analysis Three Switch Circuit

A successful simulation of isolated compulsator and flashlamp current startup is obtained with the 3 switch startup circuit shown in Figure A-1. The compulsator is represented on the left by the voltage source V, the rotationally variable effective armature inductance L_{eff}, and the temperature dependent armature resistance R_{gen}. The alternator voltage V is given by

$$V = \frac{V_o \omega}{\omega_o} \cos\left(\frac{N_p}{2} \theta_m\right) \quad \text{Volts} \tag{1}$$

where V_o is the peak alternator voltage at the initial angular rotor speed ω_p, ω is the time varying angular rotor speed, N_p is the number of generator poles, and θ_m is the time varying rotor mechanical position angle. The effective armature inductance is given by

$$L_{eff} = L_{a1} - L_{a2} \cos\left(\frac{N_p}{2} \theta_m\right) \quad H \tag{2}$$

where the maximum inductance is $L_{a1} + L_{a2}$ at $\theta_m = \pm 2\pi/N_p$ rad and the minimum inductance is $L_{a1} - L_{a2}$ at $\theta_m = 0$ rad. The compulsator output current is i_g.

The crowbar branch contains the branch inductance L_s, the crowbar resistance R_s, and the crowbar switch S_1. The crowbar switch has a programmed voltage drop V_s, so that the commutating effect of an increased

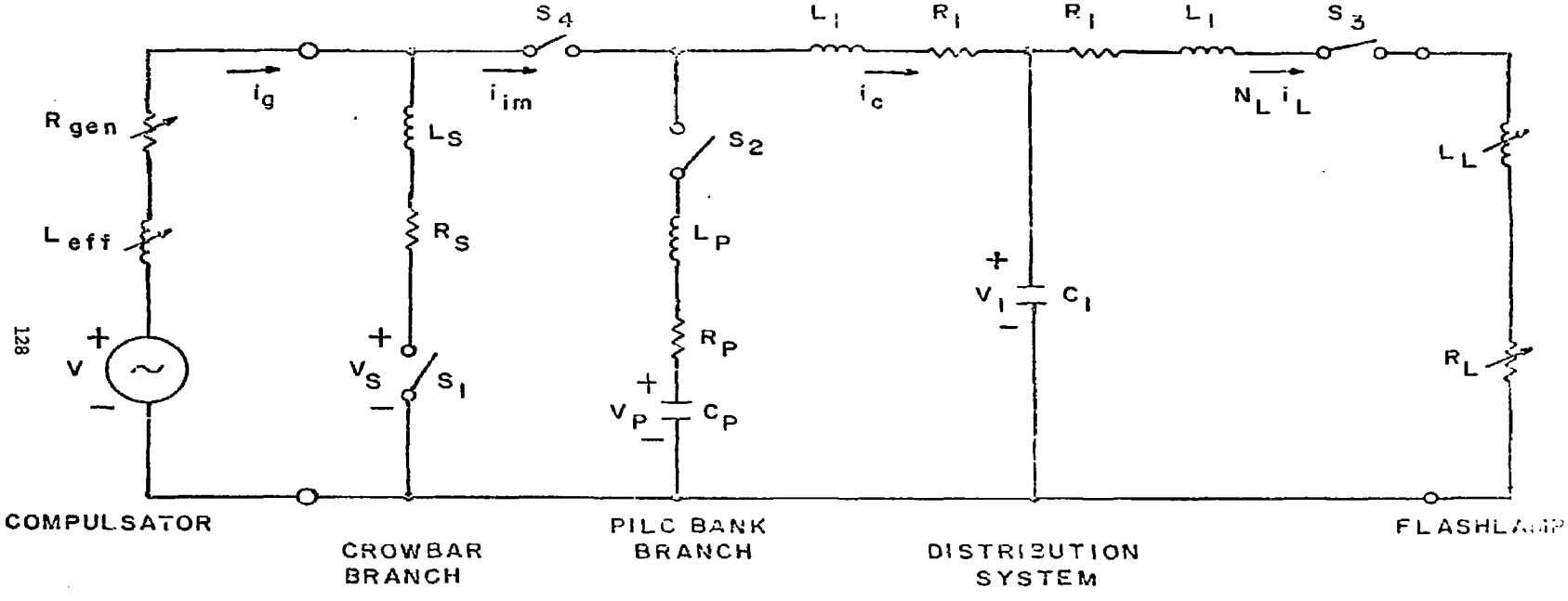

Figure A-1: Three Switch Startup Circuit

switch voltage drop on the crowbar branch current can be investigated. Presently the resistance of the crowbar resistor is constant, but a nonlinearly increasing crowbar resistance can be easily programmed.

The ideal switch S_4 connects the parallel combination of the compulsator and the crowbar branch to the flashlamps via the power distribution system represented by the network. S_4 is closed after isolated current startup is obtained in the compulsator and the lamps.

The PILC capacitor bank branch contains the ideal switch S_2, the initial lamp current rate limit inductor L_p, the PILC bank branch resistance R_p, and the PILC capacitor bank capacitance C_p. The voltage across the PILC bank is V_p. Its initial value is V_{po}. The switch S_2 is closed at some time after the compulsator current is started in the crowbar branch by closure of S_1. Analysis shows that, unless its inductance is very small compared to the compulsator minimum inductance, the lamp current limit inductor must be placed in the PILC bank branch, rather than in series with the T network. If an inductor of appreciable size is placed in series with the T network, the minimum series inductance seen by the compulsator alternator voltage source is increased and the peak alternator output current is reduced.

The T network with the elements L_1, R_1, and C_1 is an approximation to a distribution system made up of a 50 ft. parallel plate generator output bus, a protective fuse, a current equalizing reactor network, and N_L parallel coaxial cables of 100 ft length. Each coaxial cable is connected to two flashlamps in series. The capacitance C_1 is the

approximate capacitance of the system. The voltage across this capacitance is V_1. The capacitance is initially uncharged so that $V_{10} = 0$. The resistance R_1 is one half of the resistance of the distribution system, and L_1 is one half of its inductance. The current which enters the left side of the T network is i_c.

The ideal switch S_2 represents the overvoltage breakdown transition of the lamps from the nonconducting state to the conducting state. S_3 closes when V_1 reaches the lamp breakdown voltage V/am. This breakdown voltage is taken as 24 kV.

The N_L parallel flashlamp circuits are represented by the variable inductance L_L and the variable resistance R_L. After S_3 closes, but before the lamp current begins, R_L is taken as R_{fLmax}/N_L, where R_{fLmax} is 56.3 kΩ. After the lamp current begins, the equivalent lamp resistance is given by

$$R_L = \frac{K_o d_{af}}{N_L d_a(t) |i_L|^{1/2}} \quad \Omega \tag{3}$$

where K_o is the lamp impedance parameter, $d_a(t)$ is the time varying lamp arc diameter, d_{af} is the final lamp arc diameter, which is the lamp inner bore, and i_L is the current per lamp circuit.

The equivalent lamp inductance L_L is modelled as the effective inductance of N_L parallel, magnetically uncoupled go and return current filaments connected in the bucking mode. L_L is given as

$$L_L = \frac{2 \times 10^{-7}}{N_L} (L_{self} - 2M) \quad H \tag{4}$$

where $2 \times 10^{-7} L_{self}$ is the self inductance of each go and return filament and $2 \times 10^{-7} M$ is the mutual inductance of the two halves of each filament. The filament self inductance factor L_{self} is taken as[1]

$$L_{self} = \ell_a \left[\ell_n \left(\frac{4\ell_a}{d_a}\right) - .75\right] \quad H \times 5 \times 10^6 \tag{5}$$

where ℓ_a is the filament length in m and d_a is the filament diameter in m. The filament mutual inductance factor M is taken as[2]

$$M = \frac{\ell_a}{2} \left[\ell_n \left(\frac{\ell_a}{2d} + \sqrt{1 + \left(\frac{\ell_a}{2d}\right)^2}\right) - \sqrt{1 + \left(\frac{2d}{\ell_a}\right)^2} + \frac{2d}{\ell_a}\right]$$

$$H \times 5 \times 10^6 \tag{6}$$

where d is the separation of the centers of the two filament halves. Each filament half models the arc channel of one flashlamp. The arc separation distance d is taken as 5.4 cm.

Analysis shows that inclusion of this model of the flashlamp inductance in the simulations enhances the peak generator current by a few tenths of a percent. For this reason, it is usually omitted, but is included in some of the final calculations for a case.

The growth of the lamp arc diameter is based on the empirical model of Dishington, Hook, and Hilberg.[3] According to this model, the

cylindrical arc filament diameter d_a initially expands in a wall independent regime as

$$d_a = 1.5 \times 10^{-2} \left(\frac{E_L}{\ell_a \times 10^{-2}}\right)^{0.6} \quad m \tag{7}$$

where E_L is the energy absorption of one lamp circuit and is given by

$$E_L = \int_o^t \frac{R_L}{N_L} i_L^2 \, dt \quad J \tag{8}$$

The arc expansion changes to a slower, wall dependent regime at a critical diameter d_{ac} given by

$$d_{ac} = 0.657 \, d_{af}^{1.18} \quad m \tag{9}$$

In the wall dependent regime, the arc diameter is given by

$$d_a = 0.77 \, d_{af} \left(\frac{E_L}{\ell_a \times 10^{-2}}\right)^{0.077} \quad m \tag{10}$$

In the analysis, the initial diameter d_{ao} of the lamp arc is taken as $d_{ao} = 0.01 \, d_{af} = 1.5 \times 10^{-4}$ m.

A system, which gives relatively good results, is the following one. The generator rotor inertia is 708.6 J-sec^2, the initial rotor angular speed is 3140 rpm or 329 rad/sec, the number of generator poles is 4, the initial armature copper rotor resistance at 20°C is 19.57 mΩ, the initial armature copper stator resistance at 20°C is 14.40 mΩ, the rotor armature heat capacity is 3.560×10^4 °C/J, the stator armature heat capacity is 4.772×10^4 °C/J, the generator inductance parameter

L_{al} is 3143 μH, and the inductance parameter L_a^2 is 25.61 μH. The crowbar switch S_1 is closed at $\theta_m = -\pi/4$ rad = -0.7854 rad when the alternator voltage V = 0. The peak no-load alternator voltage for constant angular speed should occur at $\theta_m = 0$ rad and be V_{max} = 15 kV, but, due to generator loading, the peak alternator voltage occurs at $\theta_m = -8.814 \times 10^{-2}$ rad and has the value V_{max} = 14.45 kV.

The crowbar inductance L_s = 2μH; the crowbar resistance R_s = 1mΩ. The crowbar switch voltage V_s varies as

$$V_s = 0 \text{ for } V < 5\text{kV}$$
$$V_s = 100 \text{ V for } V \geq 5 \text{ kV}, S_4 \text{ open} \qquad (11)$$
$$V_s = 5 \text{ kV for } S_4 \text{ closed}$$

The PILC bank capacitance C_p = 100 μF with an initial voltage V_{po} = 20 kV. The PILC bank energy storage is 20 kJ. The PILC branch lamp current limit inductance L_p = 5μH and the PILC branch resistance R_p = 2 μΩ.

The T network inductance L_1 = 104.8 nH and its resistance R_1 = 1.568 mΩ. The T network capacitance C_1 = 55.4 nF.

The lamp arc length ℓ_a = 88 in. = 2.235 in. The lamp impedance factor K_o = 225 $\Omega\text{-A}^{-1/2}$. The number of lamp circuits N_L = 96. The lamp arc expansion is assumed to begin after E_L = 0.104 J. The wall independant expansion ends at E_L = 140 J; the wall dependent expansion

ends at E_L = 6.66 kJ. The lamp inductance model is included in this calculation.

At t = 0, the crowbar switch is closed. At t = 1.434 msec, the generator current in the crowbar branch reaches 14.61 kA at θ_m = -0.3139 rad. At this time, the switch S_2 is closed and the PILC bank begins to pulse charge the T network capacitance.

At t = 1.437 msec, the T network capacitor voltage reaches the chosen ionization voltage of the lamps. At this time, the generator current is 14.75 kA and the T network input current i_c is 6.425 kA. The switch S_3 now closes and the lamps begin to conduct.

At t = 1.495 msec, 58 μsec after lamp conduction begins, the connection switch S_4 is closed and the voltage drop of the crowbar switch is stepped up to V_s = 5 kV. At this time, the generator current is 17.79 kA, the T network input current is 44.96 kA, and the total lamp current is 45.02 kA. The rotor is now at θ_m = -0.2939 rad.

At t = 1.545 msec, 50 μsec after connection, the generator and total lamp currents equalize at 20.51 kA. At this time, the lamp arc diameter is 11.45 mm and 200 J have been absorbed by each lamp.

The evolution of the lamp arc diameter is shown in Figure A-2. The behavior of the lamp and generator currents are also shown in Figure A-2. The wall independent expansion regime ends at about t = 1.500 msec, shortly after closure of S_4.

Fig. A-2: Lamp Arc Diameter, Generator Current, and Lamp Current for Three Switch Compulsator Startup

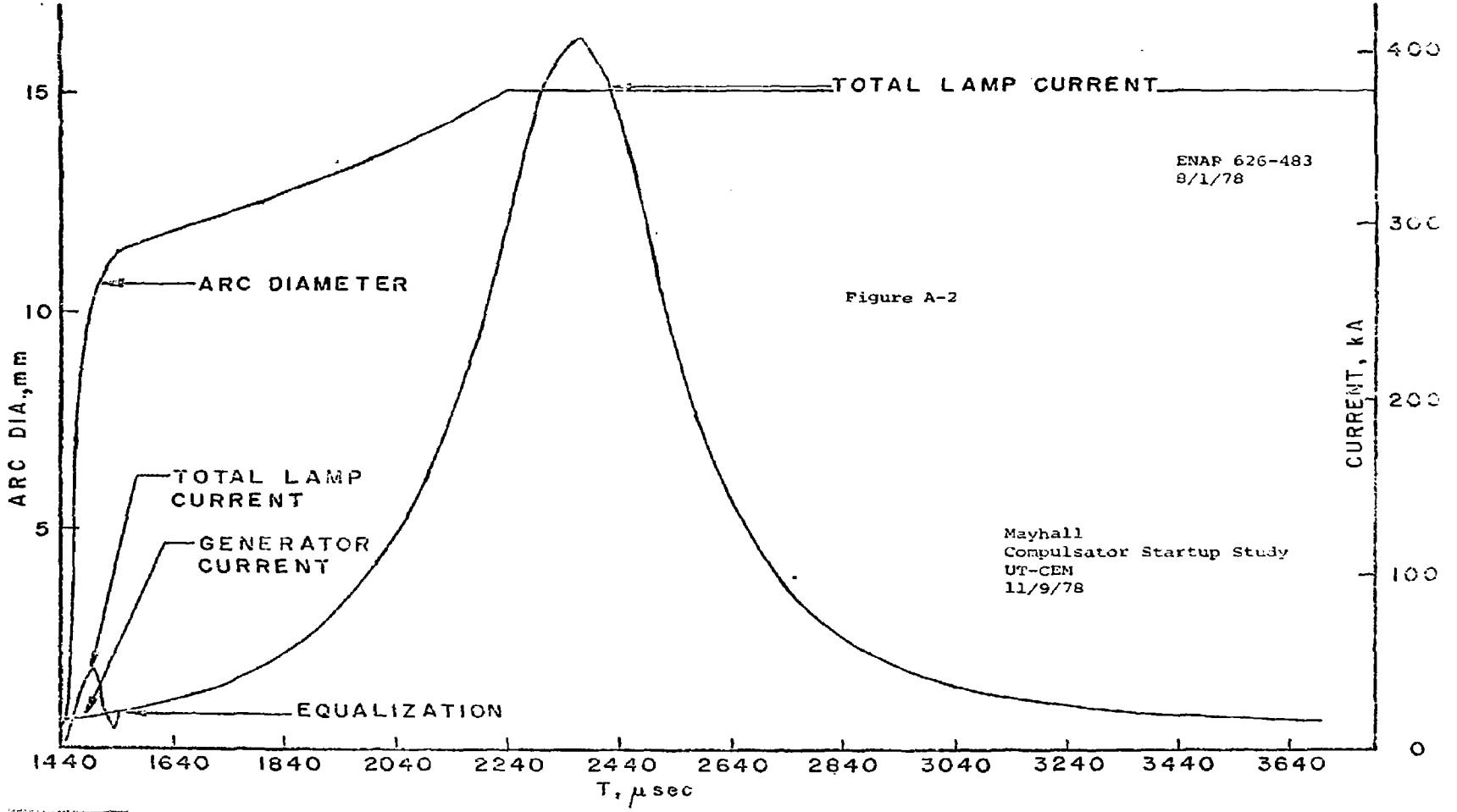

At some times between 1.565 msec and 1.605 msec, the currents in the crowbar and PILC branches go to zero and the switches S_1 and S_2 are opened. These two currents thus self commutate in this system. The peak reverse voltage on the PILC bank occurs at t = 1.535 msec and is V_p = -4.525 kV.

At about t = 2.245 msec, the lamp arc diameter reaches 15 mm, the inner diameter of the flashlamps. The lamp arc thus reaches full bore about 808 μsec after the flashlamp discharge begins. At this time the total lamp current is 304.6 kA.

At t = 2.379 msec, the total lamp current reaches its peak value of 404.5 kA. At t = 3.375 msec, when θ_m = 0.2986 rad, 2.470 MJ has been deposited in the lamps. This is 25.73 kJ per lamp circuit. The full width at half maximum of the total lamp current pulse occurs 202.3 kA and is about 418 μsec.

One possible problem with this circuit may be the nonmonatonic behavior of the lamp current from initiation to equalization with the generator current. Initially, the total lamp current rises from zero at t = 1.437 msec to 2.106 kA at t = 1.440 msec. It then drops to 457.3 A at t = 1.445 msec and then rises to 45.02 kA at t = 1.495 msec, when generator connection occurs. After generator connection, it drops to 9.811 kA at t = 1.535 μsec, undershooting the generator current. The total lamp current then rises to 20.51 kA, the value of the generator

current, at t = 1.545 msec. We presently do not know if this initial pulsation in the lamp current is detrimental to the proper operation of the lamps.

Another possible problem may be the initial rate of lamp current rise $\frac{di_L}{dt}$, which is 1.791×10^9 A/sec. This rate persists for less than 3 μsec because at t = 1.440 msec, $\frac{di_L}{dt} = 1.411 \times 10^7$ A/sec. Afterward, the maximum positive rate of lamp current rise is 1.377×10^7 A/sec at t = 1.460 msec. We presently do not know if an initial rate of lamp current rise of about 1.8×10^9 A/sec for less than 3 μsec can be tolerated by the flashlamps without adverse effects. Fountain[4] suggests that the rate of current rise should be kept below 5×10^7 A/sec, but that up to 1×10^8 A/sec may be used for standard ILC Technology seals.

The performance of this 3 switch startup circuit can probably be further optimized in desired ways by judicious selection of the various circuit and generator parameters.

References

[1]Grover, F. W., Inductance Calculations: Working Formulas and Tables, D. Van Nostrand Co., Inc., NY, 1946 or Dover S974, Formula (7), p. 35.

[2]Grover, F. W., Formula (1), p. 31.

[3]Dishington, R. H., Hook, W. R., and Hilberg, R. P., "Flashlamp Discharge and Laser Efficiency," Application Optics, 13, 2300-2312, October, 1974.

[4]Fountain, W. D., "A Flashlamp/PFN Cookbook," Lawrence Livermore Laboratory Memorandum SSL 73-426, December 20, 1973.